Copyright Warning & Restrictions

The copyright law of the United States (Title 17, United States Code) governs the making of photocopies or other reproductions of copyrighted material.

Under certain conditions specified in the law, libraries and archives are authorized to furnish a photocopy or other reproduction. One of these specified conditions is that the photocopy or reproduction is not to be "used for any purpose other than private study, scholarship, or research." If a, user makes a request for, or later uses, a photocopy or reproduction for purposes in excess of "fair use" that user may be liable for copyright infringement,

This institution reserves the right to refuse to accept a copying order if, in its judgment, fulfillment of the order would involve violation of copyright law.

Please Note: The author retains the copyright while the New Jersey Institute of Technology reserves the right to distribute this thesis or dissertation

Printing note: If you do not wish to print this page, then select "Pages from: first page # to: last page #" on the print dialog screen

NJIT New Jersey's Science & Technology University

The Van Houten library has removed some of the personal information and all signatures from the approval page and biographical sketches of theses and dissertations in order to protect the identity of NJIT graduates and faculty.

ABSTRACT

ELECTRODELESS ELECTRO HYDRODYNAMIC PRINTING OF PERSONALIZED DRUG DOSAGES

by
Ezinwa Okeoma Elele

There is compelling evidence that variability in drug efficacy in individuals depends on their genetic fingerprints. These observations have given rise to the concept of personalized therapy whose ultimate goal is to develop medicinal agents designed for each niche of the population and individual patients according to their genetic background. The drawback in current pharmaceutical technologies is that most processes are designed to target large population and are unable to meet the demand of small-scale manufacturing of tailored therapeutics with diverse range of physical properties. One of the major challenges lie in developing efficient and cost effective methods of manufacturing personalized treatments.

Noncontact drop-on-demand (DOD) systems (i.e., drops are formed only as required) appear to be the most promising platform technology for small-scale manufacturing of personalized treatments. As a digital technology, DOD dosing is able to deposit precisely controlled amounts of material at exact locations without waste, rendering it especially attractive for use with expensive pharmaceutical products. It would provide the capability to form an individual dosage unit by printing a vast array of predefined amounts of therapeutics arranged in a specific pattern on a carrier substrate to achieve a desired drug release profile. However, current DOD methods developed for chemically and thermally stable, low-viscosity inks are of limited use for pharmaceuticals due to fundamentally different functional requirements.

In this dissertation, a recently developed DOD method for gentle printing of personalized medicines is presented. To eliminate adverse effects of electrochemical reactions at the fluid-electrode interface, the fluid was infused into an electrically insulating nozzle to form a pendant drop that served as a floating electrode capacitively coupled to external electrodes. A short voltage pulse was applied to the electrodes to stretch the drop into a liquid bridge that broke up creating a sessile drop on the substrate which could be post-processed into a final dosage form. Versatility was proved in experiments on fluids spanning over three orders of magnitude in viscosity and electric conductivity. This method can be used for printing fluids of different physical properties in pharmaceutical, biomedical, and biotechnology applications. Model for pendant drop and scaling analysis which captured the essential physics of electrodless electrohyrodynamic drop dynamics is presented. This analysis describes the characteristics of the operating regimes and provides critical design guideline.

To demonstrate the capability of electrodeless DOD for printing personalized dosages, assembled unit dosages were prepared by precisely loading porous hydroxy methylcellulose film matrix with controlled drops of model drugs dissolved in lowly volatile polyethylene glycol carrier. Dissolution tests were performed following United States Pharmacopeia (USP) protocol, and the drug release data was analyzed to identify the underlying drug release mechanisms from the assembled unit dosages. Data showed that the DOD method met the reproducibility requirement critical for content uniformity and that the porous film rapidly disintegrated resulting in instant release of drug which could be useful in fast orally dissolvable medicinal film dosage forms.

ELECTRODELESS ELECTRO HYDRODYNAMIC PRINTING OF PERSONALIZED DRUG DOSAGES

by
Ezinwa Okeoma Elele

A Dissertation
Submitted to the Faculty of
New Jersey Institute of Technology
in Partial Fulfillment of the Requirements for the Degree of
Doctor of Philosophy in Chemical Engineering

Otto H. York Department of
Chemical, Biological and Pharmaceutical Engineering

May 2011

Copyright © 2011 by Ezinwa Okeoma Elele

ALL RIGHTS RESERVED

APPROVAL PAGE

ELECTRODELESS ELECTRO HYDRODYNAMIC PRINTING OF PERSONALIZED DRUG DOSAGES

Ezinwa Okeoma Elele

Dr. Boris Khusid, Dissertation Advisor — Date
Professor of Chemical, Biological and Pharmaceutical Engineering, NJIT

Dr. Robert Barat, Committee Member — Date
Professor of Chemical, Biological and Pharmaceutical Engineering, NJIT

Dr. Rajesh Dave, Committee Member — Date
Distinguished Professor of Chemical, Biological and Pharmaceutical Engineering, NJIT

Dr. Kamalesh Sirkar, Committee Member — Date
Distinguished Professor of Chemical, Biological and Pharmaceutical Engineering, NJIT

Dr. Paul Takhistov, Committee Member — Date
Associate Professor of Food Engineering, Rutgers the State University of NJ

BIOGRAPHICAL SKETCH

Author: Ezinwa Okeoma Elele

Degree: Doctor of Philosophy

Date: May 2011

Undergraduate and Graduate Education:

- Doctor of Philosophy in Chemical, Biological and Pharmaceutical Engineering, New Jersey Institute of Technology, Newark, NJ, 2011
- Master of Science in Mechanical Engineering, New Jersey Institute of Technology, Newark, NJ, 2005
- Bachelor of Engineering in Mechanical Engineering, University of Nigeria, Nsukka, Nigeria, 1999

Major: Chemical Engineering

Publications:

Elele Ezinwa, Shen Yueyang, and Khusid Boris, (2010). "Electrodeless electro-hydrodynamic printing of personalized medicines," Applied Physics Letters, 97 (23), 233501-233503.

Elele Ezinwa, Shen Yueyang, Sursala Ramana, Michniak-Kohn Bozena, and Khusid Boris, (2011). "Electrodeless drop-on-demand printing of fast dissolvable assembled unit dosage," JOURNAL OF PHARMACEUTICAL SCIENCES, (In preparation).

Shen Yueyang, Elele Ezinwa, and Khusid Boris, (2011). "A novel concept of dielectrophoretic engine oil filter," Electrophoresis, (Accepted for publication).

Khusid Boris, Elele Ezinwa, Palle Prashanth, Shen Yueyang, Basaran Osman, Collins Robert T., McGough Patrick T., (2010). "Drop-on-demand printing of personalized medicines," Proceedings of the 16th U.S. National Congress of Theoretical and Applied Mechanics, USNCTAM2010-1089-1-2, State College, Pennsylvania.

Kumar Anil, Elele Ezinwa, Yeksel Mike, Khusid Boris, Qiu Zhiyong, and Acrivos A., (2006). "Measurements of the fluid and particle mobilities in strong electric fields," Physics of Fluids, 18 (12), 123301-10.

Presentations

Khusid Boris, Shen Yueyang, Elele Ezinwa, Palle Prashanth, and Siginer Dennis, (2010). "Electro-hydrodynamic drop-on-demand printing of personalized medicines on porous film," American Institute of Mechanical Engineers (ASME) International Congress and Exposition, November 12-18, Vancouver, British Columbia.

Khusid Boris, Elele Ezinwa, and Shen Yueyang, (2010). "Electrodeless Drop-on-demand printing of personalized unit doses," 63rd Annual Meeting of the American Physical Society (APS), Division of Fluid Dynamics, November 21-23, Long Beach, California.

Shen Yueyang, Elele Ezinwa, Palle Prashanth, Khusid Boris, and Michniak-Kohn Bozena, (2010). "Electrodeless drop-on-demand printing of personalized doses," American Institute of Chemical Engineers, AIChE Annual meeting, Salt Lake City, Utah, November 9.

Elele Ezinwa, Shen Yueyang, and Khusid Boris, (2010). "Electrodeless drop-on-demand printing of personalized medicines," Biotech Conference, 10th Anniversary symposium, October 28, Philadelphia, Pennsylvania.

Elele Ezinwa, Shen Yueyang, and Khusid Boris, (2010). "Electrodeless electro-hydrodynamic printing of personalized unit dosages," Metro Area MEMS/NEMS Workshop:NanoManufacturing, July 26, Stevens Institute of Technology, Hoboken, New Jersey.

Shen Yueyang, Elele Ezinwa, Palle Prashanth, Khusid Boris, and Basaran Osman, (2009). "Electro-hydrodynamic printing of drugs onto edible substrates," 62nd Annual Meeting of the American Physical Society (APS), Division of Fluid Dynamics, November 22-24, Minneapolis, Minnesota.

Shen Yueyang, Elele Ezinwa, and Khusid Boris, (2009) "Electrodeless electro-hydrodynamic printing of personalized drug dosage," American Institute of Mechanical Engineers (ASME) International Congress and Exposition, November 13-19, Lake Buena Vista, Florida.

Elele Ezinwa O., Khusid Boris, and Shen Yueyang, (2009). "Electrical conductivity of aqueous solutions of surfactants with added electrolytes," American Institute of Chemical Engineers, AIChE Annual meeting, November 9, Nashville, Tennessee.

Khusid Boris, Shen Yueyang, and Elele Ezinwa O., (2009). "Electrodeless electro-hydrodynamic printing of personalized medicines," American Institute of Chemical Engineers, AIChE Annual Meeting, November 8-13, Nashville, Tennessee.

Elele Ezinwa, (2009). "Electrodeless electro-hydrodynamic printing of personalized drug dosages" The Dana Knox Student Research Showcase, April 18, New Jersey Institute of Technology, Newark, New Jersey.

Elele Ezinwa O., and Khusid Boris, (2008). "Electrical conductance of aqueous surfactant solution with added salt," American Institute of Chemical Engineers, AIChE Annual meeting, November 17, 2008, Philadelphia, Pennsylvania.

Elele Ezinwa O., and Khusid Boris, (2008). "Premiceller association in dodecyl sulfate-salt-water system," American Institute of Mechanical Engineers (ASME) International Congress and Exposition, October 31-November 6, Boston, Massachusetts.

Elele Ezinwa, (2008). "Electro hydrodynamic filtration of polarizable microparticles in a flowing suspension," Fourth Annual student research showcase, April 9, New Jersey Institute of Technology, Newark, New Jersey.

Elele Ezinwa, (2007). "Simultaneous measurement of fluid and particle mobilities in strong electric fields," Third Annual student research showcase, April 11, New Jersey Institute of Technology, Newark, New Jersey.

To Alpha and Omega, the First and the Last, the Beginning and the End

ACKNOWLEDGEMENT

My profound thanks and appreciation goes to my thesis advisor Dr. Boris Khusid, Professor, Otto York Department of Chemical, Biological and Pharmaceutical Engineering, NJIT for his deep understanding, support and guidance throughout the course of my study and research. His advisement is pivotal to the success if this dissertation. My experience will not be complete without the painstaking support of Dr. Rajesh Dave, Distinguished Professor, Otto York Department of Chemical, Biological and Pharmaceutical Engineering, NJIT and director of Engineering Research Center for Structured Organic Particulates Systems (ERC-SOPS) which provided funding for this research under National Science Foundation (NSF) grant no. EEC-0540855.

My in-depth gratitude goes to my thesis committee members for their invaluable advisements and contributions, Dr. Robert Barat, Professor, Otto York Department of Chemical, Biological and Pharmaceutical Engineering, NJIT, Dr. Kamalesh Sirkar, Distinguished Professor, Otto York Department of Chemical, Biological and Pharmaceutical Engineering, NJIT and Dr. Paul Takhistov, Associate Professor of Food Engineering, Rutgers the State University of New Jersey.

I would also like to thank Dr. Yueyang Shen, Assistant Research Professor, Otto York Department of Chemical Biological and Pharmaceutical Engineering, NJIT for his encouragements and fundamental insights in this research. I greatly thank my family members for their encouragement and moral support especially my wife Goodness. My appreciation also goes to my uncle, Mr. Alexander Njoku and his family for their deep support and commitments to my success. Finally, to Alpha and Omega, the First and the Last, the Beginning and the End, I give all the glory!

TABLE OF CONTENTS

Chapter	Page
1 INTRODUCTION……...	1
1.1 Motivation…….	1
1.2 Challenges…….	2
1.3 Research Objectives and Overview……..	3
2 BACKGROUND AND LITERATURE REVIEW……..	5
2.1 Drop Formation…….	5
2.2 Applications……..	7
2.3 Inkjet Printing……	7
2.3.1 Continuous Inkjet……	9
2.3.2 Drop on Demand Inkjet……...	10
2.4 Drop on Demand Printing in Biomedical and Pharmaceutical Applications	16
3 MATERIALS AND METHOD……...	19
3.1 Overview of Electrodeless EHD Drop on Demand printing…….	19
3.2 Experimental Setup and Description…….	19
3.3 Experimental Materials……	22
3.3.1 Fluids……...	22
3.3.2 Active Pharmaceutical Ingredients (API)……...	23
3.3.3 Film Materials and Preparation Methods……	23
3.4 Material Properties and Dimensionless Parameters……..	23

TABLE OF CONTENTS
(Continued)

Chapter	Page
4 EXPERIMENTAL RESULTS…….	28
4.1 Regimes of Drop Deposition…….....	28
4.1.1 Drop Relaxes Back……..	28
4.1.2 Single Sessile Drop…….	29
4.1.3 Multiple Sessile Drops……	30
4.2 Critical Parameters……	30
4.3 Examples of Printed Patterns ……...	30
4.4 Conclusions……...	34
5 MODELING AND SCALING ANALYSIS OF DROP DYNAMICS……	36
5.1 Modeling for Pendant Drop as Harmonic Oscillator……	36
5.2 Electrostatic Forces acting on Pendant Drop……	37
5.3 Oscillation of Pendant Drop…….....	40
5.4 Estimate of Model Parameters…….....	40
5.5 Prediction of Critical Liquid Bridge Lines for Fluids with Oh≤1…….	44
5.5.1 Damped Harmonic Oscillator ……	44
5.5.2 Limiting Case of Negligible Viscous Force……	46
5.6 Design Guidelines…….....	48
5.6.1 Liquid Bridge Stability Study…….	49
5.6.2 Scaling Analysis for Drop Dynamics……..	52
5.7 Conclusions……...	55

TABLE OF CONTENTS
(Continued)

Chapter **Page**

6 PRINTING OF FAST DISSOLVABLE UNIT DOSAGES…..... 57

6.1 Objectives and Overview…….. 57

6.2 Materials…… 58

6.2.1 Model Drugs…… 58

6.2.2 Drug Carrier…… 59

6.2.3 Porous Film Material……... 59

6.3 Preparation of Porous and Non Porous Substrates……..... 59

6.4 Preparation of Drug Solutions……... 60

6.5 Printing of Assembled Unit Dosages…… 61

6.6 Dissolution Tests……... 64

6.6.1 Dissolution Test of Assembled Unit Dosages……. 64

6.6.2 Dissolution Test of Drug Solutions……. 69

6.7 Experimental Results…… 69

6.7.1 Images of Freeze Dried Film, Cast and Assembled Unit Dosage…... 69

6.7.2 Reproducibility of Release Profiles…… 69

6.7.3 Analysis of Drug Release Profiles…….. 71

6.7.4 Drug Release Mechanism……... 72

6.8 Conclusions……... 75

TABLE OF CONTENTS
(Continued)

Chapter	**Page**
7 CONCLUDING REMARKS……...	76
7.1 Summary……...	76
7.2 Future Studies…….....	78
APPENDIX A MINIMIZATION OF VARIATION IN DROP POTENTIAL…..	80
APPENDIX B ELECTRIC FORCE DEFORMATION OF PENDANT DROP…	82
APPENDIX C PARAMETERS FOR TRIANGULAR PULSE…….	84
APPENDIX D FORMATION OF CAST AND MICROPOROUS SUBSTRATE	86
APPENDIX E MEASUREMENT OF FLUID DIELECTRIC PROPERTIES…..	88
APPENDIX F THERMO-OPRTICAL MEASUREMENTS.....	92
APPENDIX G CHARGE RELAXATION TIME AND FLUID BEHAVIOR…..	96
APPENDIX H CRITICAL PULSE AND RESONANCE TIME……...	97
REFERENCES…….	98

LIST OF TABLES

Table		Page
2.1	Drop on Demand Inkjet and Technology Companies (Le 1998)……	11
2.2	Applications of Inkjet Printing (Le 1998)……...	15
2.3	Inkjet Fluids (Kipphan 2001)……..	17
3.1	Material Properties……..	25
3.2	Dimensionless and Characteristic Parameters…….	26
5.1	Parameters for Low-Viscosity fluids……...	44
5.2	Geometrical Parameters……..	55
5.3	Ohnesorge Number and Electrical Impulse for Operating Regime……	56
6.1	Reproducibility of The Release Profiles of Drugs in Porous Film…….	70
6.2	Reproducibility of The Release Profiles of Drugs Solutions……..	70
6.3	Mechanisms for Drug Release From Polymeric Matrix…….	72
6.4	Determined Parameters for Drug Release from Freeze Dried Polymeric Matrix…….	73
6.5	Determined Parameters for Drug Release from Solutions……..	73
B.1	Pulse Forcing Functions for Different Intervals within the Pulse……...	83
D.1	Film Configurations……	87

LIST OF FIGURES

Figure		Page
1.1	Concept of small-scale manufacturing of personalized unit dosages (Rex Reklaitis, Purdue University).....	2
2.1	Basic methods of drop formation (a) dripping(b) jet break up (c) liquid bridge breakup (c) EHD jetting (Basaran 2002)……...	6
2.2	Classification of non-impact printing (Kipphan 2001)…….....	8
2.3	Inkjet technologies map (Le 1998)…….....	9
2.4	Operation principle of a continuous inkjet print head…….	10
2.5	Piezoelectric inkjet printing ……	12
2.6	Thermal inkjet…….	13
2.7	Acoustic Inkjet drop ejection process and dependence of drop size on acoustic frequency (Hadimioglu, Elrod et al. 2001)……..	14
3.1	Experimental setup for electrodeless EHD DOD printing……..	20
3.2	Electrodeless EHD drop deposition steps……...	21
4.1	PEG 200: (a) phase diagram "peak voltage (U_p) - pulse length (t_p)":(1) drop relaxes back, (2) single sessile drop, (3) multiple drops; H=1mm, v_i= 0.1 μL, R_{OD}=0.38mm……	29
4.2	Drop evolution: U_p=7kV, t_p=3ms; v_i=0.1μL, H=1.5mm, R_{OD}=0.38mm	30
4.3	Effect of conductivity; v_i=0.2μL, H=1.2mm, R_{OD}=0.38mm……...	31
4.4	Effect of Ohnesorge Number; v_i=0.2μL, H=1.2mm, R_{OD}=0.38mm…..	32
4.5	(a) 0.1uL drops of PEG200 with 2(w/w)% fenofibrate & dye, 1mm center-to-center separation; (b). 0.1μL drops of PEG200 with dye, 1.5mm center-to-center separation (c). 0.2μL drops of PEG3350 with 20 (w/w)% aceclofenac printed at ~70^{o}C, 3mm center-to-center separation…….	33

LIST OF FIGURES
(Continued)

Figure		Page
4.6	20 (w/w)% Ibuprofen solution in PEG400 deposited on (a) 80%-porous HPMC film; drop 0.2μL. (b) HPC film; drops with volumes: (1) 2μL, (2) 1μL, (3) 0.5μL, (4) 0.2μL, (5) 0.1μL……..	34
5.1	Model of a pendant drop as a harmonic oscillator …….....	36
5.2	(a) Schematics of the displacement of the pendant (b) high speed image of deformation of DI-water pendant drop into a hemispheroid by electric forces…….....	39
5.3	High speed images of oscillations of DI-water drop ……..	42
5.4	DI-water oscillations: fitting ($\Gamma \sim 80$, $\Omega \sim 3.3$) and experiment ……	42
5.5	High speed images of the motion of PEG 400 drop ……...	43
5.6	PEG 400 aperiodic motion: fitting ($\Gamma \sim 11.5$, $\Omega \sim 3.3$) and experiment.	43
5.7	Periodic displacement of pendant drop to touch dielectric film (substrate) placed on the ground electrode (DI-water at B_e=0.8)……	45
5.8	Critical lines for drops of relatively low viscosity fluids. Symbols show experimental data; solid lines represent values computed with equation 5.2 and parameters listed in Table 5.1…….	46
5.9	Critical line computed using equation 5.9. Symbols represent experimental data……	48
5.10	Liquid bridge stability study (a) pendant drop (b) liquid bridge schematics……	49
5.11	Drop evolution into a stable liquid bridge; PEG 400 on 80um HPC film, U_p=7kV, t_p=5ms; v_i=0.2μL, H=0.85mm, R_{OD}=0.38mm, h=80um……	50
5.12	Drop evolution into an unstable liquid bridge: PEG 200 on 80um HPC film, U_p=7kV, t_p=5ms; v_i=0.2μL, H=1.2mm, R_{OD}=0.38mm, h=80um……	50

LIST OF FIGURES
(Continued)

Figures		Page
5.15	Stability limits of PEG 200 bridges for K, B_g, and R_{OD}: 1) 0.7, 0.02, 0.38mm; 2) 0.8. 0.06, 0.55mm; 3) 0.6, 0.2, 1.1mm. Open and filled symbols indicate measurements by decreasing volume and increasing height. Curves show computations (Meseguer, Slobozhanin et al. 1995; Slobozhanin and Alexander 1998) for various K and B_g=0……..	51
5.16	Operating modes for various fluids listed in Table 3.1: A) drop relaxes back, B) single sessile drop formed, C) multiple sessile drops formed; α, H/R_{OD}, Δ/R_{OD}, ξ: (1) *fluids No. 1-13, Table 3.1*; 0.32, 3.16, 1.55, 0.74; (2) *fluid No 15, Table 3.1*: -0.095, 3.95, 2.83, 0.74; (3) *fluid No 16, Table 3.1*; 0.32, 3.95, 2.34, 0.74; *fluid No 14, Table 3.1*: (4) -0.095, 2.63, 1.51, 0.74; (5) 0.32, 3.16, 1.55, 0.74; (6) 0.22, 2.73, 1.33, 0.73; (7) 0.54, 3.27, 1.31, 0.73; (8) -0.22, 1.82, 0.95, 0.76. Solid lines show the critical line asymptotics…….....	54
6.1	A schematic cross-section view of an assembled unit dose……	58
6.2	Drug solutions…….	60
6.3	(a) Electrodeless DOD setup. (b) drop of 20(w/w)% Griseofulvin in PEG 400/SDS on 95%-porous HPMC film; U_p=7kV, t_p=5ms, H=1.5mm, R_{OD}=0.38mm, v_i=0.2μL……	62
6.4	Freeze dried 95% porous HPMC film of 500um film thickness. (b) Casted HPMC film of 60um thickness formed from a 5 (w/w)% solution. (c) 112 drops of 20(w/w)% griseofulvin in PEG400/SDS on 35mm x 20mm, freeze dried 95% porous HPMC of thickness 500um. (d) assembled unit dosage (5.12mg) of griseofulvin covered on top with 60um cast HPMC film……...	63
6.5	Water absorption and disintegration of an assembled unit dosage of Griseofulvin in an unstirred beaker containing 500ml DI-water……	64
6.6	Dissolution apparatus (Prof. Bozena Michniak-Kohn Lab, Rutgers University, New Jersey)…….....	65
6.7	Calibration curve for (a) Ibuprofen in PEG 400. (b) Griseofulvin in PEG 400/SDS…….....	66

LIST OF FIGURES
(Continued)

Figures		Page
6.8	Dissolution profiles of drugs in 95% porous HPMC film (a) Ibuprofen (b) Griseofulvin.....	67
6.9	Dissolution profiles of drugs solutions (a) Ibuprofen (b) Griseofulvin...	68
6.10	Comparison of dissolution profiles of ibuprofen from porous film and Solution.....	74
6.11	Comparison of dissolution profiles of griseofulvin from porous film and solution.....	75
A.1	Nozzle configuration and minimization of variation in drop potential...	80
B.1	Triangular pulse applied to the pendant drop (for $t_p=t_c$).....	82
C.1	Deformation of pendant drop by electric force.....	84
D.1	Labconco Benchtop Freeze Drier.....	86
E.1	Novocontrol Broadband Dielectric Spectrometer (BDS).....	88
E.2	Broadband Dielectric Spectrometer Schematics.....	89
E.3	Conductivity spectrum of different fluids.....	90
E.4	Spectrum of real part of dielectric permittivity for different fluids.....	90
F.1	Experimental Setup for thermo-optical analysis.....	92
F.2	DSC Thermograms at 5^{o}C/min showing the melting temperature of different materials.....	93
F.3	DSC Thermograms of 7.2mg Ibuprofen powder and 36mg solution of 20 (w/w)% Ibuprofen solution in PEG 400 at 5^{o}C/min.....	93
F.4	DSC Thermograms of 7.5mg Ibuprofen powder and 37.5mg solution of 20 (w/w)% griseofulvin solution in PEG 400 at 5^{o}C/min.....	94
F.5	DSC Thermograms of 1.5mg HPMC powder and 1.5mg porous freeze dried HPMC film at 5^{o}C/min.....	94

LIST OF FIGURES
(Continued)

Figures		Page
G.1	Charge relaxation time compared to pulse length for fluids with Oh≤1.	96
H.1	Comparison of resonance time and pulse length for fluids with Oh≤1...	97

LIST OF SYMBOLS

Symbol	Definition
ρ_f	Density of fluid
γ_f	Fluid surface tension
η_f	Fluid dynamic viscosity
σ_f	Fluid conductivity
ε_o	Permittivity of space
ε_f	Fluid dielectric constant
ε_r	Film dielectric constant
v_i	Infused volume
v_s	Sessile volume
V_p	Pendant drop volume
R_{OD}	Nozzle outer radius
H	Gap between nozzle exit and ground electrode
U_p	Peak value of alternating voltage
U_e	Instant voltage
U_f	Final voltage across the drop
t_p	Pulse length of alternating voltage
B_e	Electric Bond number
I_p	Electrical impulse
B_g	Gravitational Bond number

e	Hemispheroid eccentricity
Oh	Ohnesorge number
Δ	Drop displacement required for touching the film
W_e	Weber number
h	Film thickness
R_f	Liquid bridge radius on the film
K	Inequality between nozzle and bridge radius on film
t_c	Capillary time
t_e	Charge relaxation time
t_v	Viscous time
v	Fluid velocity
ξ	Nozzle inner-to-outer radius ratio
C_w	Nozzle capacitance
C_g	Capacitance between the lower electrode and the drop
Γ	Damping parameter
Ω	Resonance parameter
ϕ	Film porosity
α	Drop size parameter
t	Time
x	Displacement
τ	Dimensionless time
$\overline{x}$	Dimensionless displacement
R_c	Foci radius of Hemispheroid

R_{ID}	Nozzle internal diameter
θ	Drop tip angle
L_{Nozzle}	Nozzle length across the electrode
T_m	Melting Temperature
g	Gravitational Acceleration
L	Major Radius of Hemispheroid
σ	Electrical Conductivity
f	Frequency
ε''	Imaginary Part of Complex Permittivity

LIST OF ACRONYMS

API	Active pharmaceutical ingredient
BCS	Biopharmaceutics Classification System
DI-Water	Deionized water
DOD	Drop on demand
DSC	Differential Scanning Calorimetry
EHD	Electro hydrodynamics
FDA	Food and drug administration
HPC	Hydroxypropyl cellulose
HPMC	Hydroxypropyl methylcellulose
KCl	Potassium chloride
PEG	Polyethylene glycol
SDS	Sodium dodecyl sulfate
USP	United States Pharmacopeia

CHAPTER 1

INTRODUCTION

1.1 Motivation

In medicine, one size does not fit all: Studies over the past two decades show that a substantial portion of drug response variability is genetically determined (Hood, Heath et al. 2004; Katsanis, Javitt et al. 2008). Hence, a drug that works for one individual may not work for another or may even cause adverse effects. These observations have given rise to the concept of personalized therapy whose ultimate goal is to develop medicinal agents designed for each niche of the population and/or individual patients according to the vagaries and variance of their genes. With advances in the sequencing of the human genome, new tools for successful transition into personalized medicine are being acquired. Genome mapping could help build biomarkers for targeted drug administration and consequently increase efficiency in disease treatment.

Under a personalized medicine scheme, drug prescribing and dosing should be carefully tailored to a patient's genetic background (Jørgensen 2007). This method would enable physicians to use genomic testing to choose the best treatment for a patient with less guesswork. There is already evidence that use of companion diagnostics to exclude patients based on genomic analysis would improve clinical trial data of new drugs for targeted patient populations and boost the odds of Food and Drug Administration (FDA) approval. This will remedy the setback associated with failure of a drug to acquire regulatory approval. However, innovative small-scale pharmaceutical technologies are required for manufacturing of tailored therapeutics since the existing technologies have

evolved around processes for mass production. The ideal technology should be precise, simple, efficient and cost effective.

1.2 Challenges

Noncontact drop-on-demand (DOD) principle (i.e., drops are formed only as required) commonly used in graphic arts printing, electronics, and micromachining (Eggers 1997; Kipphan 2001; Basaran 2002) appears to be a particular promising approach for small scale manufacturing of personalized treatments (illustrated in Figure 1.1). It would provide the ability to form an individual dosage unit by printing a vast array of predefined amounts of therapeutics arranged in a specific pattern on a carrier substrate to achieve a desired drug release profile.

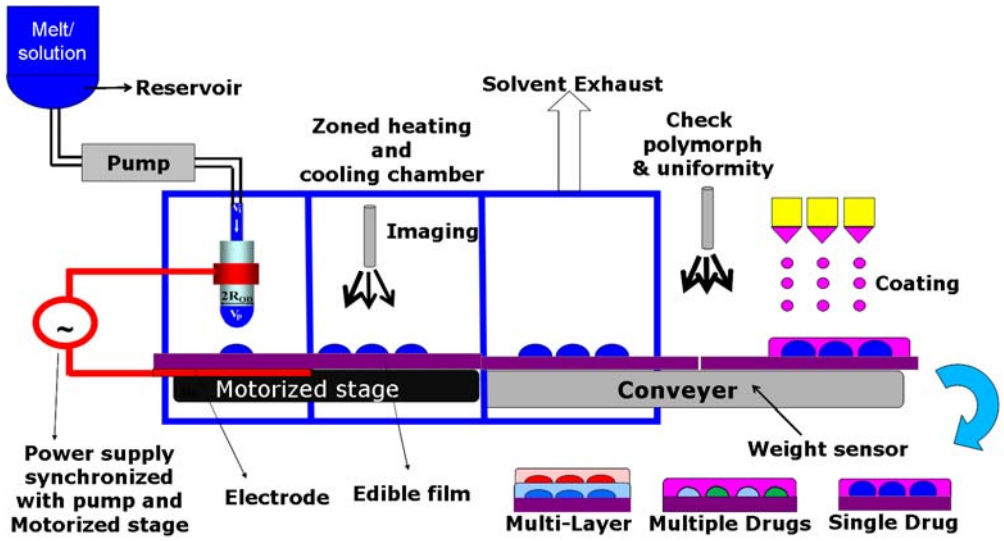

Figure 1.1 Concept of small-scale manufacturing of personalized unit dosages (Rex Reklaitis, Purdue University).

However, current DOD methods developed for printing chemically and thermally stable, low-viscosity inks are of limited use for pharmaceuticals due to fundamentally different functional requirements:

- A pharmaceutical product is a unique, delicate formulation composed of active therapeutic ingredients and inactive substances to ensure a desired absorption rate in the human body and stability over long-term storage (Allen, Popovich et al. 2004)
- Pharmaceutical products have to be protected against chemical changes, excessive heating, and high shear stress during drop deposition.
- Formulations with widely different properties should be printed with high volume accuracy.

The development of DOD inkjet printing systems thus far has focused on high-speed throughput and delivery of drops in the nano- and pico-liter range (Le 1998; Kipphan 2001; Yogi, Kawakami et al. 2001; Roth, Xu et al. 2004; Schena 2005). Also, DOD inkjet technology is typically restricted to liquids having viscosities of few centipoises (cp) and is generally believed to be unfeasible if the liquid viscosity exceeds 20-30 cp. Therefore, existing DOD methods such as thermal, piezoelectric, electrostatic, etc. (Le 1998; Kipphan 2001; Yogi, Kawakami et al. 2001; Basaran 2002; Roth, Xu et al. 2004; Schena 2005) do not meet the functional requirements to print pharmaceutical products.

1.3 Research Objectives and Overview

This dissertation is addressing limitations of current DOD techniques in handling pharmaceutical product for personalized medicine and distributed manufacturing of dosages through precise and controllable deposition of drops containing active pharmaceutical ingredients onto/into edible substrates.

This dissertation seeks to:

- Carry out fundamental study and develop an electric field based method for DOD printing of pharmaceutical products which addresses the critical limitations facing current DOD methods.
- Determine operating regimes for precise deposition of drops.
- Study operating regimes and understand mechanisms governing the formation, deposition and layering of drops.
- Develop a dynamic model for the field driven evolution of a pendant drop and scaling analysis for prediction of drop deposition regimes.
- Develop method of printing unit dosages and conduct dissolution studies on assembled unit dosage.

The first chapter outlines the motivation, challenges and research objectives; the second summarizes the literature survey of mechanisms and dynamics of drop formation and background of various technological applications using drop formation with emphasis on DOD printing. The limitations of extending these technologies to meet the needs of cost effective small-scale manufacturing of personalized treatments are highlighted. The third chapter presents a proposed method of DOD printing that overcomes the limitations of currently available DOD methods. In this chapter, the details of the method and experiments on fluids with diverse physical properties are described. The fourth presents results and operating regimes and includes a summary of the critical milestones achieved. The fifth chapter discusses a pendant drop model and scaling analysis for drop dynamics for prediction of operating regimes and providing critical design guidelines. Chapter 6 demonstrates the use of the proposed method in the preparation of personalized unit dosages to meet reproducibility requirements and presents characteristics of the drug release from a porous polymer film.

CHAPTER 2

BACKGROUND AND LITERATURE REVIEW

2.1 Drop Formation

Drop formation is a surface flow phenomenon whose driving force is the surface tension; this driving force usually favors minimum surface area leading preferably to spherical drop configurations (Eggers 1997; Basaran 2002). Drops can be formed by dripping, jet breakup or liquid bridge breakup. When a liquid is released very slowly from a nozzle, dripping occurs if the gravitational force exceeds the capillary force; the liquid then begins to fall and drops eventually separate (Figure 2.1(a)). If the flow rate is large, a liquid jet emanating from the nozzle can become unstable and breaks up into liquid droplets (Figure 2.1(b)).

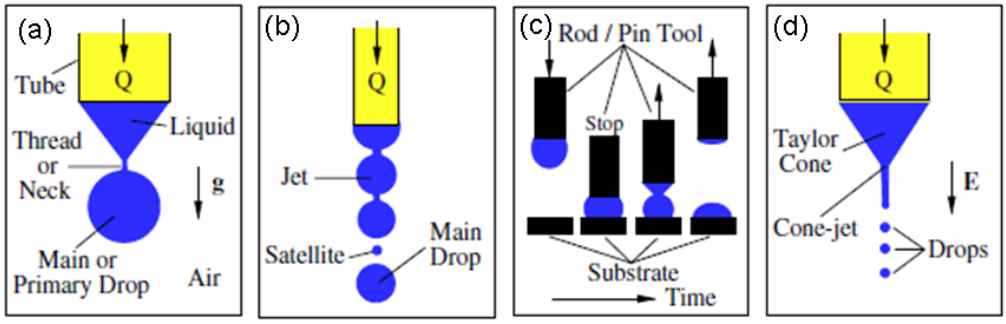

Figure 2.1 Basic methods of Drop Formation (a) dripping (b) jet break up (c) liquid bridge breakup (d) EHD jetting, (Basaran 2002).

Jet breakup has been studied for years; Plateau observed that jets break up in segments of equal length such that a spherical drop formed from these segments gives minimum surface energy if the drop is formed from each segment (Lin and Reitz 1998). Consequently, Rayleigh showed that jet breakup is as a result of hydrodynamic instability

(Rayleigh 1878). Different drop size distributions are obtainable depending on the flow regimes (Lin and Reitz 1998). The third mode of drop formation is the liquid bridge configuration. A drop hanging on a disk under the action of capillary forces can form a liquid bridge with an opposite disk and breaks up to produce a drop (Figure 2.1(c)). Generally, the drop dynamics is governed by three non-dimensional numbers (Basaran 2002); the Weber number, W_e, that incorporates the Reynolds number of the flow; the Ohnesorge number, Oh, that shows the relative importance of viscous forces compared to inertia and capillary forces; and the gravitational Bond number, B_g that scales the contribution of the gravitational force. These parameters are designated as $W_e = \rho_f v R_{OD} / \gamma_f$, $Oh = \eta_f \Big/ \sqrt{\rho_f R_{OD} \gamma_f}$ and $B_g = \rho_f g R_{OD}^2 \Big/ \gamma_f$, where ρ_f, γ_f, η_f are the fluid density, surface tension, viscosity; R_{OD} is the nozzle outer radius and v is the fluid velocity. Dripping occurs, when W_e is not too large and B_g is not too small.

As the Weber number, W_e, increases, dripping transforms into jetting. Furthermore, the liquid bridge drop formation requires B_g to be sufficiently small, such that the gravity force does not dominate the capillary force. Dripping and jetting are affected by an electric field. If the fluid is conducting and $W_e << 1$ the regime known as electrohydrodynamic (EHD) jetting occurs. Thus a drop placed in an electric field, becomes polarized and the induced surface charges are pulled apart. A greater drop elongation is reached with increasing field strength; when the electric field strength is raised above a critical value, these shapes become unstable and a conical tip appears at the end of the drop, from which a tiny jet is ejected (Figure 2.1(d)). Taylor (1964) showed that a cone is a local equilibrium solution in which the surface tension and electric forces are balanced. The cone, which has a definite opening angle of 98.6°, is

known as Taylor's cone (Taylor 1964).

2.2 Applications

Many applications, such as inkjet printing, integrated circuit printing, automatic pipetting, fiber spinning, silicon chip technology, spraying, atomization and mixing, make use of one type of drop formation or the other. Furthermore, technologies in medicine and drug delivery are also utilizing some methods of drop formation in their operations, such as in DNA arraying, micro particle encapsulation and deposition of reagents on diagnostic strips (Eggers 1997; Le 1998; Basaran 2002; Schena 2005). The critical requirements in these operations are that the drop size should be controllable, the process should be fast, repeatable and the products to be defects free. These requirements appear to be satisfied in DOD printing where drops are formed and delivered only as required. Each DOD method is suitable in certain operations and capable of handling specific fluid properties and functional requirements.

2.3 Inkjet Printing

Inkjet is a non-impact dot-matrix printing technology in which droplets of ink are jetted from a small aperture directly to a specified position on a media to create an image. The mechanism by which a liquid stream breaks up into droplets was described by Rayleigh in 1878 (Rayleigh 1878). In 1951, Elmqvist of Seimens patented the first practical Rayleigh break-up ink-jet device (Elmqvist 1951). This invention led to the introduction of the Mingograph, one of the first commercial inkjet chart recorders for analog voltage signals.

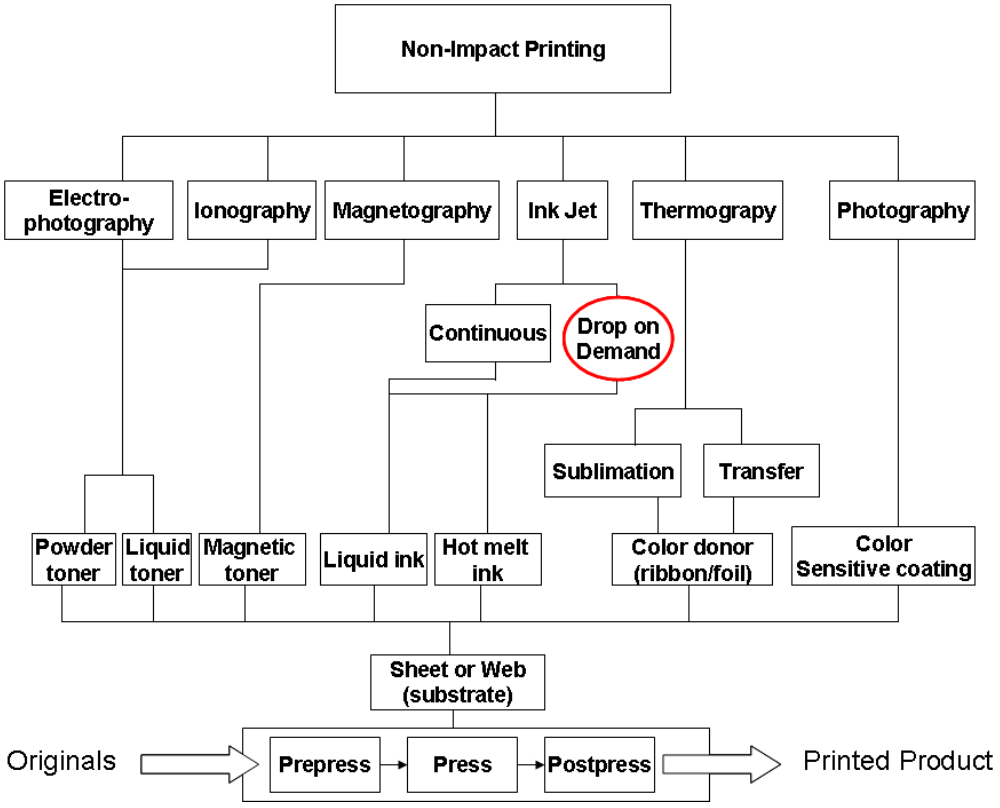

Figure 2.2 Classification of non – impact printing (Kipphan 2001).

As classified in the handbook for printing media (Kipphan 2001), inkjet is categorized into continuous and DOD methods, depending on mechanism type (Figure 2.2). Further classification based on the mode of operation, is shown on the inkjet technology map in Figure 2.3.

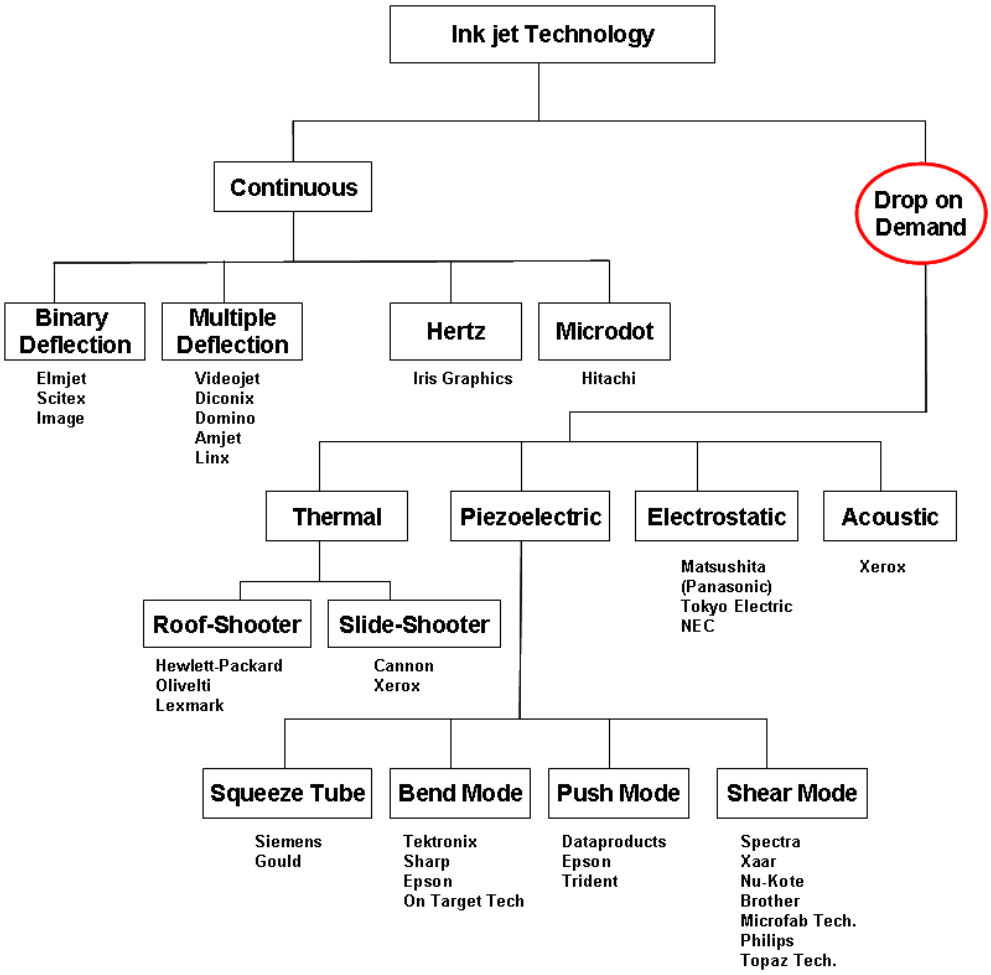

Figure 2.3 Inkjet technologies map (Le 1998).

2.3.1 Continuos Inkjet

Continuous inkjet generates a constant stream of droplets. Ink is pressured by an ink supply pump and flows from an ink reservoir to a nozzle. Ultrasonic vibration breaks a pressurized ink stream into small droplets as it leaves the nozzle (Figure 2.4). Droplets are ejected from the nozzle at a high speed and pass through the charging electrode tunnel and then between the deflection electrodes. The droplets are deflected depending on the amount of charge imparted onto them by the charging electrode.

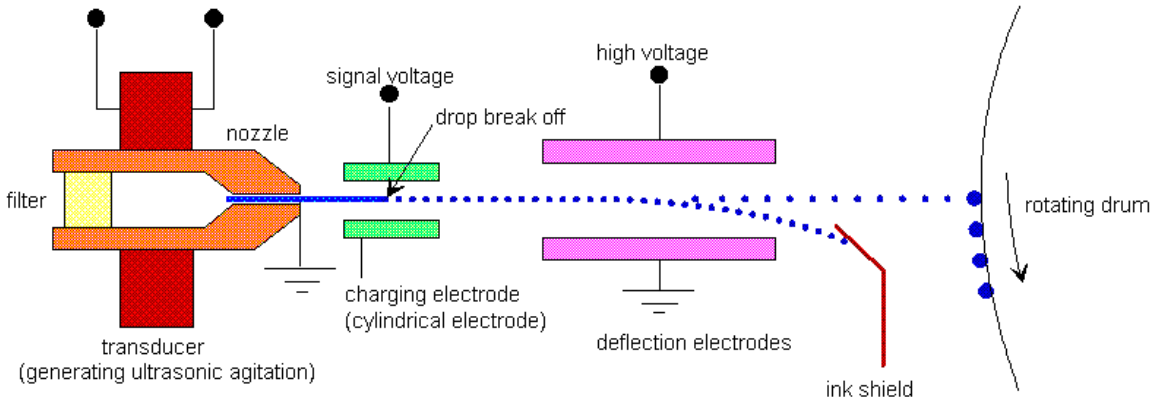

Figure 2.4 Operation principle of a continuous ink jet print head.

Source: Microsensor and actuator Technology Center, "A Micromachined Continuous Ink Jet Print Head for High Resolution printing," http://www-mat.ee.tu-berlin.de/

As a droplet leaves the deflection region, it continues to travel in a new direction until it passes out of the print head to the substrate. Drops that are not utilized for printing are then caught by the gutter and subsequently recycled back to the ink reservoir. Further classification of continuous inkjet includes binary deflection, multiple deflection, hertz and microdot.

2.3.2 Drop on Demand Inkjet

Zoltan, Kyser and Sears (Zoltan 1972; Kyser and Sears 1976) are among the pioneer inventors of the DOD inkjet systems. Their inventions were used in the Siemens PT-80 serial character printer (1977) and by Silonics (1978). In these printers, on the application of voltage pulses, ink drops are ejected by a pressure wave created by the mechanical motion of a piezoelectric crystal. Many of the DOD inkjet ideas and systems were invented, developed, and produced commercially in the 1970s and 1980s. Table 2.1 shows some major corporations manufacturing DOD printing systems.

Table 2.1 Drop on Demand Inkjet and Technology Companies (Le 1998)

Drop on Demand Type	**Technology Companies**
Piezoelectric	Siemens, Gould, Tektronix, Sharp Trident, Microfab, Philips
Thermal	Hewlett-Packard, Lexmark, Canon, Xerox
Electrostatics	NEC, Panasonic
Acoustic	Xerox

2.3.2.1 Piezoelectric. This type of inkjet printing employs the deformation of a piezo crystal under the influence of a tiny electrical charge (Magdassi 2009) at the back of the ink reservoir. In essence, whenever a dot is required, a current is applied to the piezo element which flexes, generating force to expel a droplet of ink out of the nozzle (Figure 2.5). The use of piezo technology in inkjet printing provides a better control over the shape and size of ink droplets. Tiny variation of the piezo crystal length allows for smaller droplet sizes. Compared to thermal inkjet printing, the major advantages of the piezo inkjet technology include increasing the print speed and eliminating heating and cooling ink steps between each cycle.

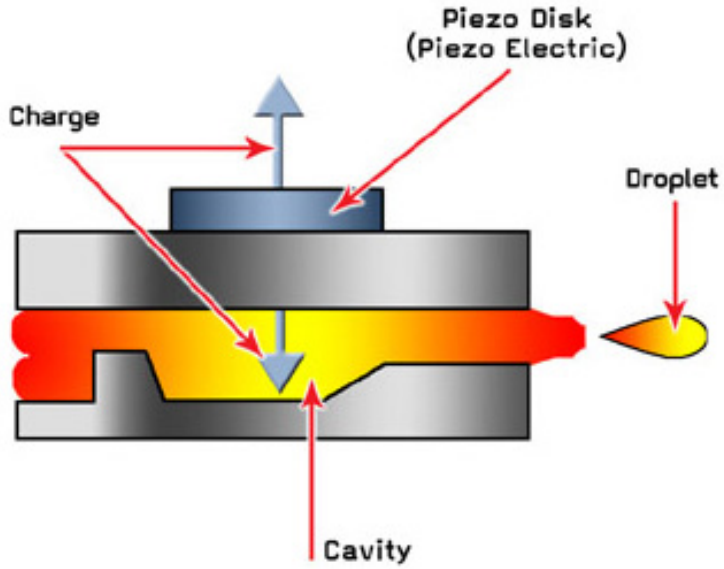

Figure 2.5 Piezoelectric inkjet printing.

Source: OKI's Guide to Piezoelectric Printing, http://www.askoki.co.uk/

Therefore, the ink design for piezoelectric printing can be based solely on the ink light absorption properties, whereas its ability to withstand high temperatures is critical for thermal printing

2.3.2.2 Thermal. Thermal DOD printing is also referred to as bubble jet printing. A bubble jet printer is one of the more useful and versatile inventions of the last decade. The active component of the printer is the 'head' through which liquid ink passes before striking the page.

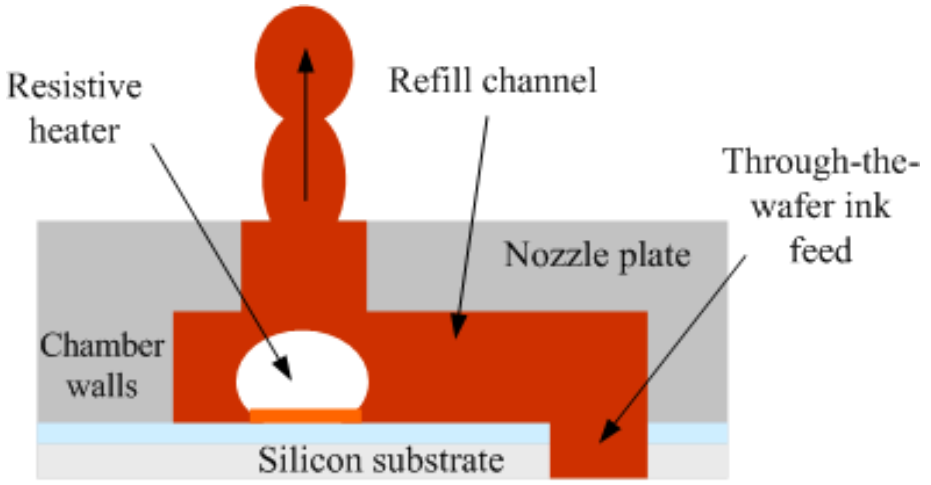

Figure 2.6 Thermal inkjet.

Source: The Inkjet Printhead for KODAK EASYSHARE AIO Printers
http://pluggedin.kodak.com/

When the heater is pulsed on, it heats the ink and causes a vapor bubble to expand. The bubble pushes ink out of the nozzle, where surface tension breaks it into droplets. After the heater is pulsed off, the bubble is vented to atmosphere and the chamber refills with ink. The chamber is now ready to be fired again (Figure. 2.6).

2.3.2.3 Electrostatic. Electrostatic inkjet are based on the Taylor cone phenomenon where jets protruding from an orifice induced by an electric field forms a meniscus called the Taylor cone and separates from the meniscus tip as fine droplets much smaller than the orifice diameter. Electrostatic inkjet has a greater advantage compared to piezoelectric inkjet and thermal inkjet in the ability to eject fine droplets and in the simplicity of the structure, also Electrostatic printers are far faster than other inkjet systems. Furthermore, electrohydrodynamic (EHD) atomization has recently attracted attention for printing micro/nano-sized patterns because (i) it can eject droplets that are

much smaller than the nozzle diameters, (ii) operate on versatile materials, including metal, organic, and even biological material, and can be used without thermal damage, and (iii) the nozzle structure is simpler than in other types of DOD systems. In EHD atomization, the charged liquid is ejected from the nozzle when the electrical force locally overcomes the liquid surface tension (Cloupeau and Prunet-Foch 1994; Lin and Reitz 1998).

2.3.1.4 Acoustics. In acoustic inkjet printing (AIP), an ultrasonic beam is focused on the free surface of the ink to eject discreet droplets of controlled diameter (Figure 2.7). Since the lateral dimensions of the acoustic beam determine the drop size, this "nozzleless" process enables generation of extremely small drops without sensitivity to small defects in the nozzle geometry (Hadimioglu, Elrod et al. 2001).

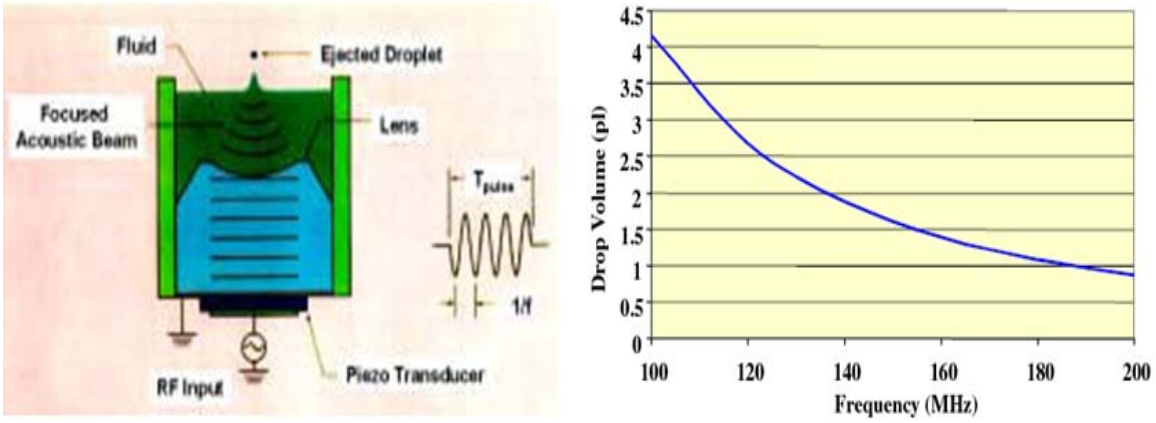

Figure 2.7 Acoustic Inkjet drop ejection process and dependence of drop size on acoustic frequency (Hadimioglu, Elrod et al. 2001).

Table 2.2 Applications of Inkjet Printing (Le 1998)

	Market/Application	**Key Player**
Current Markets and Applications	Small home, small office	Hewlett-Packard, Canon Epson
	Office network	Tektronix, Hewlett-Packard
	Graphic arts	Iris, Tektronix, Epson
	Industrial/postal marking	VideoJet, Marsh, Image, Willet
	Large format	ColorSpan, Encad, Hewlett Packard, Mimaki
3Emerging Markets and Applications	Home Photo	Hewlett-Packard, Epson, Canon
	Color copier	Hewlett-Packard, Canon
	Multifunction	Hewlett-Packard, Canon
	Digital color press Grand format	Scitex, ACS, Tektronix Idanit, Vutek, Nur, ColorSpan, Mutoh
	Textile	Canon, Seiren, Stork, Toxot
	Medical imaging	Iris, Sterling Diagnostics
	3-D printing	3D System, Z Corporation
	Computer-to-plate	Polychrome, Iris

2.4 Drop on Demand in Biomedical and Pharmaceutical Applications

Apart from inkjet dot matrix printing technology in which droplets are jetted from a small aperture directly to a specified position on a media to create an image (as in application listed in Table 2.2), application of printing in the biomedical and pharmaceutical fields is the area of active research and development. Advances in genomic microarray technology have evolved to include molecules other than DNA, such as proteins, ligands, cells, carbohydrates and tissues (Schena 2005). The use of micro arrays is moving rapidly from basic scientific studies into drug discovery and commercial diagnostic format across a number of industries. The current platform is predominantly based on the use of capillary pins and solid pins which can readily yield pico-liter size transfers of genomic reagents to solid-like substrates.

Both continuous and drop-on-demand (DOD) inkjet printing has been adapted for non contact dispensing in micro array systems. Though DOD technology has been successfully implemented for biomedical and tissue engineering applications (Roth, Xu et al. 2004; Xu, Jin et al. 2005), its use for pharmaceutical applications has been less explored. Basaran et al. (Yeo, Basaran et al. 2003) developed a novel microencapsulation technique which utilizes interfacial mass transfer between two mutually soluble liquids. A dual micro dispenser system based on the principle of piezoelectric printing was developed to produce reservoir-type PLGA poly(lactic-co-glycolic acid), microcapsules encapsulating an aqueous fluid. Trost et al. (Radulescu, Trost et al. 2005) used a JetLab printing system based on inkjet printing to produce PLGA biodegradable microspheres containing paclitaxel. Määttänen et al. also studied the use of inkjet for printing of drug on porous substrate for personalized dosing applications and Kane et al. investigated the

use of thermal inkjet for preparation of oral dosage forms (Meléndez, Kane et al. 2008; Sandler, Määttänen et al. 2011). In another study, Yan et al. (Yu, Yan et al. 2008) used piezoelectric DOD printing to evaluate the printability of microemulsions with different oils, ibuprofen was used as a model drug and soybean lectin as an emulsifier. They evaluated the effects of the rheological properties of emulsions to improve printability. As these methods are developed for low viscous chemically and thermally stable materials (Table 2.3), they are of little use in handling pharmaceutical formulations with wide range of diverse physical properties.

Table 2.3 Inkjet Fluids (Kipphan 2001)

Ink jet Printing	Ink/Fluid Description	Drying	Drop Volume pL	Dynamic Viscosity cP
1. Drop on Demand				
Thermal	Pigment in base, fluid, water	Evaporation/absorption	6 - 30	1 - 5
Piezoelectric	Conventional (dyes/ pigments in base fluid, oil or water	Evaporation/absorption	4 – 30	5 - 20
	Hot Melts (pigments in base fluid, oil or water	Hardening through cooling	20 – 30	10 - 30
	UV (pigments in liquid monomer, etc)	Radiation cross-linking	10 – 30	15 - 30
2. Continuous	(Dyes in solvent, water MEK, etc)	Evaporation/absorption	5 – 100	1 - 5

The proposed electrodeless field based DOD printing method is the first demonstration of an appropriate DOD system for small-scale manufacturing of personalized treatments that overcomes the critical challenges facing current DOD technologies.

Earliest experiments on field driven drops carried out by Taylor (Taylor 1969) where jets and drops of conducting and dielectric fluids were drawn from a conducting tube by electric forces showed that jets or drops could be obtained by applying continuous electric field across a fluid meniscus at the end of the tube. Sato et al. considered oscillations of hanging drops where a drop is connected to the top plate of a parallel plate capacitor and deformed by an applied electric field (Tsukada, Sato et al. 1987). In their case, the pendant drop was stretched from an initial equilibrium position to a final equilibrium position by an electric field. Consequently, finite amplitude axisymmetric oscillation of the pendant drop was generated by turning off the field. Their intent focused on studying the oscillation of pendant drops.

Recently, Barton et al. also studied DOD printing with a pulsed electrohydrodynamic jet using a conducting nozzle (Mishra, Barton et al. 2010). Drop deformation through electric field was also studied theoretically and experimentally by Basaran et al. where an electric field is used to stretch or deform a drop hanging on a tube or rod to generate drop oscillation (Harris and Basaran 1993; Basaran and DePaoli 1994; Wilkes and Basaran 1997). In the field-based methods of drop manipulation available in the literature, a contact between a fluid and electrodes renders them unattractive for use in pharmaceutical applications due to the adverse effects of electrochemical reactions at the fluid-electrode interface which could damage pharmaceutical formulations.

CHAPTER 3

MATERIALS AND METHOD

3.1 Overview of Electrodeless EHD DOD Printing

In the proposed method for DOD printing of personalized medicines, a fluid was infused into an electrically insulating nozzle (Figure. 3.1) to form a stable stationary pendant drop. The drop size was sufficiently small for the capillary force to dominate the gravitational force. The fluid served as a floating electrode capacitively coupled to external electrodes; therefore, there is no contact between fluid and electrode to eliminate undesirable electrochemical reaction at the fluid-electrode interface. A short electrical pulse of an alternating voltage was applied across the pendant drop to form a liquid bridge which broke up forming a single sessile drop on an edible substrate. A unit dosage was formed by printing an array of drops on an edible substrate which could be post-processed into a final dosage form. This method is appropriate for printing fluids with diverse physical properties in pharmaceutical, biomedical, and biotechnological applications.

3.2 Experimental Setup and Description

Figure 3.1 illustrates the concept of the proposed electrodeless EHD DOD method for gentle printing of pharmaceuticals. An electrically insulating nozzle was equipped with the energized electrode mounted externally. Drops were printed on an electrically insulating edible film placed on the ground electrode.

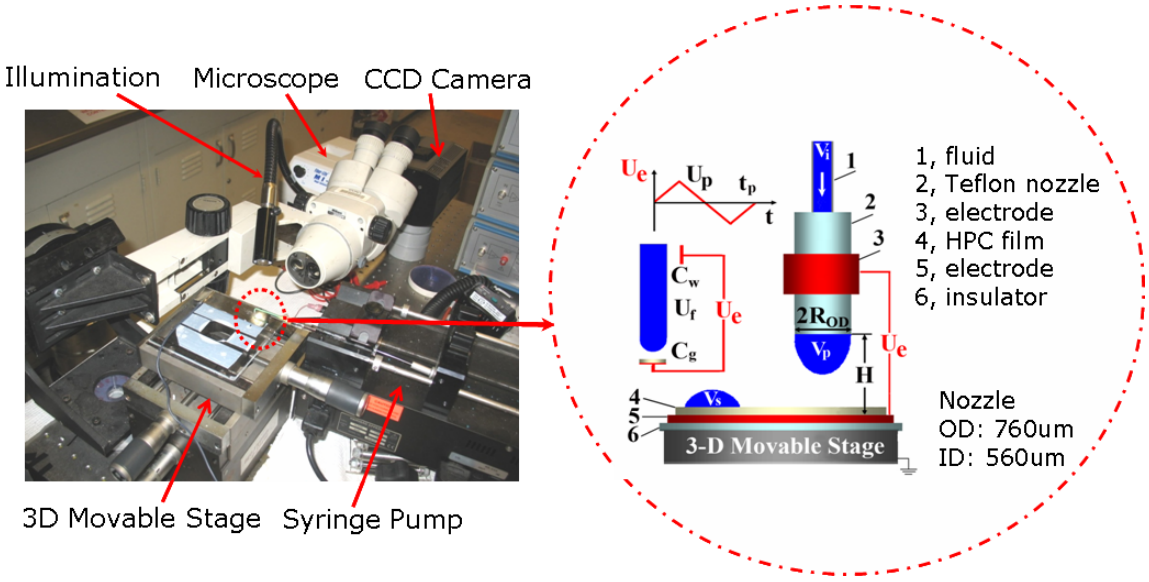

Figure 3.1 Experimental setup for electrodeless EHD DOD printing.

Three Teflon nozzles (Small Parts) with relatively large orifices were used to avoid clogging: 1) outer diameter (OD)=0.76mm and inner diameter (ID) =0.56 mm; 2) OD= 1.10mm and ID =0.80mm; and 3) OD=2.2mm and ID=1.68mm. A pulse was produced by a high-voltage amplifier (TREK Model 10/40) controlled by a programmable signal generator (Agilent 33220a). The lower electrode was mounted on the upper translation stage of a micromanipulator comprised of two independently adjustable stages having three degrees of translational freedom (Figure. 3.1). The nozzle was brought to the field of view of an initially vertical microscope (Nikon SMZ-2T). The microscope was then rotated by 90 degrees in the vertical plane to view the nozzle from the side and control the height of the nozzle exit (Figure. 3.1). A pendant drop was formed by infusing a fluid specimen into the nozzle with the flow rate and volume controlled by a programmable microsyringe pump (Harvard Apparatus PHD 2000). A heater pad (New Era Pump System) wrapped around the syringe and the nozzle and a

gentle-heat compressed-air blower (McMaster Carr) were used for printing a fluid with a melting point above room temperature. The drop evolution was recorded with a high-sensitivity CCD camera (a high-resolution CoolSNAP HQ2 or a high-speed Cascade 128+, both from Photometrics) mounted on the microscope.

Printing consists of three key steps, (Figure. 3.2). (1) A predefined fluid volume, v_i, was infused into a nozzle under a moderate pressure to form a pendant drop which was smaller than the critical size for dripping (Eggers 1997; Basaran 2002). The nozzle was positioned over a desired film location. (2) A voltage pulse was applied to the electrodes to stretch the pendant drop by an electric force until it touches the polymer film and forms a liquid bridge. During the pulse, the drop served as a floating electrode capacitively coupled to the external electrodes, (Figure.3.1).

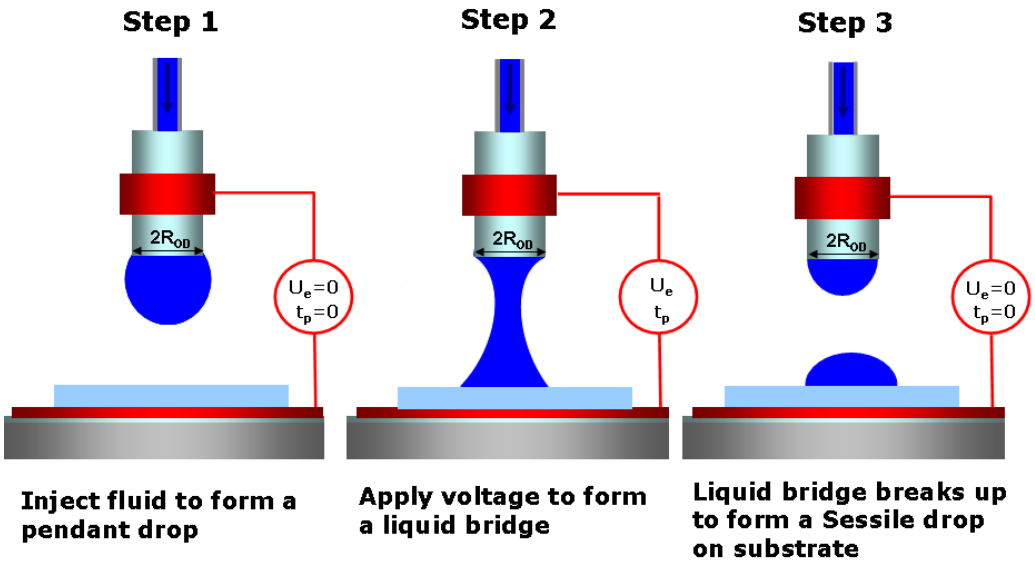

Figure 3.2 Electrodeless EHD drop deposition steps.

The pulse consists of two symmetric, phase-alternating short signals to suppress undesirable field effects on the fluid. (3) As the liquid bridge is intentionally formed in an unstable configuration, it broke up, creating two drops, one on the film and the other hanging from the nozzle. Once formed, the sessile drop spreads over the film and also imbibes into, if the film is porous. The field presence was not required during this period. It was found that producing *a single sessile drop per pulse* provided a precise control over its volume as it equals v_i for steady state operation regardless of the fluid properties and pulse characteristics in the operating regime. After a drop was printed, the stage was moved to a new location for a new drop to be printed.

3.3 Experimental Materials

3.3.1 Fluids

Experiments were conducted on de-ionized DI-Water, KCl (Sigma Aldrich) solution in DI-Water, solutions of DI-Water in glycerol (Sigma Aldrich) and Polyethylene Glycols (PEG) of different molecular weight (PEG 200, 400, 3350, 35000; Sigma-Aldrich, the number indicates the molecular weight), and drug solutions in PEG 400 and 3350. A 2mM solution of potassium chloride was used to increase conductivity over three orders of magnitude from that of water. Also, solutions of glycerol in water and PEG 35000 in water were prepared to increase the viscosity over three orders of magnitude while maintaining Newtonian properties.

3.3.2 Active Pharmaceutical Ingredients (API)

Cholesterol reducing medication fenofibrate with molecular formula, molecular mass and melting temperature: $C_{20}H_{21}ClO_4$, 360.83g/mol 80^oC (Sigma-Aldrich) and non-steroidal

anti-inflammatory medications aceclofenac, $C_{16}H_{13}Cl_2NO_4$, 354.18g/mol, 150^oC (samples provided by Prof. Lynne Taylor, Purdue University) and ibuprofen a non-steroidal anti-inflammatory drug, $C_{13}H_{18}O_2$, 206.29g/mol, 76^oC (BASF) were chosen as common drug models. Fluorescent dyes PF-38 Tropical Sunlight Orange, PF-13 Palm Leaf Green, and PF–14 Blue Tang (all from Risk Reactor) were used to color drug solutions.

3.3.3 Film Materials and Preparation

Hydroxypropyl cellulose (HPC, molecular weight 80000) and hydroxypropyl methylcellulose (HPMC, E15LV), edible biocompatible polymers were respectively used to form a non-porous and porous substrate on which the fluid and drug solutions were deposited. HPC was obtained from Sigma Aldrich while HPMC from Dow Chemical company. HPC non porous films were formed by preparing a 10(w/w)% aqueous solution and spreading it on a non-wettable plastic plate using a BYK-Gardner film-casting knife and then drying in a laboratory oven at 60^oC. A film thickness of about 80um was obtained after drying. 80%-porous hydroxypropyl methylcellulose (HPMC) films were prepared from an aqueous solution of 20(w/w)% HPMC. The solution was poured into a well formed with a rubber ring (McMaster Carr) placed on a glass slide coated with a 3M-release liner. The well covered with another glass slide, also coated with the 3M-liner, was kept in a freezer for 12 hrs and then transferred to a Labconco Freeze Drier for 18 hrs to sublimate water (APPENDIX D).

3.4 Material Properties and Dimensionless Parameters

The fluid density, viscosity, and surface tension were measured using graduated cylinders, a Cannon–Fenske tube viscometer, and a Surface Tension Apparatus (all from

Fisher Scientific). The melting point of materials was measured on a Mettler-Toledo hot stage FP82HT/84HT (APPENDIX F). The fluid dielectric constant and conductivity were measured on a Novocontrol broadband dielectric spectrometer BDS-80 (APPENDIX E). The fluid properties are listed in Table 3.1 & 3.2.

Contributions of capillary, gravity, electric, and viscous forces to drop evolution are represented (Eggers 1997; Basaran 2002) by the gravity Bond number $B_g = \rho_f g R_{OD}^2 / \gamma_f$, the pulse electric Bond number $B_e = \varepsilon_0 U_p^2 R_{OD} / 2\gamma_f H^2$, and the Ohnesorge number $Oh = \eta_f / \sqrt{\rho_f R_{OD} \gamma_f}$, where ρ_f, γ_f, η_f are the fluid density, surface tension, viscosity; $2R_{OD}$ is the nozzle outer diameter, H is the separation between the electrodes, and U_p is the peak voltage (Figure. 3.1). These characteristics in Table 3.2 are calculated for a typical experimental regime $R_{OD} = 0.38$mm, H=1.2mm and U_p=7kV.

Table 3.1 Material Properties

No	Sample	Density (g/cm^3)	Viscosity (cP)	Surface Tension (dyn/cm)	Conductivity ($\mu S/cm$)	Dielectric Constant
1	DI-Water at 18°C	1.0	1.0	72	0.8	78
2	DI-Water with 2 mM of KCL at 18°C	1.0	1.0	72	290	78
3	Glycerol with 60 (w/w) % of DI-Water at 18°C	1.1	4.0	68	4.5	69
4	Glycerol with 35 (w/w) % of DI-Water at 18°C	1.2	15	66	1.7	64
5	PEG 200 at 18°C	1.1	76	44	3.0	20
6	PEG 400 at 18°C	1.1	142	46	0.3	14
7	Glycerol with 6 (w/w) % of DI-Water at 18°C	1.2	320	63	0.08	48
8	Glycerol with 4 (w/w) % of DI-Water at 18°C	1.3	450	63	0.05	46
9	Glycerol with 3 (w/w) % of DI-Water at 18°C	1.3	694	63	0.05	46
10	Glycerol with 2 (w/w) % of DI-Water at 18°C	1.3	1045	63	0.02	44
11	30 (w/w)% PEG 35000 in of DI-water at 18°C	1.1	1212	37	64	63
12	35 (w/w)% PEG 35000 in of DI-Water at 18°C	1.1	1911	36	62	60
13	40 (w/w)% PEG 35000 in DI-Water at 18°C	1.1	3112	35	61	58
14	PEG 400 with 20 (w/w)% Ibuprofen at 21°C	1.1	136	42	0.2	16
15	PEG 200 with 2 (w/w)% fenofibrate at 21°C	1.1	62	39	3.0	20
16	PEG 3350 with 20 (w/w)% aceclofenac at 70°C	1.2	234	41	0.2	9

Table 3.2 Dimensionless and Characteristic Parameters

No	Sample	Capillary Time (ms)	Gravity Bond Number	Ohnesorge Number	Electric Bond No.	Charge Relaxation Time (μs)
1	DI-Water at 18°C	0.8	0.02	0.006	0.8	8.6
2	DI-Water with 2 mM of KCL at 18°C	0.8	0.02	0.006	0.8	0.02
3	Glycerol with 60 (w/w) % of DI-Water at 18°C	0.9	0.02	0.02	0.8	1.3
4	Glycerol with 35 (w/w) % of DI-Water at 18°C	1.0	0.03	0.09	0.8	3.4
5	PEG 200 at 18°C	1.2	0.04	0.55	1.3	0.6
6	PEG 400 at 18°C	1.2	0.04	1.02	1.2	4.2
7	Glycerol with 6 (w/w) % of DI-Water at 18°C	1.0	0.03	1.85	0.9	53
8	Glycerol with 4 (w/w) % of DI-Water at 18°C	1.0	0.03	2.6	0.9	81
9	Glycerol with 3 (w/w) % of DI-Water at 18°C	1.0	0.03	4.0	0.9	102
10	Glycerol with 2 (w/w) % of DI-water at 18°C	1.0	0.03	6.02	0.9	195
11	30 (w/w)% PEG 35000 in of DI-Water at 18°C	1.3	0.04	10	1.6	0.09
12	35 (w/w)% PEG 35000 in of DI-water at 18°C	1.3	0.04	15.8	1.6	0.09
13	40 (w/w)% PEG 35000 in DI-Water at 18°C	1.3	0.04	26	1.6	0.08
14	PEG 400 with 20 (w/w)% Ibuprofen at 21°C	1.2	0.04	1.0	1.4	7.1

Table 3.2 Dimensionless and Characteristic Parameters (Continued)

No	Sample	Capillary Time (ms)	Gravity Bond Number	Ohnesorge Number	Electric Bond No.	Charge Relaxation Time (μs)
15	PEG 200 with 2 (w/w)% fenofibrate at 21°C	1.2	0.04	0.48	1.5	0.6
16	PEG 3350 with 20 (w/w)% aceclofenac at 70°C	1.3	0.04	1.7	1.4	4.0

CHAPTER 4

EXPERIMENTAL RESULTS

4.1 Regimes of Drop Deposition

Despite the considerable literature (Fernández de la Mora 2006) on EHD drop formation through stationary dripping and jetting, pulsed EHD drop generation has received attention only recently (Chen, Saville et al. 2006; Lee, Cho et al. 2006; Choi, Park et al. 2008; Kim, Oh et al. 2008; Li and Zhang 2009; Stachewicz, Yurteri et al. 2009). However, these studies do not provide the understanding of how to find (i) the pulsing length, t_p, and peak voltage, U_p, to stretch a drop without excessive exposure to a field and (ii) the drop volume to form an unstable liquid bridge. To address these questions and prove the method versatility, experiments were conducted on fluids listed in Table 3.1. Drops were deposited on non-porous HPC films (h= 80μm). The drop size ranged from 0.1 to 2μL.

Three modes of drop evolution were observed for all fluids, depending on the pulse length and voltage. In all cases, the contact line of a drop practically remains pinned to the nozzle outer edge. Figure 4.1 illustrates the diagram of operating modes for PEG 200.

4.1.1 Drop Relaxes Back

Under operating conditions in region 1 (Figure 4.1), the pendant drop undergoes shape oscillations but capillary forces managed to prevent the formation of a liquid bridge. As the pulse is weak, a drop elongates, but does not touch the film and relaxes back to the initial state, oscillatory or aperiodically depending on the fluid viscosity.

The pendant drop does not touch the substrate and, therefore, a sessile drop was not formed.

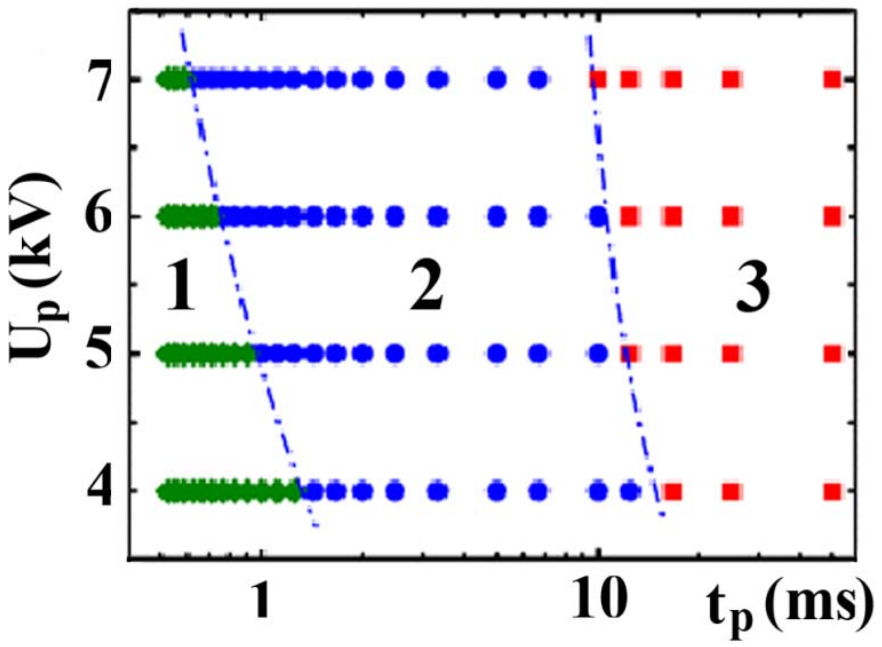

Figure 4.1 PEG 200: (a) Phase diagram "peak voltage (U_p) - pulse length (t_p)":(1) drop relaxes back, (2) single sessile drop, (3) multiple drops; H=1mm, v_i= 0.1μL, ROD=0.38mm.

4.1.2 Single Sessile Drop

The second mode (region 2, Figure. 4.1) is attributed to pulses creating a single sessile drop. In this case, the volume of a sessile drop produced after N successive depositions is $v_{s,N} = \left(1-\beta^N\right) v_i$, where β is part of the liquid bridge retreating back; $v_{s,N}$ rapidly approaches the value v_i with increasing N as β ~0.5-0.6. Contrary to contemporary techniques (Chen, Saville et al. 2006; Lee, Cho et al. 2006; Kim, Oh et al. 2008; Li and Zhang 2009; Stachewicz, Yurteri et al. 2009), the volume of sessile drops formed in this

regime is insensitive to the pulse parameters and the fluid properties. Taking the pulse parameters in the vicinity of the critical line for a transition between first and second modes (Figure 4.1 and Figure 4.2), would minimize the fluid exposure to a field and increase printing speed (field is off during liquid bridge break up). This region is the operating regime for precise drop deposition using electrodeless DOD system.

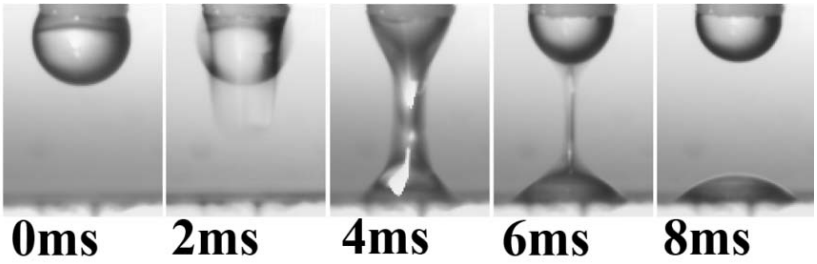

Figure 4.2 Drop evolution: Up=7kV, t_p=3ms; v_i=0.1μL, H=1.5mm, R_{OD}=0.38mm.

4.1.3 Multiple Sessile Drops

This region corresponds to sufficiently long pulses (region 3, Figure 4.1). A drop is stretched to form an unstable liquid bridge that broke up to produce a sessile drop and a pendant drop, while a field was still on. The process then repeats itself several times, creating several sessile drops. This regime is inappropriate for controlled deposition as the sessile drops have different volumes.

4.2 Critical Parameters

The phase boundary which denotes the cross-over from a drop relaxing back to forming a single sessile drop is the critical liquid bridge line. It was observed that the critical liquid bridge line tends to decrease with increasing the pulse length. Data on DI-Water modified

by adding 2mM potassium chloride to increase the ionic strength and conductivity showed that three orders of magnitude change in conductivity did not affect the critical liquid bridge line (Figure 4.3).

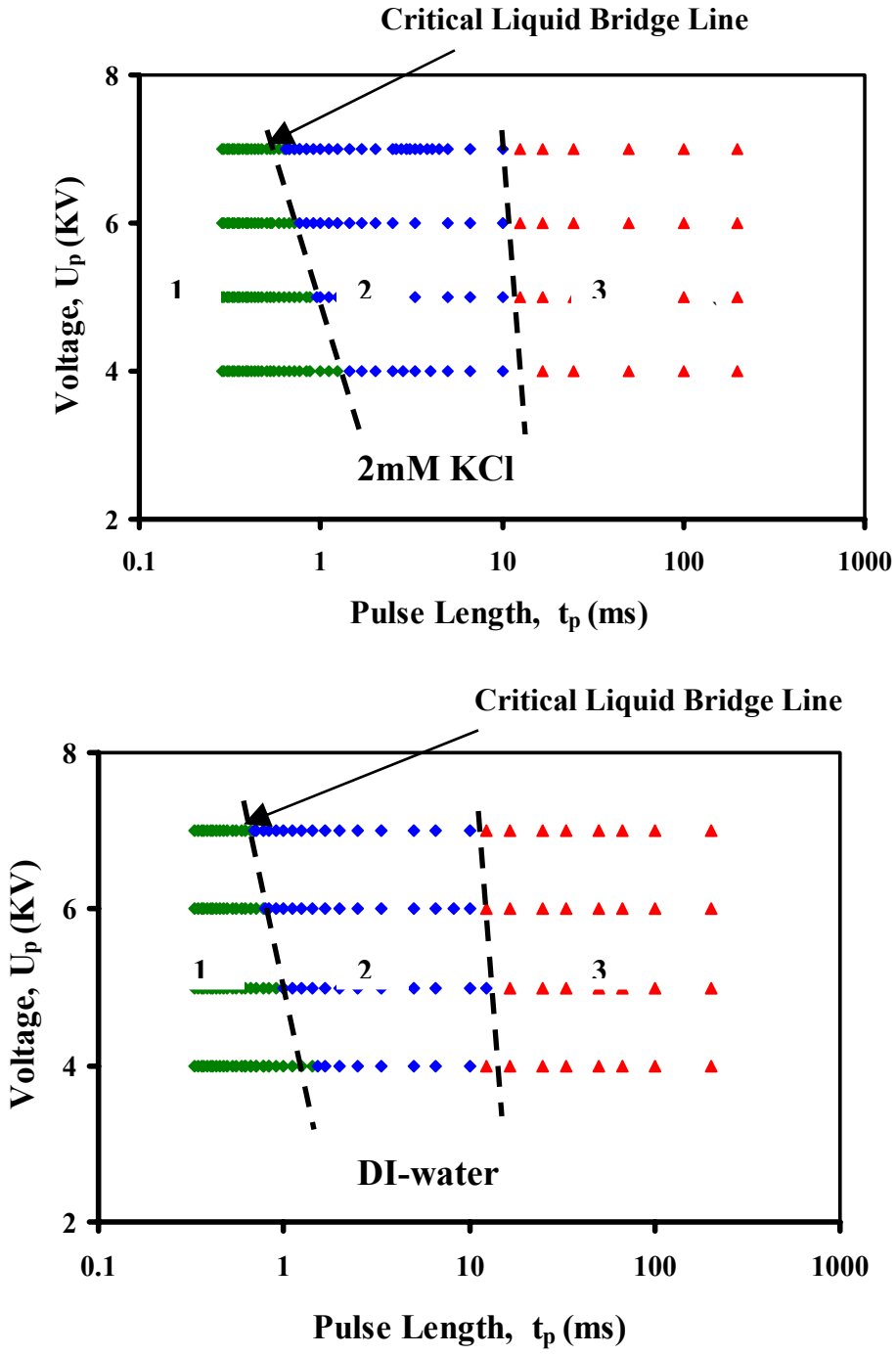

Figure 4.3 Effect of conductivity; v_i=0.2μL, H=1.2mm, R_{OD}=0.38mm.

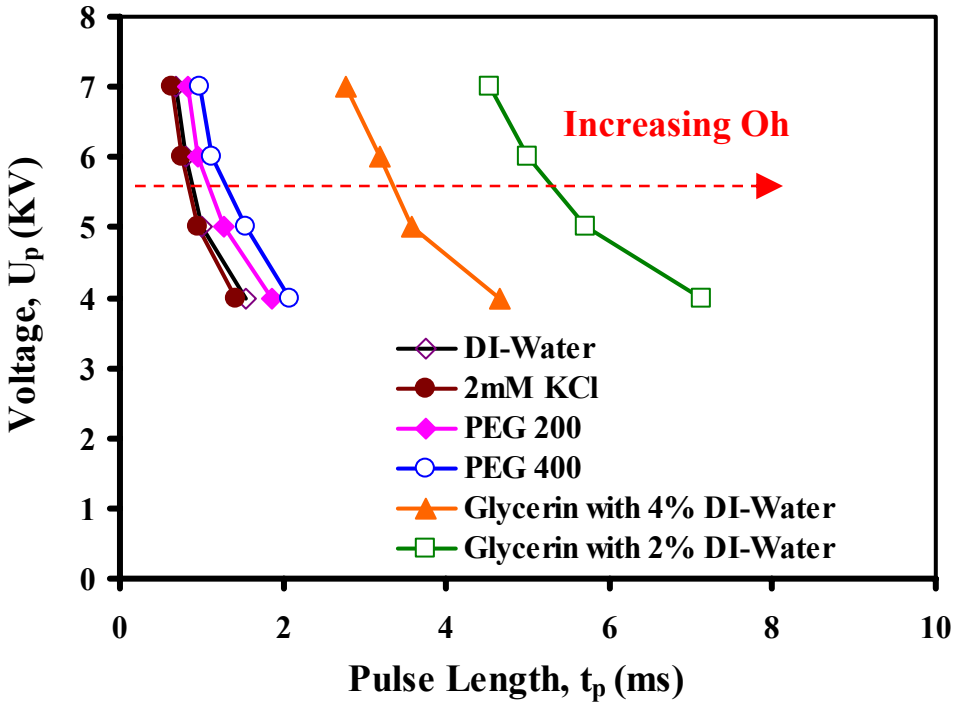

Figure 4.4 Effect of the Ohnesorge number; v_i=0.2μL, H=1.2mm, R_{OD}=0.38mm.

The critical liquid bridge line shifted to the right with increasing Ohnesorge number. This highlights the importance of the fluid viscosity in printing (Figure 4.4). The effects of the Ohnesorge number on the characteristics of a printing regime to form a single sessile mode per pulse (region 2, Figure 4.1) will be analyzed in more detail in Chapter 5.

4.3 Examples of Printed Patterns

Photos in Figure 4.5 and Figure 4.6 illustrate the ability of the proposed DOD method to arrange sessile drops into various patterns. Drugs incorporated in carriers whose melting temperature is above room temperature, such as PEG 3350, were printed by forming a melt and using a heating pad over the nozzle to maintain fluid temperature before drop

was deposited. Figure 4.6(a) shows dye-colored ibuprofen solution deposited on porous HPMC film. Figure 4.6(b) shows uniform drop sizes deposited on non-porous HPC film.

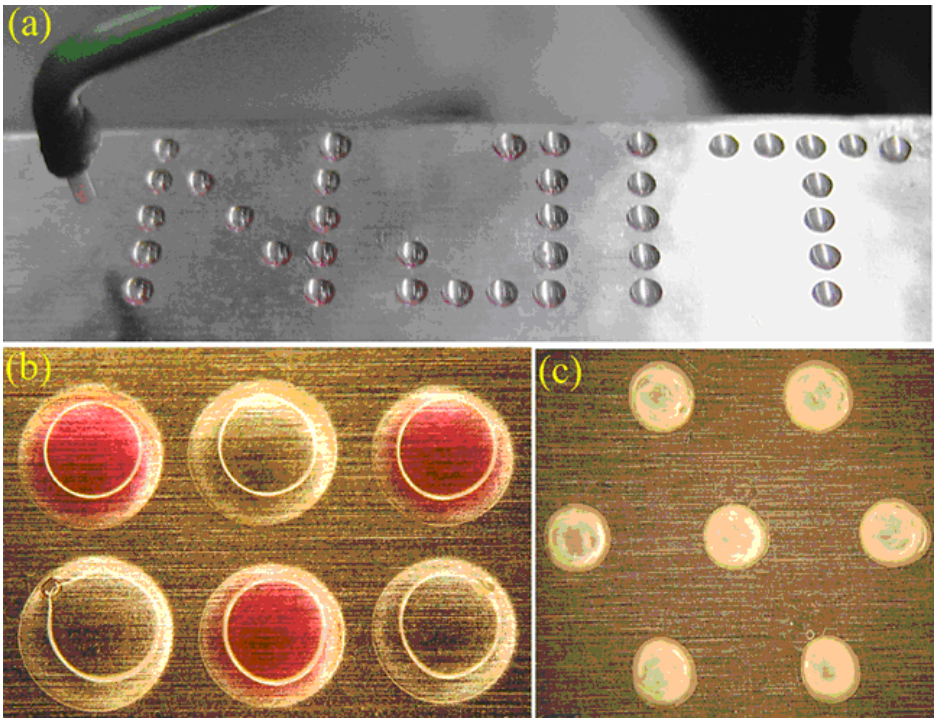

Figure 4.5 (a) 0.1-uL drops of PEG200 with 2(w/w)% fenofibrate & dye, 1mm center-to-center separation; (b). 0.1-mm3 drops of PEG200 with dye, 1.5mm center-to-center separation (c). 0.2-mm3 drops of PEG3350 with 20 (w/w)% aceclofenac printed at ~70^{o}C, 3mm center-to-center separation.

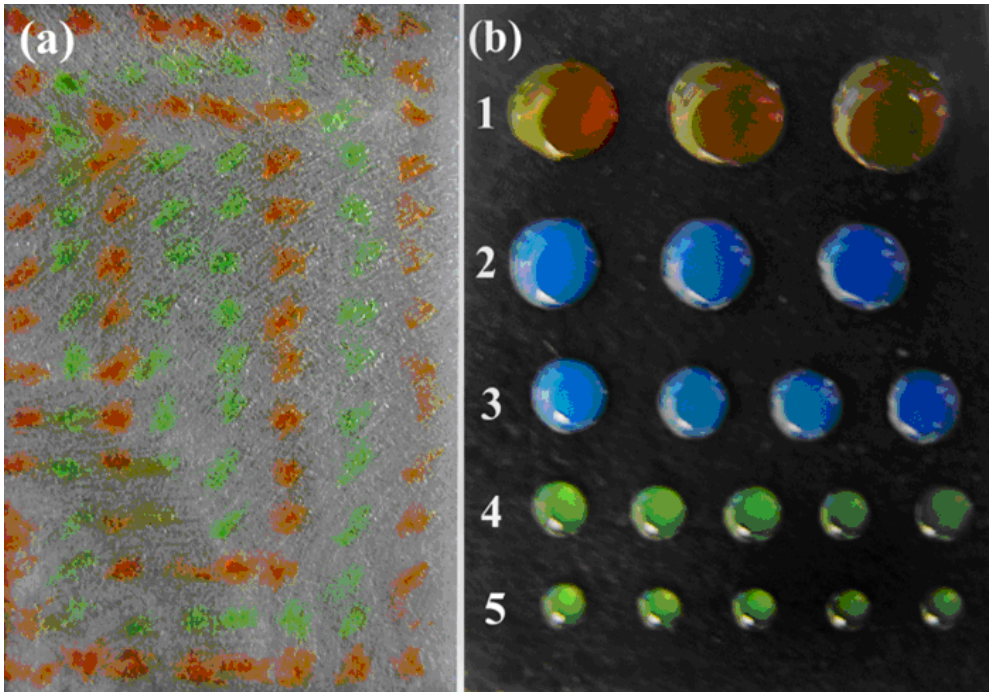

Figure 4.6 20 (w/w)% Ibuprofen solution in PEG deposited on (a) 80%-porous HPMC film; drop 0.2μL. (b) HPC film; drops with volumes: (1) 2μL, (2) 1μL, (3) 0.5μL, (4) 0.2μL, (5) 0.1μL.

4.4 Conclusions

With electrodless EHD DOD printing, fluids whose physical properties; conductivity, dielectric constant, and surface tension: 1-3112 cP, 0.02-290 μS/cm, 9-78, and 35-72 dyn/cm varied over a broad range were successfully printed, whereas current DOD techniques (Kipphan 2001) operate on fluids with viscosity below ~30 cP due to high viscous dissipation. Operating regimes for drop deposition were identified and characterized. The range of drop sizes printed was 0.1 to 2uL.

The drop size in a steady regime of printing was found to be equal to the infused volume regardless of the fluid properties and pulse parameters. This feature makes this method particularly attractive for printing expensive pharmaceutical formulations and

precise control of unit dosages. Furthermore, the absence of direct contact between fluid and electrodes due to capacitive coupling eliminates concerns of formulation degradation during printing.

CHAPTER 5

MODELING AND SCALING ANALYSIS OF DROP DYNAMICS

5.1 Modeling Pendant Drop as Harmonic Oscillator

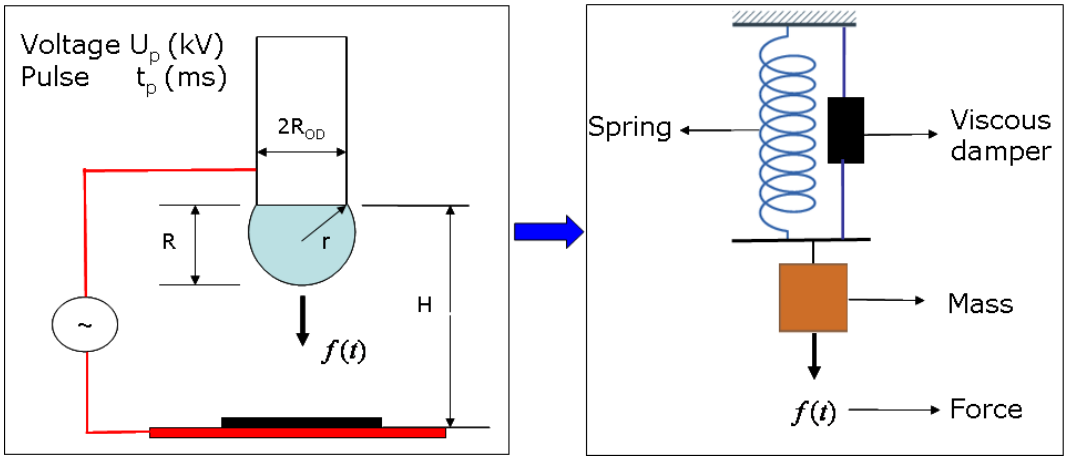

Figure 5.1 Model of a pendant drop as a harmonic oscillator.

As the capillary force prevails for $B_g << 1$, a pendant drop formed at the nozzle, Figure 5.1 adopts the shape of a sphere segment with the contact line along the nozzle outer edge (Basaran and DePaoli 1994) and volume $V_p = \pi R_{OD}^3 \bar{V}/3$, where $\bar{V} = (1+\alpha)^{1/2}(2-\alpha)/(1-\alpha)^{3/2}$ and α $(-1<\alpha<1)$ is the ratio between the distance from the nozzle exit face to the sphere center and the sphere radius (Basaran and DePaoli 1994). In order to understand the dynamics of drop deposition in the electrodeless DOD method, the motion of a pendant drop under the action of capillary and electric forces is modeled as a damped harmonic oscillator (Stachewicz, Yurteri et al. 2009)

as shown in Figure. 5.1. Depending on the fluid properties, the application of an electric force to a drop causes it to elongate. The displacement of a pendant drop is expressed by the differential equation.

$$m\frac{d^2x}{dt^2}+\Gamma R_{OD}\eta_f\frac{dx}{dt}+\Omega^2\gamma_f x = F_E(x,t) \tag{5.1}$$

where m is mass of the pendant drop, R_{OD} the nozzle radius, η_f the viscosity, γ_f the surface tension, x the pendant drop displacement, Γ the damping parameter and Ω the resonance parameter of the pendant drop. This equation is a force balance between inertia, viscous, capillary and electric forces, $F_E(x,t)$. Nondimensionalizing it with two scaling factors, (1) the capillary time t_c and (2) the nozzle radius R_{OD} such that all time scales becomes $\tau = t/t_c$, and length scales $\bar{x} = x/R_{OD}$ where $t_c = \sqrt{\rho_f R_{OD}^3/\gamma_f}$, yields Equation 5.2, where $a=\pi\bar{V}/3$, $b=\Gamma Oh$, and $c=\Omega^2$.

$$a\frac{d^2\bar{x}}{d\tau^2}+b\frac{d\bar{x}}{d\tau}+c\bar{x} = F_E(\bar{x},\tau) \tag{5.2}$$

5.2 Electrostatic Forces Acting on Pendant Drop

The drop evolution can be considered in the high-conductivity limit of the EHD equations (Saville 1997) (i.e., the fluid behaves like a conductor) since the pulse length t_p is long compared to the time scale of charge redistribution in the fluid $t_e=\varepsilon_f\varepsilon_0/\sigma_f$ ~0.02μs-0.2ms, where ε_f, σ_f are the fluid dielectric constant and conductivity and ε_0 is the vacuum permittivity (APPENDIX G). The electric force exerted on the drop consists

of two components. The first is the repulsive force generated by the upper electrode. As shown by Taylor (Taylor 1966), this force can be approximated by the force acting on a hemispheroid with the same tip position as the drop (Figure 5.2(a)). The force is written in Equation 5.3 as:

$$f_{Taylor}(\bar{x},\tau) = 2\pi B_e \left(\frac{U_f}{U_p}\right)^2 \left(\frac{\bar{L}^2(\bar{x})}{eI_2}\right)\left(1-\frac{0.75-\mathrm{Log}_e 2}{e^3 I_2}\right) f(\tau) \tag{5.3}$$

where L is the major radius of the hemispheroid, e the eccentricity, $I_2 = 1/e^2\left\{1/2e\,\mathrm{Log}_e\left((1+e)/(1-e)\right)-1\right\}$, U_f is the voltage across the gap and $f(\tau)$ is the pulse time function (APPENDIX B).

The second component is the attractive force generated by the lower electrode. As suggested by Fumagalli et al. and Hudlet et al. for nanoscale capacitance microscopy (Belaidi, Girard et al. 1997; Jean, Hudlet et al. 1999; Casuso, Fumagalli et al. 2007; Fumagalli, Ferrari et al. 2007), it can be approximated as the electric force between the spherical apex of the drop and the dielectric film placed on the lower electrode. In dimensionless variables, this force is written in Equation 5.4.

$$f_{Sperical\_apex}(\bar{x},\tau) = 2\pi B_e \left(\frac{U_f}{U_p}\right)^2 \bar{H}^2 \bar{R}_c^2 \left(\frac{(1-\sin\theta_o)}{\left(\bar{x}+\bar{h}/\varepsilon_r\right)\left(\bar{x}+\bar{h}/\varepsilon_r+\bar{R}_c(1-\sin\theta_o)\right)}\right) f(\tau) \tag{5.4}$$

Where $\bar{H}$, $\bar{R}_C$, θ_o, ε_r and $\bar{h}$ are the height, radius of curvature, the half angle of the drop, the dielectric constant of the film on the ground electrode and the film thickness respectively (APPENDIX C). Symbols with dash are nondimensionalized quantities.

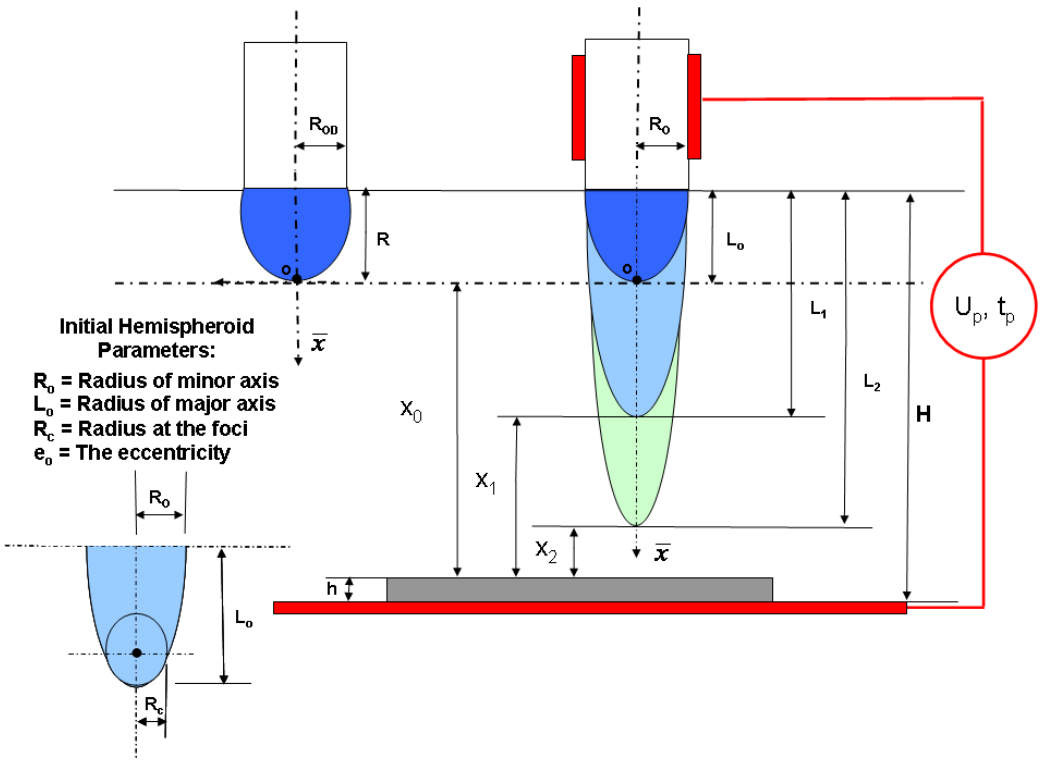

Figure 5.2 (a) Schematics of the displacement of the pendant drop.

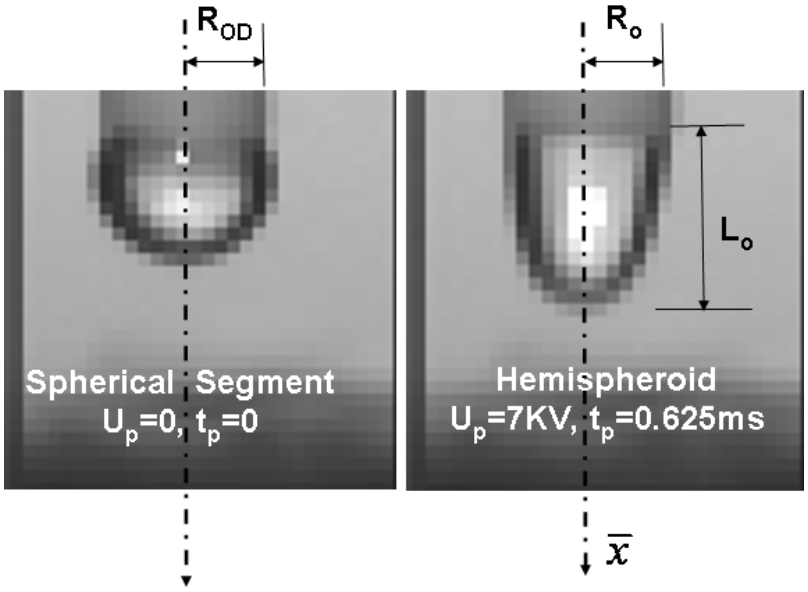

Figure 5.2 (b) High speed image of deformation of a DI-Water pendant drop into a hemispheroid by electric forces.

The total electric force in Equation 5.2 is then. $F_E(\bar{x},\tau) = f_{Taylor}(\bar{x},\tau)+f_{Sperical\_apex}(\bar{x},\tau)$ or $F_E(\bar{x},\tau) = f_E(\bar{x})f(\tau)$ where $f_E(\bar{x}) = f_{Taylor}(\bar{x})+f_{Sperical\_apex}(\bar{x})$. As the electric force overcomes inertial, viscous and capillary forces, the drop touches the film and forms a liquid bridge.

5.3 Oscillation of Pendant Drop

Following an electric pulse, a pendant drop relaxes back oscillatory or aperiodically, depending on the Ohnesorge number, Oh, that characterizes the damping factor in Equation 5.2. For small Oh, as $b^2-4ac<0$, the pendant drop oscillates following the pulse. On the other hand, for large Oh, as $b^2-4ac>0$, the pendant drop monotonically relaxes back.

5.4 Estimate of Model Parameters

Evaluation of Ω and Γ is based on measurements of the drop motion. Stani and Sabetta analyzed theoretically the oscillatory motion of a sessile drop of a low viscosity fluid and calculated the drop resonance frequency and damping factor of an oscillating drop (Strani and Sabetta 1984; Strani and Sabetta 1988). Sato et al. (Tsukada, Sato et al. 1987), Basaran et al. (Harris and Basaran 1993; Basaran and DePaoli 1994; Wilkes and Basaran 1997), studied the oscillation of a drop generated by an electric field. Kim et al. (Harris and Basaran 1993; Basaran and DePaoli 1994; Wilkes and Basaran 1997; Moon, Kang et al. 2006) studied oscillation of drops generated by acoustic disturbances. Particularly, Basaran and Wilke showed that the transition from periodic to aperiodic oscillation is determined by a critical Ohnesorge Number (Basaran and DePaoli 1994). Since experimental conditions differ from those considered in the literature, experiments were

conducted to measure Ω and Γ by fitting experimental results for the drop motion following an electric pulse, i.e., when $F_E(\bar{x},\tau) = 0$ in Equation 5.2. For example, photos in Figure 5.3 and Figure 5.4 show the oscillatory motion of a 0.2uL pendant drop of DI-water generated by the pulse, U_p=6KV, t_p =0.625ms, for H=1.2mm. Measurements of the drop tip position after the maximum displacement were fitted to Equation 5.5 which is the periodic solution of Equation 5.2 with boundary condition $\bar{x}\big|_{\tau=0} = \bar{x}_{max}$ and $d\bar{x}/d\tau\big|_{\tau=0} = 0$.

$$\bar{x}(\tau) = \bar{x}_{max} e^{r\tau}\left(\cos q\tau - \frac{r}{q}\sin q\tau\right) \tag{5.5}$$

where $r = -b/2a$ and $q = \sqrt{b^2-4ac}/2a$

For PEG 400, measurements of the drop tip position after the maximum displacement generated by applying U_p=7KV, t_p =2.5ms for H=1.2mm (Figure 5.5 and Figure 5.6) were fitted to Equation 5.6 which is an aperiodic solution of Equation 5.2

$$\bar{x}(\tau) = K_1 e^{\lambda_1 \tau} + K_2 e^{\lambda_2 \tau} \tag{5.6}$$

Where $\lambda_1 = r+q$, $\lambda_2 = r-q$, $K_1 = \lambda_2 \bar{x}_{max}/(\lambda_2 - \lambda)$, $K_2 = \lambda_1 \bar{x}_{max}/(\lambda_1 - \lambda_2)$ and $\bar{x}_{max}$ is the maximum displacement.

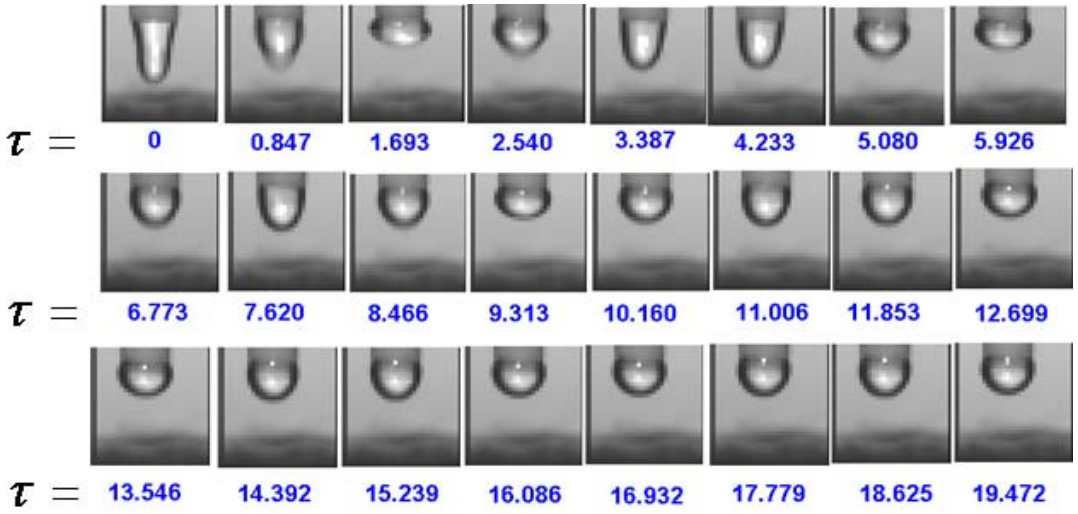

Figure 5.3 Images of oscillations of a DI-Water drop.

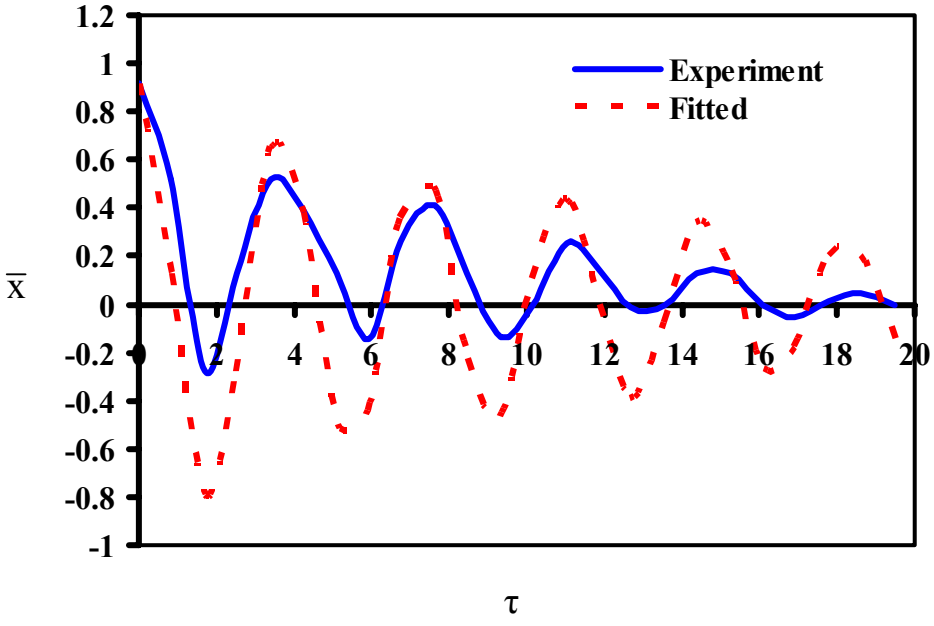

Figure 5.4 DI-Water oscillations: fitting ($\Gamma \sim 80$, $\Omega \sim 3.3$) and experiment.

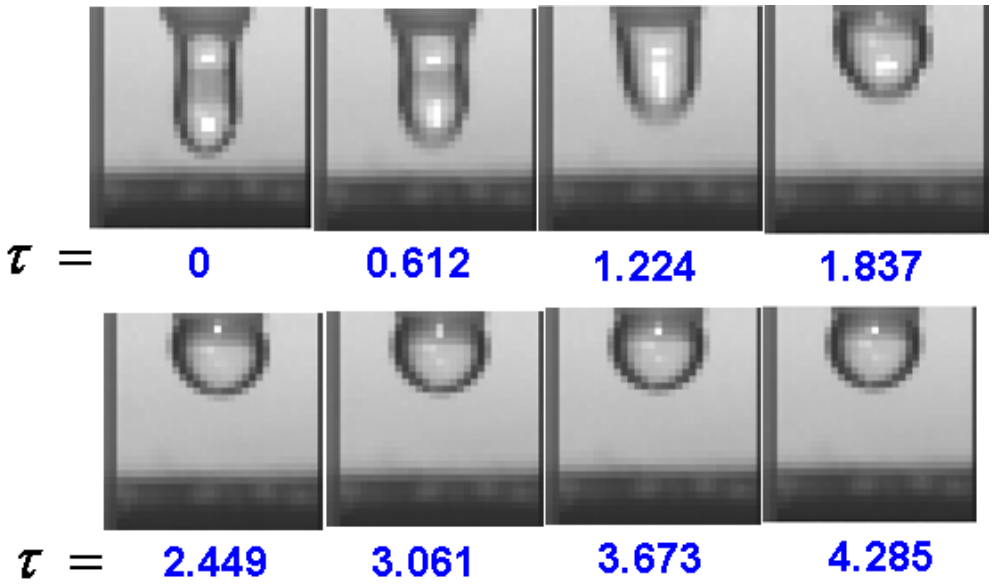

Figure 5.5 Images of the motion of a PEG 400 drop.

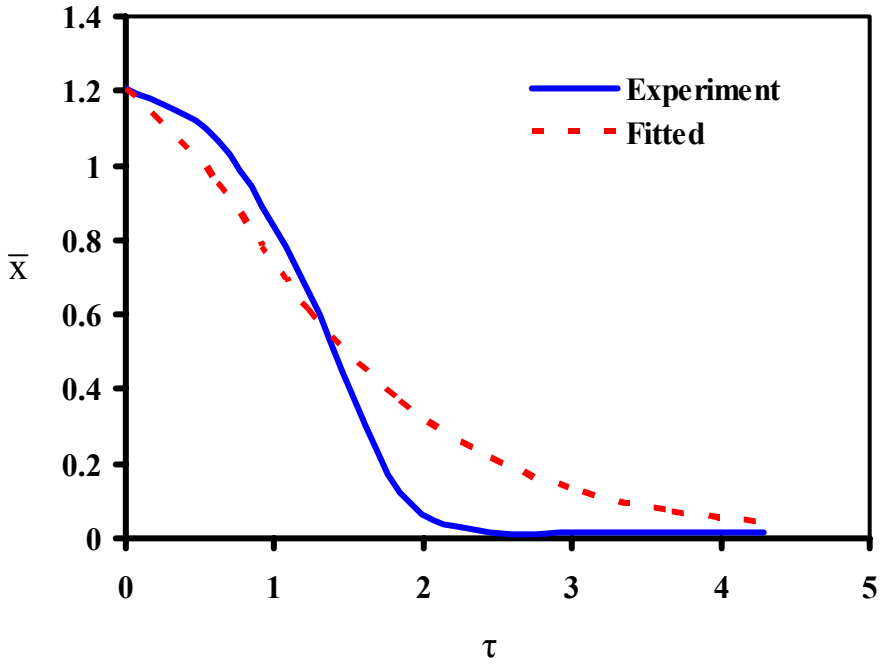

Figure 5.6 PEG 400 aperiodic motion: fitting ($\Gamma \sim 11.5$, $\Omega \sim 3.3$) and experiment.

Parameters determined for relatively low-viscosity fluids for which Oh ≤1 are shown in Table 5.1.

Table 5.1 Parameters for Low-Viscosity Fluids

Fluid	Viscosity (cP)	Oh	Ω	Γ
DI-Water	1	0.006	3.3	80
2mM KCl solution	1	0.006	3.3	80
PEG 200	76	0.56	3.3	8.6
PEG 400	142	1.02	3.3	11.5

5.5 Prediction of Critical Liquid Bridge Lines for Fluids with Oh≤1

5. 5.1 Damped Harmonic Oscillator

Parameters listed in Table 5.1 were used in equation 5.2 to predict the electrical pulse required for the drop to touch the substrate and form an unstable liquid bridge. For fluids with Oh≤1 the electrostatic force at $F_E(\bar{x}|_{\bar{x}=0},\tau)$ was sufficient to generate oscillation required for the drop to touch the substrate. Following an experimental procedure for measuring the critical line, the electrical Bond number B_e was kept constant and pulse length t_p (nondimensionalized as $\tau_p = t_p/t_c$) was increased until the pendant drop touches the substrate. An example is shown in Figure 5.7 for DI-Water at B_e=0.8.

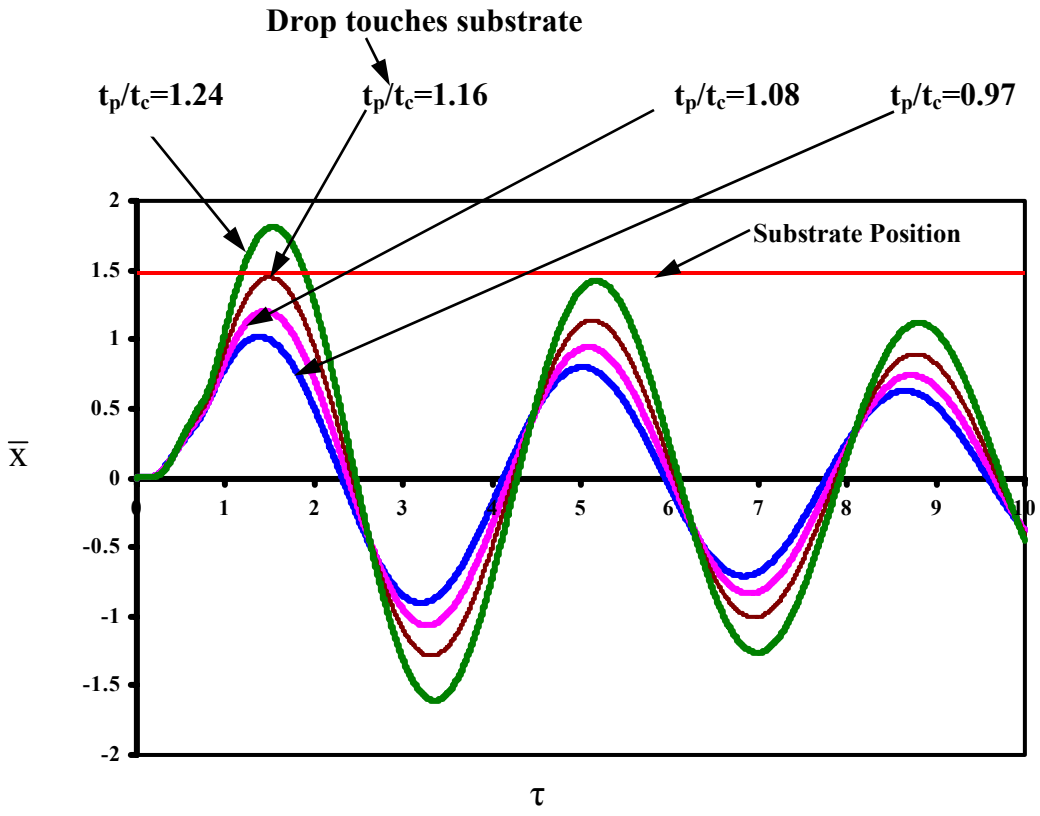

Figure 5.7 Periodic displacement of pendant drop to touch dielectric film (substrate) placed on the ground electrode (DI-Water at B_e=0.8).

The electrical impulse is $I_p = B_e t_p / 3t_c$ for the triangular pulses. It was measured to be I_p=0.22±0.07 for drops with Oh ≤1. Calculations based on parameters listed in Table 5.1 yielded I_p=0.33±0.12 .

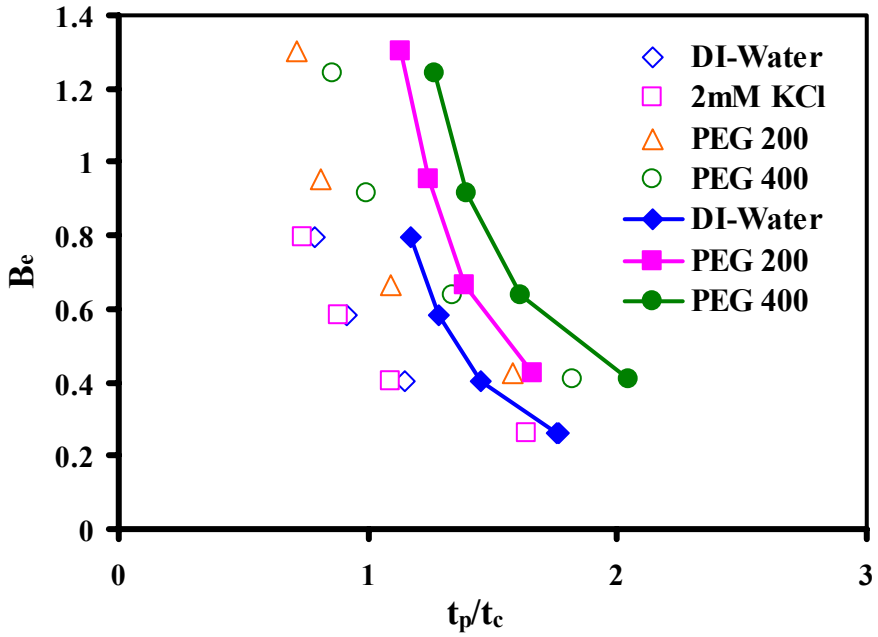

Figure 5.8 Critical lines for drops of relatively low viscosity fluids. Symbols show experimental data; solid lines represent values computed with equation 5.2 and parameters listed in Table 5.1.

This result in conjunction with measured and computed critical lines (Figure 5.8) demonstrate that Equation 5.2 with parameters listed in Table 5.1 can be used for modeling the dynamics of a pendant drop subjected to an electric pulse.

5.5.2 Limiting Case of Negligible Viscous Force

If the Ohnesorge number is small, the viscous force in the oscillating equation can be neglected. In this case Equation 5.2 can be written as:

$$a\frac{d^2\bar{x}}{d\tau^2}+c\bar{x}=F_E(\bar{x},\tau) \qquad (5.7)$$

As the drop distortion for short pulses can be neglected, such that $F_E(\bar{x},\tau) = F_E(\bar{x}=0,\tau) = f_E(\bar{x}=0)f(\tau)$. In this case, the electric pulse imparts the drop with a velocity $v_o = f_E(\bar{x}=0)\tau_p / 3a$ such that the drop continues on its inertia driven elongation and touches the substrate. The solution of Equation 5.7 is a balance between the kinetic and surface energy of the drop as shown in Equation 5.8.

$$\frac{av^2}{2} + \frac{\Omega \bar{x}^2}{2} = \frac{av_o^2}{2} \tag{5.8}$$

At the instant of touching the substrate the drop velocity is zero ($v=0$) and the drop have been displaced by a quantity $\bar{x}=\Delta$ yielding Equation 5.9 which is the minimum pulse required for touching the substrate for low Ohnesorge number fluids (Oh≤1).

$$\tau_p = \frac{3a^{1/2}\Omega\Delta}{f_E(\bar{x}=0)} \tag{5.9}$$

Estimate based on Equation 5.9 yielded an electrical impulse, $I_p \sim 0.32$ and the predicted critical lines are shown in Figure 5.9**.** This value is also in agreement with both experimental data and calculations based on the full equation (Figure 5.8). Comparison of the pulse length for liquid bridge lines for fluids with Oh≤1 shows the critical pulses were below resonance (APPENDIX H).

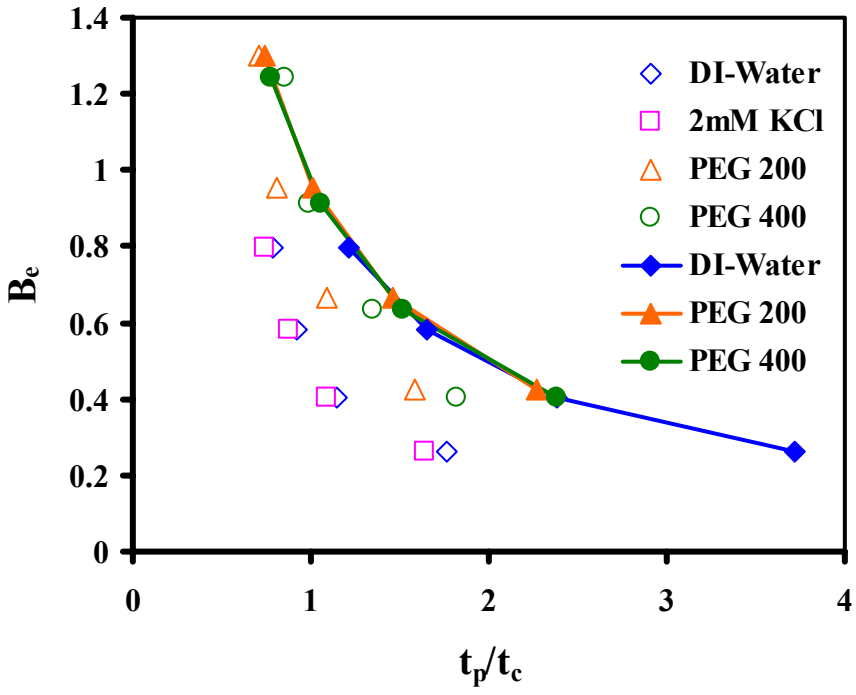

Figure 5.9 Critical line computed using Equation 5.9. Symbols represent experimental data.

5.6 Design Guideline

With respect to fluid properties and electrical parameters, the critical questions that will provide design guideline for an electrodeless DOD system are:

- How to determine pulse length, t_p, and peak voltage, U_p or electrical impulse I_p, to stretch a pendant drop to touch the film without an excessive exposure to a field.

- How to determine an infused volume v_i required to form an unstable liquid bridge so as to produce a sessile drop on the substrate.

The first question partly addressed in Sec. 5.5 will be discussed later. Now, consideration will be given for an infused volume v_i for which a liquid bridge will be unstable.

5.6.1 Liquid Bridge Stability Study

A drop of volume V_p stretched by a pulse forms a liquid bridge of length H-h anchored by capillary forces to the nozzle exit and the film (Figure 5.10). One of the criteria for obtaining a precise single sessile drop within the operating regime is the formation of an unstable liquid bridge to create a sessile drop. In other words, the liquid bridge should not retain stability indefinitely as in Figure 5.11 but must break up to form a sessile drop (Figure 5.12).

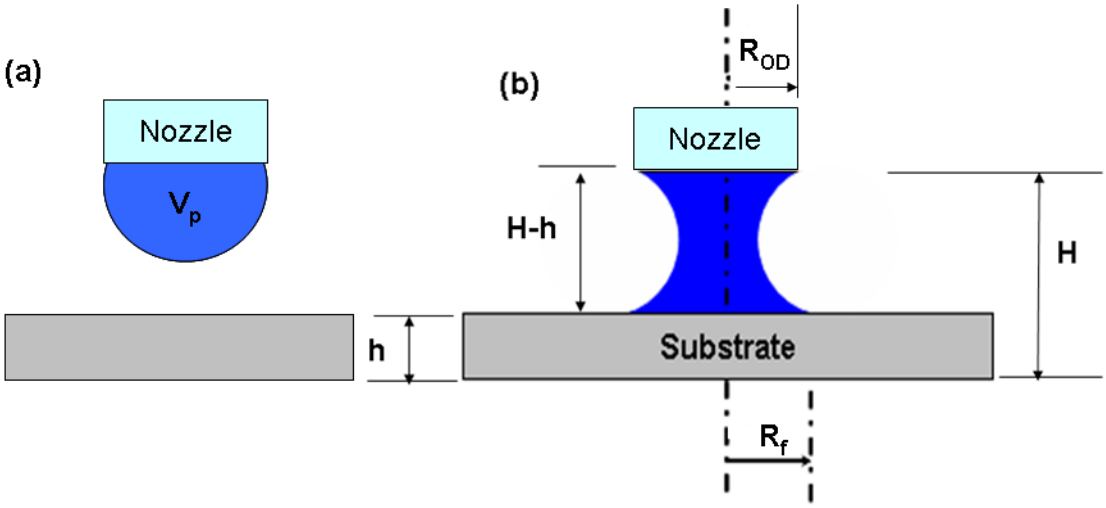

Figure 5.10 Liquid bridge stability study (a) pendant drop (b) liquid bridge schematics.

The minimum volume stability of an axisymmetric liquid bridge pinned between two coaxial equal-in-diameter disks can be measured by changing the pendant drop volume while keeping the aspect ratio (slenderness) constant until bridge becomes unstable (Espino, Meseguer et al. 2002; Slobozhanin, Alexander et al. 2002) Conversely, this can also be achieved by keeping the aspect ratio constant while changing the bridge volume until it becomes unstable. As liquid bridges formed in experiments are not

pinned, the experimental measurements were compared with studies of the stability of a liquid bridge formed between disks of different radii (Meseguer, Slobozhanin et al. 1995; Slobozhanin and Alexander 1998; Meseguer, Espino et al. 2003).

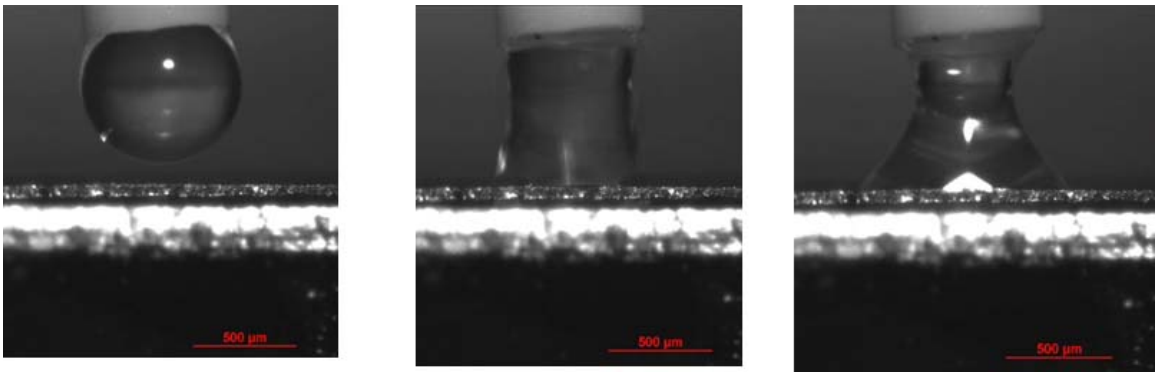

Figure 5.11 Drop evolution into a stable liquid bridge; PEG 200 on 80um HPC film, U_p=7kV, t_p=5ms; v_i=0.2µL, H=0.85mm, R_{OD}=0.38mm, h=80um.

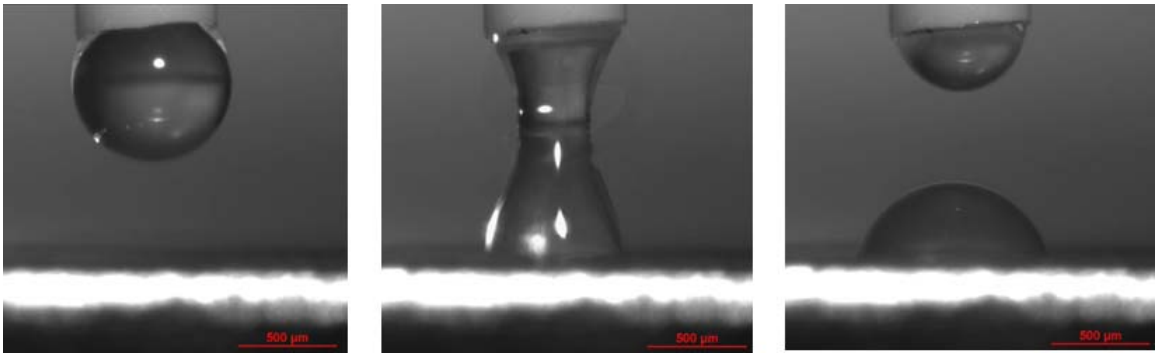

Figure 5.12 Drop evolution into an unstable liquid bridge: PEG 200 on 80um HPC film, U_p=7kV, t_p=5ms; v_i=0.2µL, H=1.2mm, R_{OD}=0.38mm, h=80um.

To find V_p and H-h such that a bridge produced by a critical pulse is unstable, PEG 200 bridges were made on a nonporous HPC film one by one, starting with V_p and H for which the bridge remained stable and successively decreasing V_p at the same H or increasing H at the same V_p, until a bridge broke up. Data on the bridge stability limits are depicted in Figure 5.13 as $V_{br}=V_p/\pi(H-h)R_0^2$, $\Lambda_{br}=(H-h)/2R_0$, $K=R_{OD}/R_f$, where

$2R_0 = R_{OD} + R_f$ and R_f is the bridge radius on the film. Results of both types of measurements are similar, suggesting that the effects of deposition regimes are insignificant.

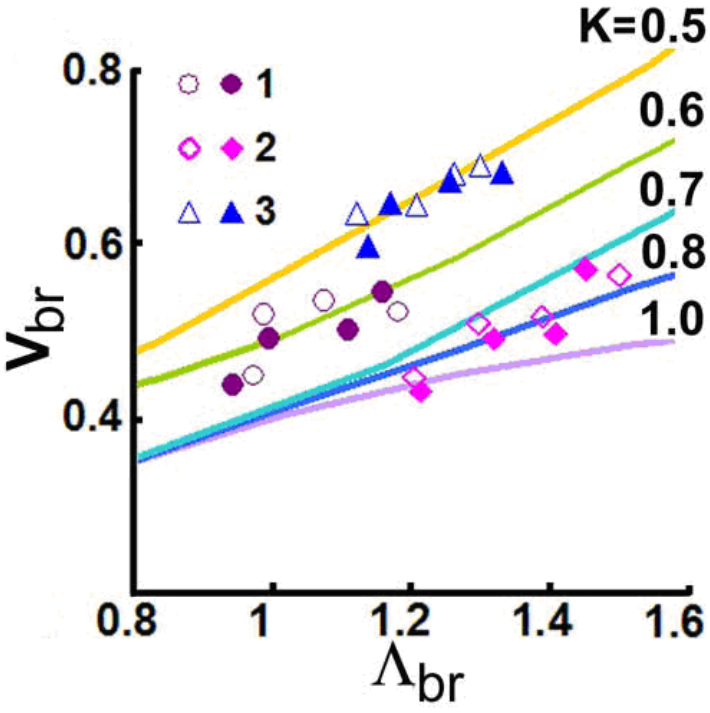

Figure 5.13 Stability limits of PEG 200 bridges for K, B_g, and R_{OD}: 1) 0.7, 0.02, 0.38mm; 2) 0.8. 0.06, 0.55mm; 3) 0.6, 0.2, 1.1mm. Open and filled symbols indicate measurements by decreasing volume and increasing height. Curves show computations (Meseguer, Slobozhanin et al. 1995; Slobozhanin and Alexander 1998) for various K and B_g=0.

As can be seen from Figure 5.13, computations (Slobozhanin and Alexander 1998) of the minimum-volume stability of a bridge anchored to unequal coaxial disks at negligible gravity provide a reasonable estimate of a drop size to form an unstable bridge by taking K as the disk radii ratio. A larger drop can be printed on a porous film since a bridge would become unstable as its volume decreases due to fluid imbibitions.

5.6.2 Scaling Analysis for Drop Dynamics

To simplify exploring the parameter space governing drop evolution, a large upper electrode is used for the capacitance C_w between it and the fluid to be large compared to the capacitance C_g between the lower electrode and the fluid (Figure. 3.1). In this case, the variation of the drop potential, $U_f \sim U_e \big/ \left(1+C_g/C_w\right)$, during its elongation can be neglected as $U_f \sim U_e$ for $C_w >> C_g$ (Figure 3.1 and APPENDIX A). Therefore, the force acting on the drop depends on its instantaneous shape and the instant value of the applied voltage U_e. Invoking the classical argument for the response of a resting fluid to localized impulsive forcing (Batchelor 1967), it was found that the temporal component of the fluid acceleration and the pressure gradient dominate for short pulses $t_p << t_v$ and $\int_0^{t_p} v dt << R_{OD}$, where v is the fluid velocity and $t_v = \rho_f R_{OD}^2 / \eta_f$ is the time scale of the diffusion of velocity variations across the drop (Batchelor 1967). As the drop deformation $\sim \int_0^{t_p} v dt$ is relatively small during such pulses, the capillary force contribution to the fluid momentum flux is insignificant. It is therefore entirely due to the electric stress over the drop surface during the pulse, $\sim \varepsilon_0 U_e^2(t) / H^2$, that imparts the drop with velocity $v(t_p) \sim \left(\varepsilon_0 / \rho_f H^2 R_{OD}\right) \int_0^{t_p} U_e^2(t) dt$. If viscous contribution was also neglected in the subsequent inertia-driven drop evolution, equating the drop kinetic energy after the pulse to an increase in the surface energy once the apex touches the film yields $v(t_p) t_c \sim \sqrt{\Delta R_{OD}}$, where Δ is the drop apex displacement and $t_c = \sqrt{\rho_f R_{OD}^3 / \gamma_f}$

is the capillary time (Basaran 2002). Hence, a transition between the first and second modes of deposition Figure. 4.1, occurs at the critical value of

$$I_p = \left(B_e/t_c\right)\int_0^{t_p}\left(U_e(t)/U_p\right)^2 dt \tag{5.10}$$

that depends solely on the geometrical parameters α, H/R_{OD}, Δ/R_{OD}, and the nozzle inner-to-outer radius ratio ξ. This limiting case corresponds to $t_p << t_c/Oh$ and $Oh << 1$.

In the opposite case of long pulses $t_p >> t_v$, the fluid inertial forces are negligible compared to viscous forces. Accordingly, the drop evolution can be considered in the creeping-flow approximation described by the linear Stokes equations (Batchelor 1967). If the ratio of the electric stress to the capillary pressure is sufficiently large, the balance of electric and viscous forces yields $\varepsilon_0 R_{OD} U_e^2(t)/\eta_f H^2$ for the scale of the instantaneous fluid velocity. As $\int_0^{t_p} v dt \sim \Delta$ in this case, a transition between the first and second modes occurs at the critical value of I_p/Oh that also depends solely on the geometrical parameters α, H/R_{OD}, Δ/R_{OD}, and ξ. This case corresponds to $Oh >> 1$.

Both asymptotics are consistent with data on the I_p-Oh diagram ($I_p = B_e t_p/3t_c$ for the triangular pulses applied) of operating modes for printing various fluids on HPC films at the same set of geometrical parameters, Figure 5.13. Namely, solid lines in Figure 5.13 approximate the critical line as $I_p \approx 0.2$ for $Oh \le 1$ and $I_p \approx 1.2Oh$ for $Oh \ge 10$; inset shows I_p/Oh along the critical line for large Oh. Data in Figure 5.13 and

Table 5.2 also demonstrate that the same range of pulse parameters can be used in printing with different nozzles and drop volumes.

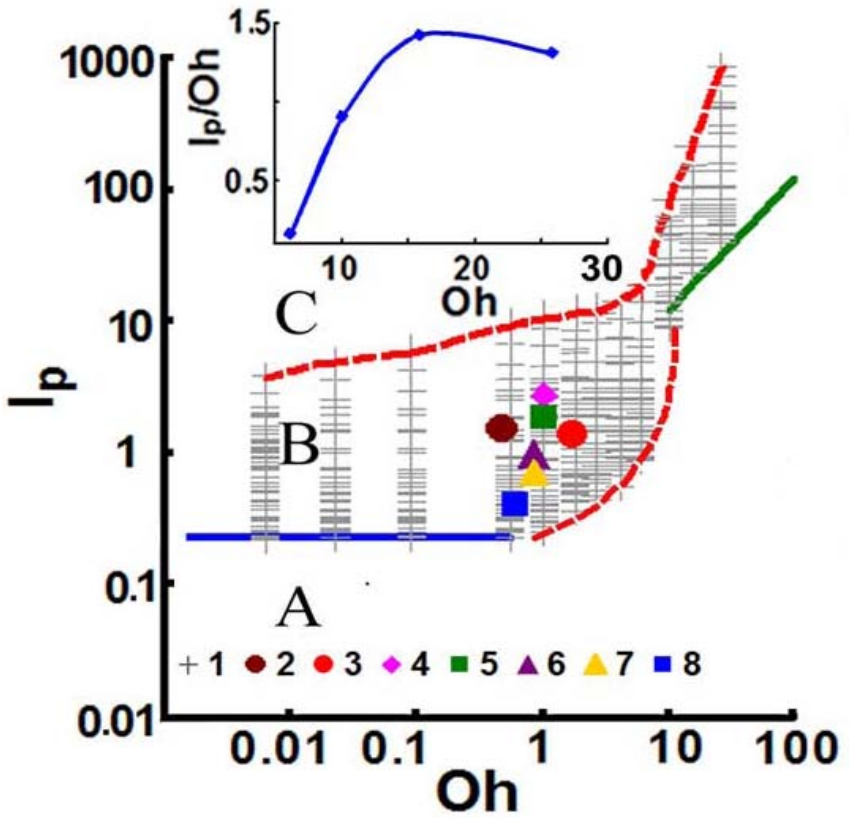

Figure 5.13 Operating modes for various fluids listed in Table 3.1: A) drop relaxes back, B) single sessile drop formed, C) multiple sessile drops formed; α, H/R_{OD}, Δ/R_{OD}, ξ: (1) *fluids No. 1-13, Table 3.1*; 0.32, 3.16, 1.55, 0.74; (2) *fluid No 15, Table 3.1*; -0.095, 3.95, 2.83, 0.74; (3) *fluid No 16, Table 3.1*; 0.32, 3.95, 2.34, 0.74; *fluid No 14, Table 3.1*: (4) -0.095, 2.63, 1.51, 0.74; (5) 0.32, 3.16, 1.55, 0.74; (6) 0.22, 2.73, 1.33, 0.73; (7) 0.54, 3.27, 1.31, 0.73; (8) -0.22, 1.82, 0.95, 0.76. Solid lines show the critical line asymptotics.

Table 5.2 Geometrical Parameters

No	Fluids	R_{ID} mm	R_{OD} mm	v_i mm	H mm	Δ mm	ξ	α	H/R_{OD}	$Δ/R_{OD}$
1	Fluids with Oh 0.006-26	0.28	0.38	0.2	1.2	0.74	0.59	0.33	3.16	1.55
2	PEG 200 with 2(w/w%) fenofibrete	0.28	0.38	0.1	1.5	0.74	1.07	0.09	3.95	2.83
3	PEG 3350 with 20 (w/w%) Aceclofenac	0.28	0.38	0.2	1.5	0.74	0.89	0.89	3.95	2.34
4	PEG 400 with 20w/w% Ibuprofen	0.28	0.38	0.1	1.0	0.74	0.57	0.09	2.63	1.51
5	PEG 400 with 20w/w% Ibuprofen	0.28	0.38	0.2	1.2	0.74	0.59	0.33	3.16	1.55
6	PEG 400 with 20w/w% Ibuprofen	0.4	0.55	0.5	1.5	0.73	0.73	0.22	2.73	1.33
7	PEG 400 with 20w/w% Ibuprofen	0.4	0.55	1.0	1.8	0.73	0.72	0.54	3.27	1.31
8	PEG 400 with 20w/w% Ibuprofen	0.84	1.1	2.0	2.0	0.76	1.05	0.22	1.82	0.95

5.7 Conclusion

This section described the essential physics of drop evolution and provided estimate of parameters required for printing of drops with diverse range of physical properties. Regimes of printing are characterized by Ohnesorge number, Oh which contains the fluid physical properties and the electrical impulse I_p that is required for printing a drop. Data

presented in Figure 5.13 and Table 5.3 demonstrates the versatility of electrodeless DOD printing method and summarized the guidelines for the design of printing apparatuses.

Table 5.3 Ohnesorge Number and Electrical Impulse for Operating Regime

Fluids	**Electrical Impulse, I_p**	
	Oh ≤ 1	**Oh ≥ 10**
Experimental Results	$I_p \sim 0.22$	$I_p \sim 1.2Oh$
Damped Harmonic Oscillator (Full equation)	$I_p \sim 0.32$	
Damped Harmonic Oscillator (Limiting case)	$I_p \sim 0.3$	
Scaling Analysis	$I_p \sim$ constant	$I_p/Oh \sim$ constant

CHAPTER 6

PRINTING OF FAST DISSOLVING UNIT DOSAGES

6.1 Objectives and Overview

This section demonstrates the ability of electrodeless DOD printing method to produce assembled unit doses which meet reproducibility requirements critical for content uniformity. Ibuprofen and griseofulvin chosen as model drugs were printed onto a porous freeze dried HPMC film. The drug strip was then covered on the top by a casted HPMC film. Due to fast disintegration and dissolution, printed unit dosages will not only provide accurate doses for patient's compliance but also have the potential to be used as fast orally unit dosages which is rapidly gaining interest in the pharmaceutical industry over traditional tablet technology (Dixit and Puthli 2009; Hariharan and Bogue 2009).

Fast orally dissolvable strip films are especially advantageous for pediatric and geriatric patients and patients experiencing nausea and vomiting during pregnancy or chemotherapy as they have difficulties in swallowing or chewing solid dosage forms. A drug loading of about 9% (w/w) was achieved in the prepared assembled unit dosages. A schematic cross-sectional view of unit doses is shown in Figure 6.1. Dissolution tests were conducted in the laboratory of Prof. Bozena Michniak-Kohn at the Department of Pharmaceutics of Rutgers, The State University of New Jersey. A unit dose comprised a porous polymer film containing drops of a Drug-PEG mixture, with the top covered by a casted polymer film (Figure 6.1).

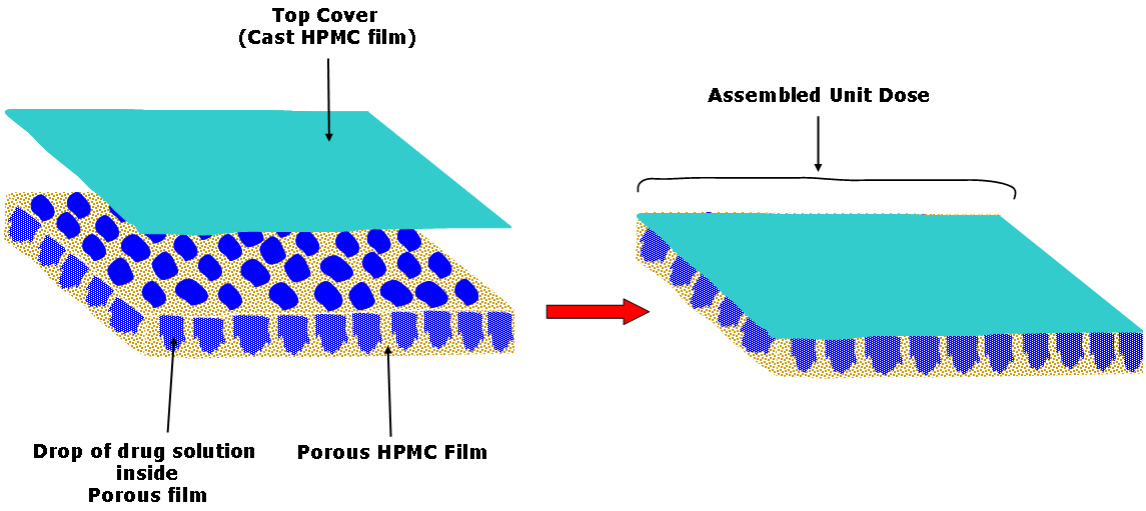

Figure 6.1 A schematic view of an assembled unit dose.

Electrodeless DOD printing was used to load the porous polymer film with a Drug-PEG mixture. Dissolution tests were performed following the USP-NF 1092; 711 protocol, and the drug release profiles from six samples were compared for unit doses of ibuprofen and griseofulvin. The release profiles show that majority of the drug is released within the first 15 minutes and the disintegration tests confirmed that the film dissolved very quickly. The drug release data were fitted to various models available in the literature to identify the best mechanism describing the release data. The percentage of drug release from the fully assembled unit dosages was 90% for ibuprofen and 75% for griseofulvin.

6.2 Materials

6.2.1 Model Drugs

Ibuprofen (BSAF) and griseofulvin (Sigma Aldrich), an antifungal drug with formula $C_{17}H_{17}ClO_6$, molecular weight 352.76g/mol, and melting temperature 218^{o}C, were

chosen as model drugs. Both drugs can be administered as and oral suspension and also delivered in a strip film format.

6.2.2 Drugs Carrier

Pharmaceutical grade polyethylene glycols (PEG) are mainly used as excipients for ointments, gelatin capsules, suppositories, globules, and for coated tablets. PEGs can also serve as drug carriers as they dissolve many active pharmaceutical ingredients (Mashkevich 2007). PEG 400 was chosen since ibuprofen is known to exhibit good solubility in PEG 400. The solubility of giseofulvin in PEG400 was increased by adding sodium dodecyl sulfate (SDS) obtained from Sigma Aldrich.

6.2.3 Porous Film Material

Hydroxypropyl methylcellulose (HPMC) is a very important biodegradable hydrophilic carrier material used for the preparation of oral drug delivery systems (Siepmann and Peppas 2001; Li, Martini et al. 2005). Hydroxypropyl methylcellulose (HPMC) grade E15LV is a non cross-linked polymer soluble in aqueous solutions with demonstrated high release rate of many API.

6.3 Preparation of Porous and Non Porous Films

To fabricate a 95% porous HPMC film, a 5 (w/w)% HPMC E15LV aqueous solution was prepared following Dow Chemical Protocol. A hollow plastic boundary of 500um thickness was placed on a 3M flouropolymer release liner taped onto a glass slide such that the hollow section forms a well of 500 microns thickness. The polymer solution was poured into the well and covered on the top with another glass slide such that the solution

was sandwiched between the glass plates while maintaining a thickness of 500 microns. The assembly was carefully placed inside a refrigerator and allowed to freeze for 12hrs after which it was transferred to a Labconco freeze drier operated in vacuum mode for 24hrs and water was sublimated leaving a porous film (Figure 6.4a). The film porosity expressed as $\varphi = \frac{\varphi_w \rho_p}{\varphi_w \rho_p + \varphi_p \rho_w}$ can be varied by changing the HPMC concentration in the aqueous solution, where ρ_p~1000 kg/m^3 and ρ_w ~ 1000 kg/m^3 are the bulk densities of HPMC and water respectively. Non-porous films were prepared by casting a 5 (w/w)% E15LV solution onto a steel plate with a casting knife (BYK) set at 1 mm gap. The casted film was then dried in a conventional oven at 40^{o}C for 3 hrs to produce a film of ~60um thickness.

6.4 Preparation of Drug Solution

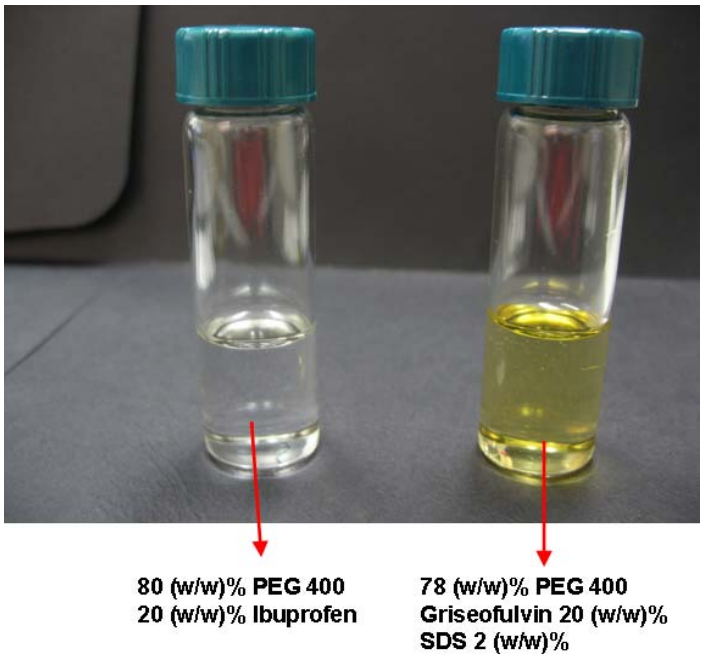

Figure 6.2 Drug solutions.

Ibuprofen and Griseofulvin are Biopharmaceutics Classification System (BCS) class-II drugs as they exhibit very poor solubility and high permeability (Amidon, Lennernäs et al. 1995; Yu, Amidon et al. 2002; Fujioka, Metsugi et al. 2008; Moneghini, Bellich et al. 2008). One of the major problems is how to increase their solubility to enhance bioavailability (BALAKRISHNAN, REGE et al. 2004; Newa, Bhandari et al. 2007; Chow, Tong et al. 2008). Therefore they were dissolved in PEG 400 before printing on HPMC porous films.

A 20 (w/w)% ibuprofen solution in PEG 400 was prepared by mixing a weighed amount of ibuprofen with PEG 400. The mixture was maintained at 50^{o}C for 30 min to dissolve ibuprofen and form a transparent solution (Figure 6.2). Subsequently, the solution was left to cool down to room temperature and was observed to be stable for more than a month. This observation was consistent with the reported solubility of ibuprofen of about 26.7 (w/w)% in PEG 400 at 25^{o}C (Haddadin, Qian et al. 2008). A 20 (w/w)% griseofulvin solution in PEG 400 was also prepared with 2 (w/w)% SDS. SDS usually increases solubility of griseofulvin in PEG (Wulff and Aldén 1995; Wulff, Aldén et al. 1996). The mixture was heated at 80^{o}C for 24hrs to completely dissolve the drug and then cooled down to room temperature. Likewise, griseofulvin solution (yellowish color, Figure 6.2) was also observed to be stable. Both solutions were packed in airtight containers since PEG 400 is highly hygroscopic.

6.5 Printing of Assembled Unit Dosage

To prepare a unit dosage, an array of drops of a drug solution was printed on a porous film. A porous HPMC film of length L=35mm, width W = 20mm and thickness

h=500um was placed on the lower ground electrode of the DOD printing setup (Figure 6.3(a)). The drug solution (20 (w/w)% ibuprofen or griseofulvin in PEG 400) was then printed on the film to form an array of non-overlapping imbibed 0.2 µL-droplets.

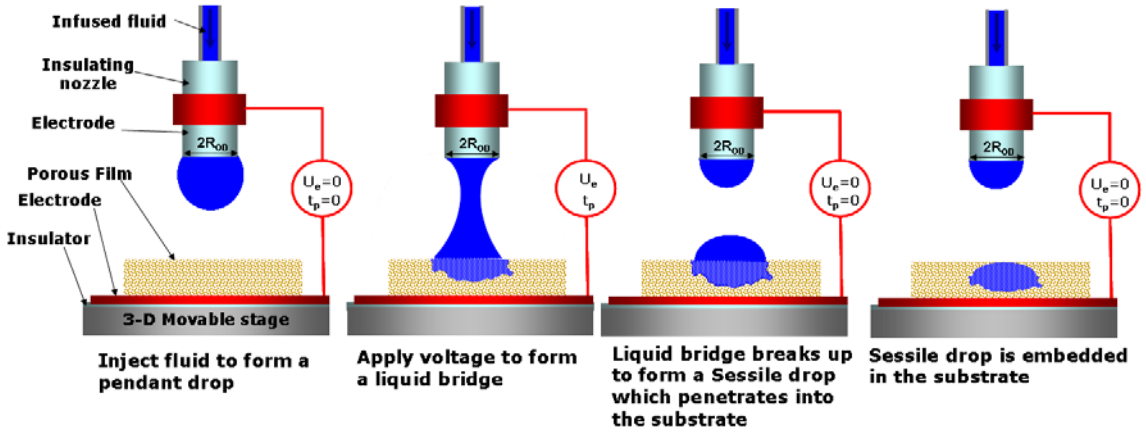

Figure 6.3 (a) Electrodeless DOD setup and process.

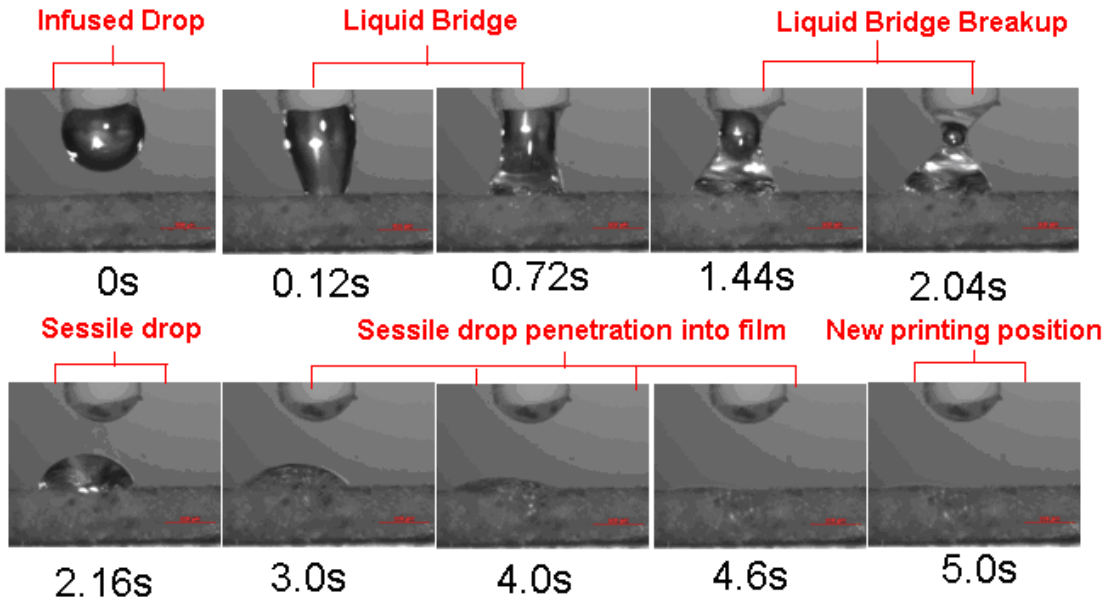

Figure 6.3 (b) Drop of 20(w/w)% griseofulvin in PEG400/SDS on 95%-porous HPMC film; U_p=7kV, t_p=5ms, H=1.5mm, R_{OD}=0.38mm, v_i=0.2µL.

The separation between the ground electrode and the nozzle exit was maintained at height, H =1.5mm. 112 Droplets were printed one by one by applying a triangular pulse t_p = 5ms and voltage U_p = 7KV to each drop (Figure 6.3(b)). Since electrodeless EHD DOD printing enables precise volume control and exact positioning of drops, the printed weight of the solution was calculated by multiplying the volume of a single drop by the total number of drops to give 22.4 μL. The densities of solutions were measured using a 10mL calibrated beaker giving 1.1g/mL and 1.15g/mL for ibuprofen and griseofulvin solutions; hence the drug loading in the porous film was 4.92mg and 5.12mg for ibuprofen and griseofulvin, respectively. An assembled unit dosage was completed by covering the top of the drug-loaded film with a non porous casted HPMC film as shown in Figure 6.4(d).

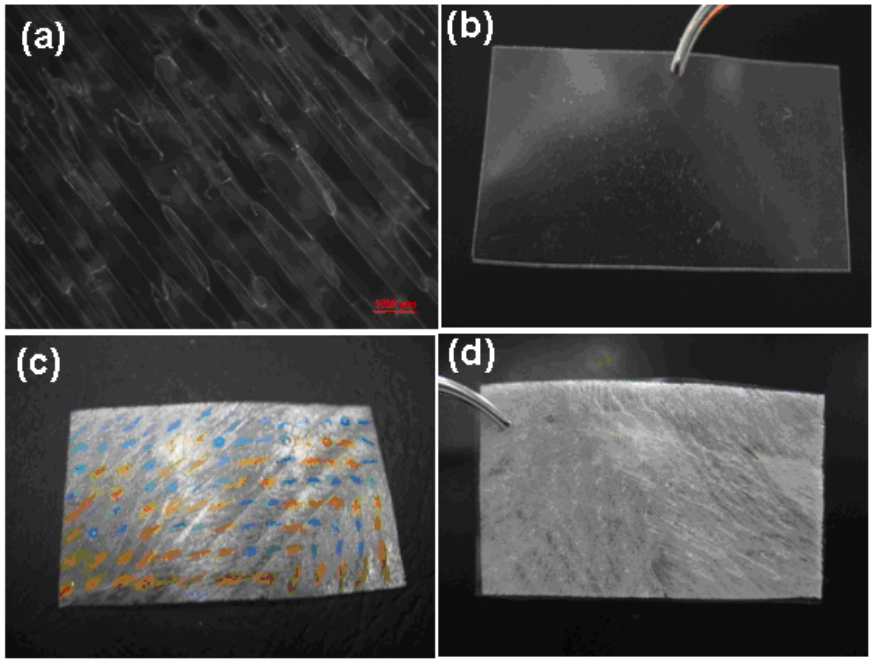

Figure 6.4 (a) Freeze dried 95% porous HPMC film of 500um thickness; (b) casted HPMC film of 60um thickness formed from a 5 (w/w)% solution; (c) 112 drops of 20(w/w)% griseofulvin in PEG400/SDS on 35mm x 20mm, freeze dried 95% porous HPMC film of thickness 500um; (d) assembled unit dosage (5.12mg) of griseofulvin covered on top with 60um cast HPMC film.

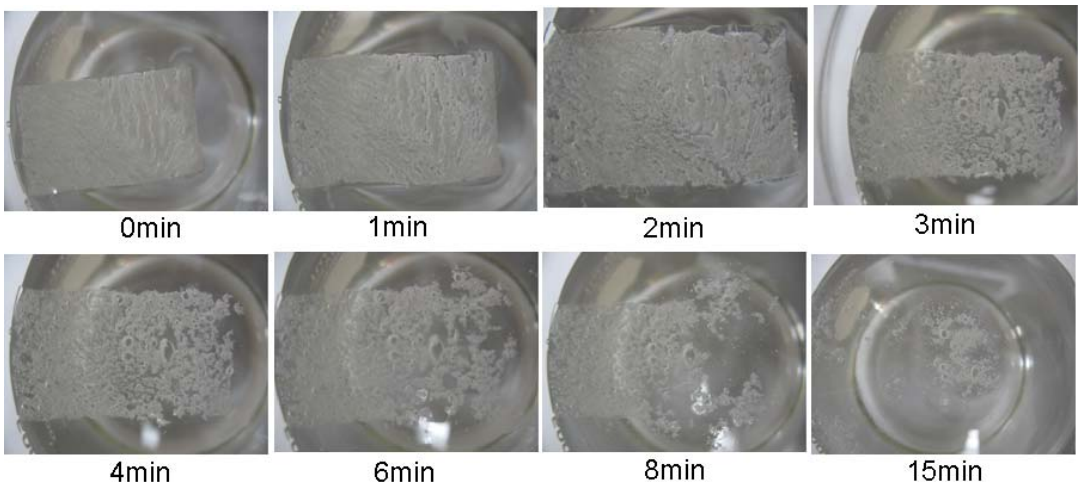

Figure 6.5 Water absorption and disintegration of an assembled unit dosage of griseofulvin in an unstirred 500ml beaker containing 500ml DI-water.

6.6 Dissolution Tests

6.6.1 Dissolution Test of Assembled Unit Dosage

Dissolution tests were conducted on assembled unit dosages in accordance with standard USP <711> protocol. To obtain a calibration curve that covers this range, four standard concentrations 0.011, 0.0055, 0.00275 and 0.001375mg/mL of ibuprofen in a buffer solution was prepared and the absorbance peaks was measured at a wavelength of 221.5nm. A plot of absorbance vs. concentration in Figure 6.7(a) showed a linear calibration curve with high correlation coefficient required by the USP protocol (USP 2004). The calibration curve also included the absorbance value of the blank buffer solution. Similarly, the calibration curve of griseofulvin also showed a good linear relationship at a peak absorbance wavelength of 293nm (Figure 6.7(b)). A verification test showed that the presence of PEG 400 and SDS in the solution did not affect the absorbance values or the wavelength. Drug release profiles from HPMC films loaded

with ibuprofen and griseofulvin were measured using a standard USP Type I apparatus (basket), Figure 6.6. To check the reproducibility of dissolution profiles, test on all six samples were carried out simultaneously. The baskets filled with the buffer solution was maintained at 37^{o}C and rotated at 100 rpm.

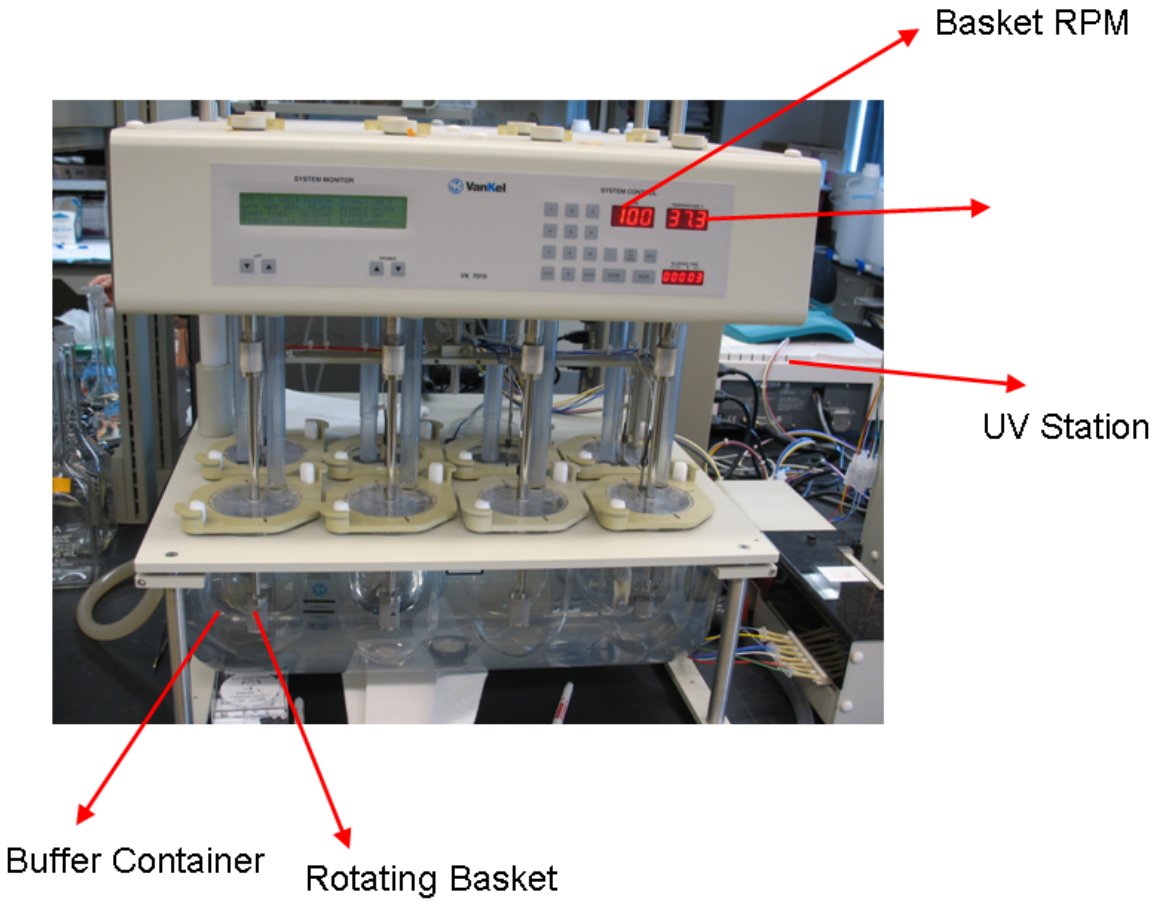

Figure 6.6 Dissolution apparatus (Prof. Bozena Michniak-Kohn Lab, Rutgers, The State University of New Jersey).

Sampling was performed at 3-minute intervals and experiments were carried out over 4 hours so that the release profile attained a steady peak value. The dissolution profiles obtained from the experiments are shown in Figure 6.8(a) and Figure 6.8(b).

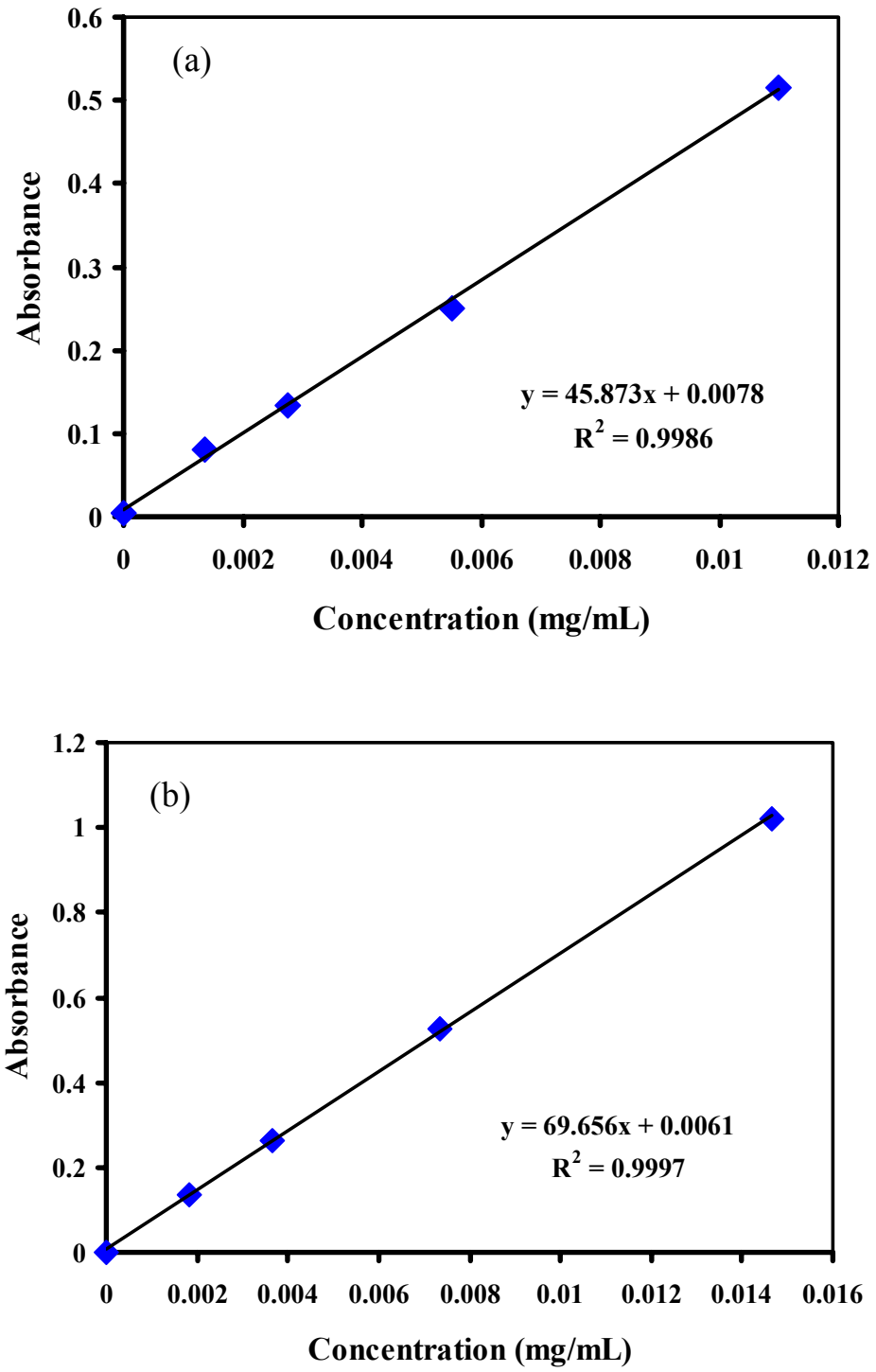

Figure 6.7 Calibration curve for (a) ibuprofen in PEG 400. (b) griseofulvin in PEG/SDS.

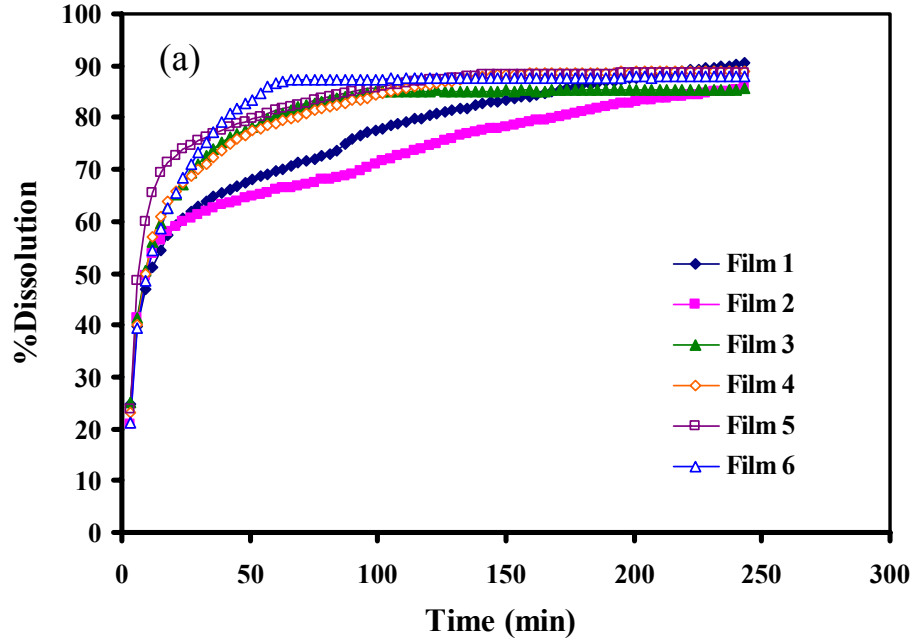

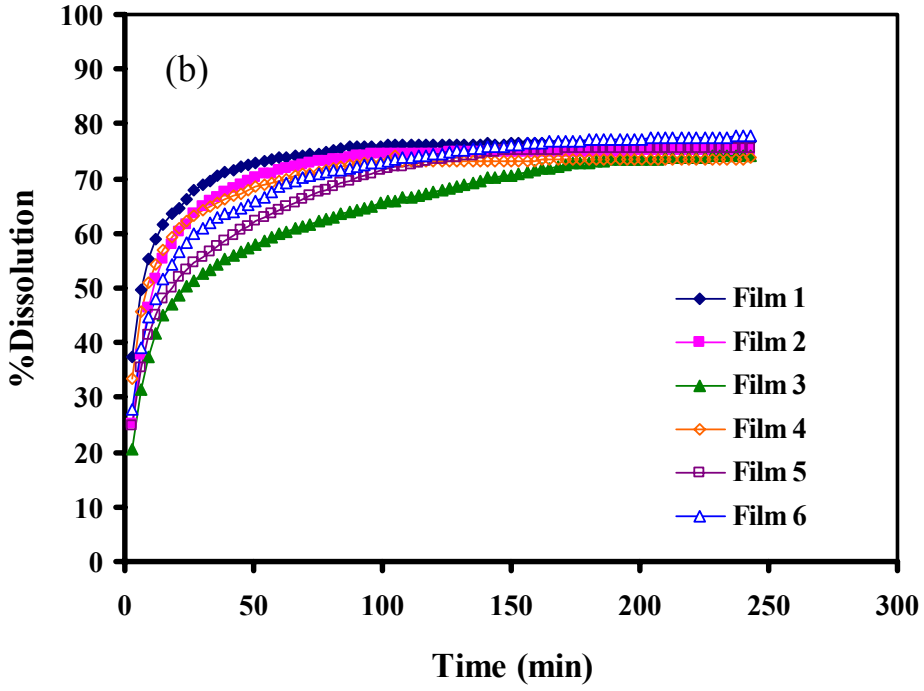

Figure 6.8 Dissolution profiles of drugs in 95% porous HPMC film (a) ibuprofen (b) griseofulvin.

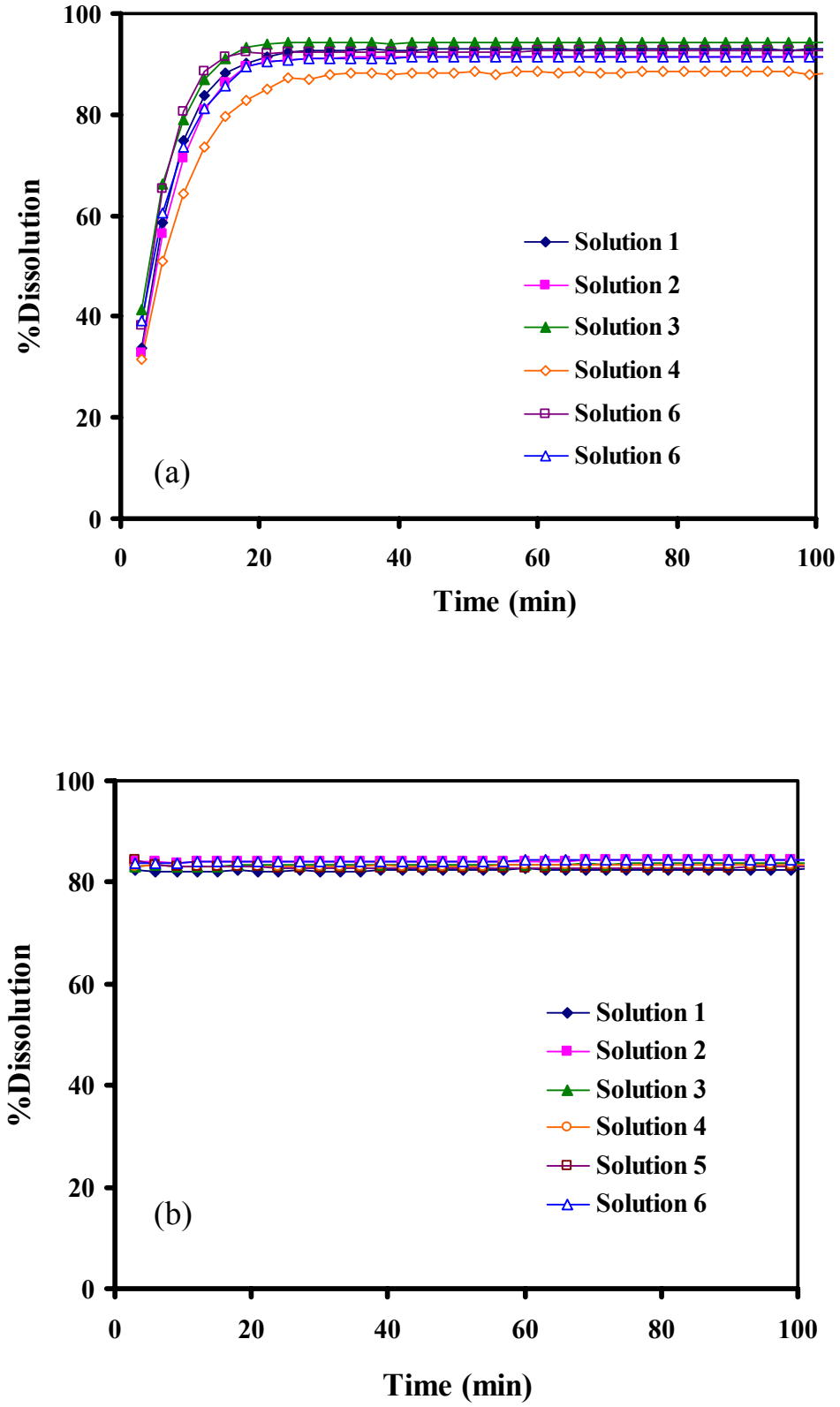

Figure 6.9 Dissolution profiles of drugs from solutions (a) ibuprofen (b) griseofulvin

6.6.2 Dissolution Test of Drug Solution

To evaluate the effects of the porous film matrix on the drug release profiles, dissolution tests were also conducted on drug solutions containing the same amount of a drug as in assembled unit doses. In this case, the drug was not confined inside the film matrix and the influence of the porous film on the drug release profiles is eliminated. A required mass of a drug solution was weighed out on an impermeable plastic plate and inserted into the basket to carry out dissolution tests similar to those conducted on the films. The results for ibuprofen and griseofulvin solutions are shown in Figures 6.9(a) and 6.9(b).

6.7 Experimental Results

6.7.1 Images of Freeze Dried Film, Cast and Assembled Unit Dosage

As shown in Figure 6.4a, a freeze dried film is a porous network of HPMC fibers after sublimation of water. A typical 35mm x 20mm porous film weighed 30mg. On the contrary, a cast film was a dense continuous impermeable matrix (Figure 6.4b). It had a smooth surface and was transparent compared to a freeze dried film which had a rough surface. The drug loading in an assembled unit dosage was about 9%. As a drop was deposited on a porous film, it quickly and completely imbibed into the substrate as shown in Figure 6.3b and Figure 6.4c. The thickness of the film was sufficient for the drop not to exit through the opposite side. As a result, a drug is entirely embedded inside the film.

6.7.2 Reproducibility of Release Profiles

The reproducibility of the release profiles of ibuprofen and griseofulvin from the films was analyzed by calculating the difference f_1 and similarity f_2 factors for the release curves (Costa and Sousa Lobo 2001).

$$f_1 = \frac{\sum_{j=1}^{m} \left| R_j - T_j \right|}{\sum_{j=1}^{m} R_j} \times 100 \quad (6.1)$$

$$f_2 = 50 \times \mathrm{Log} \left\{ \left(1 + (1/n) \sum_{j=1}^{m} W_j \left| R_j - T_j \right|^2 \right)^{-0.5} \times 100 \right\} \quad (6.2)$$

f_1 (Equation 6.1) measures the percent error between two curves over all time points, while the f_2 value (Equation 6.2) is a logarithmic transformation of the sum-squared error of differences between the test T_j and reference R_j over all time points.

Table 6.1 Reproducibility of The Release Profiles of Drugs in Porous Film

	Drugs in Porous Film	f_1	f_2
1	Ibuprofen	7.23±1.28	68.88±10.9
2	Griseofulvin	6.21±3.5	63.92±10.32

Table 6.2 Reproducibility of The Release Profiles of Drugs Solutions

	Drug Solution	f_1	f_2
1	Ibuprofen	2.28±1.85	81.55±10.01
2	Griseofulvin	1.46±0.72	90.22±5.86

Release curves are considered similar when the calculated f_1 value is close to 0 (preferably from 0-15) and f_2 is between 50-100 respectively (Dixit and Puthli 2009; Hariharan and Bogue 2009). The release profile satisfied the reproducibility requirements

as the values of f_1 and f_2 for ibuprofen and griseofulvin films were in the acceptability region.

6.7.3 Analysis of Drug Release Profiles

The release profile of ibuprofen from the porous film showed a peak value of about $88\% \pm 1.8$. However, more than 50% of the drug was released at the same rate after the first 15min which was estimated to be the time for the disintegration of the assembled unit dosage. After this period, the disintegrated film components followed different release rate to converge to a maximum release value. Similarly, for films loaded with griseofulvin, the drug release during the first 15min was $53\% \pm 6$ and then reached a maximum peak value of $75\% \pm 1.5$.

The drug release profiles from ibuprofen and griseofulvin solutions showed that the maximum peak values of solutions are greater than those of films. The maximum release from ibuprofen solutions was achieved in about 20min with a higher release rate compared to that of porous films. Griseofulvin solution had an instantaneous peak value with no initial release rate. In both cases the peak values were achieved faster in solutions than in films. As shown in Figure 6.5, an assemble unit dosage of griseofulvin in an un-agitated 500mL beaker quickly swells up and disintegrates in less than 15min. It was also observed in the release curves that more than 50% of the drug was released within the first 15min. Compared to a drug solution; it may suggest that the porous film matrix slows down the drug release.

6.7.4 Drug Release Mechanism

Among the models found in literature, drug release kinetics from a polymeric material is usually modeled by Krosmeyer-Papas generic Equation (Equation 6.1).

$$\frac{M}{M_\infty} = K_p t^n \tag{6.1}$$

Where $\frac{M}{M_\infty}$ is the fractional release of drug and K_p is a constant incorporating structural and geometrical characteristic defining the dosage form, n is the release exponent characterizing the release mechanism. This model is used in analyzing the release of pharmaceutical dosage forms when the release mechanism is not well known or when one or more mechanisms are involves. To use this model, the release from the dosage form must also be one-dimensional thus the width-thickness or length-thickness relation must be at least 10 (Costa and Sousa Lobo 2001). The interpretation of different release mechanisms following the Krosmeyer-Papas model is given in Table 6.3.

Table 6.3 Mechanisms for Drug Release from Polymeric Matrix

Release Exponent n	**Drug Transport Mechanism**	**Rate as a function of Time**
0.5	Fickian Diffusion	$t^{-0.5}$
$0.5 < n < 1.0$	Anomalous Transport	t^{n-1}
1.0	Case-II Transport	Zero Order Release
Higher than 1.0	Super Case-II Transport	t^{n-1}

The model was used to analyze the release mechanism of drugs from assembled unit dosages where micro drops containing active pharmaceutical ingredients were loaded into

a freeze dried microporous polymer films. Table 6.4 shows that the value of the release exponent for griseofulvin is close to the anomalous regime while that of ibuprofen is close to the fickian diffusion regime.

Table 6.4 Determined Parameters for Drug Release from Freeze Dried Polymeric Matrix

Drug	Release Exponent n	K_p	Drug Transport Mechanism
Ibuprofen in Porous Film	0.64±0.13	7.33±1.31	Close to Anomalous Transport
Griseofulvin in Porous Film	0.44±0.07	4.4±1.1	Close to Fickian Diffusion

The release of active pharmaceutical ingredients from solution was analyzed following the same method used for the films. The result as in Table 6.5 and Figure 6.10 showed that though the averaged release exponent for ibuprofen solution is higher than that of the film, they appear to fall within the same margin of error indicating that the initial release of ibuprofen from the freeze dried microporous HPMC film is similar to that of ibuprofen solution in PEG 400. This gives an indication that the film does not necessarily constitute a barrier to initial drug release and this is a good property for materials employed as carriers or matrixes especially in the design of fast release dosages form.

Table 6.5 Determined Parameters for Drug Release from Solutions

Drug	Release Exponent n	K_p	Drug Transport Mechanism
Ibuprofen Solution	0.72±0.07	7.33±1.31	Anomalous Transport
Griseofulvin Solution	-	-	-

However the release of griseofulvin from solution was observed to be instantaneous compared to that of film and good comparison could not be made between the two (Figure 6.11).

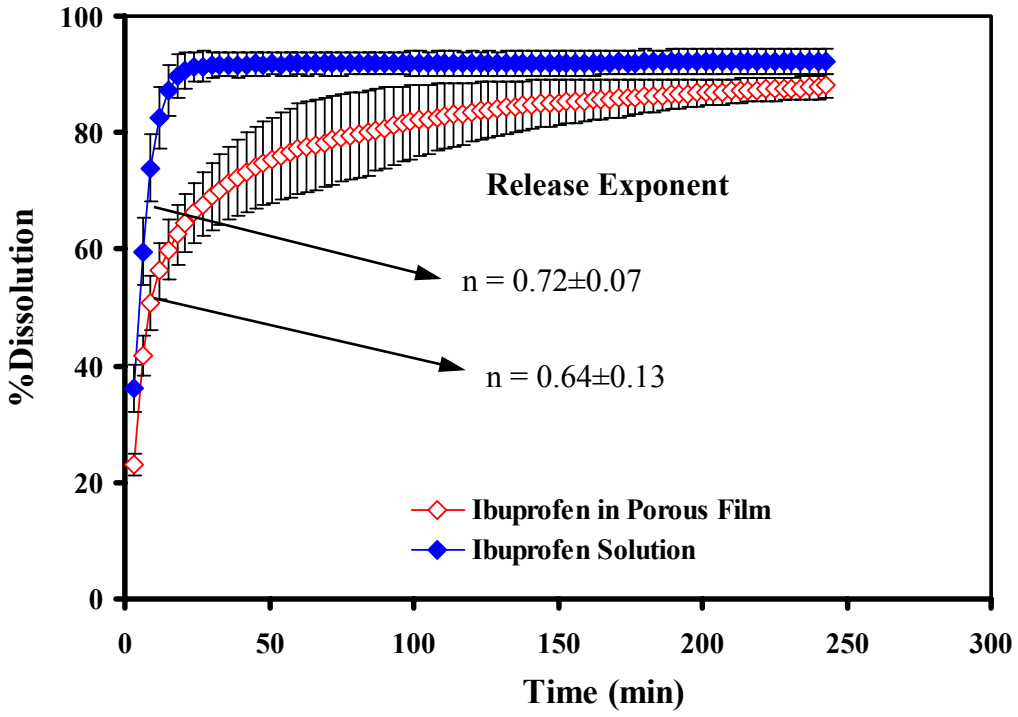

Figure 6.10 Comparison of dissolution profiles of ibuprofen from porous film and solution.

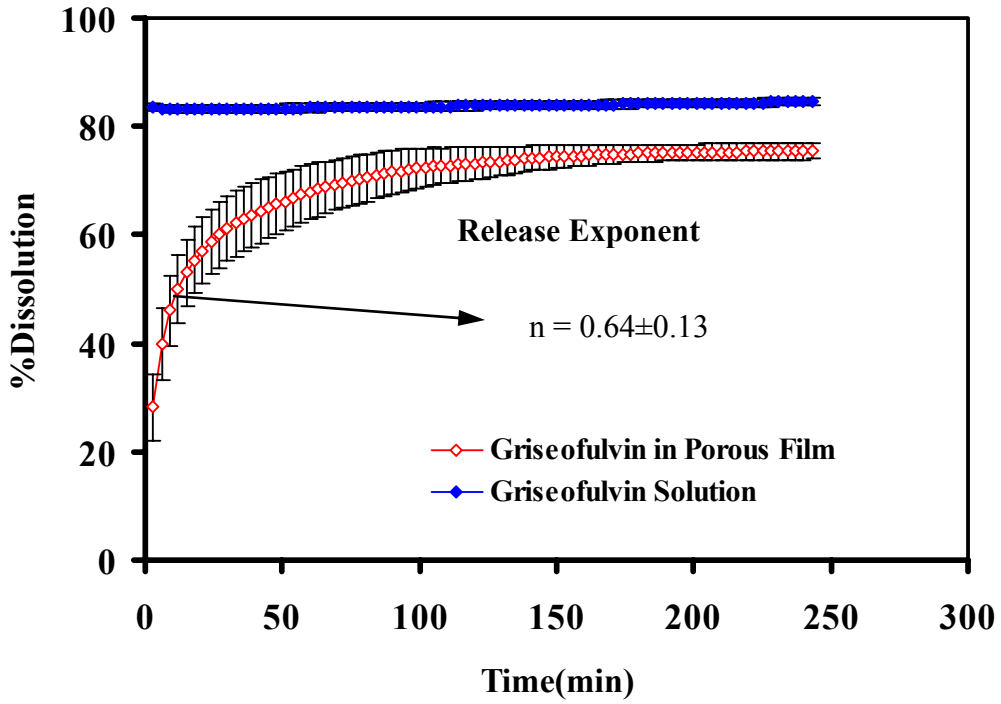

Figure 6.11 Comparison of dissolution profiles of griseofulvin from porous film and solution.

6.8 Conclusions

Tests of assembled unit dosages demonstrated the ability of the developed electrodeless DOD method for fabricating personalized medicines. The proposed method meets the regulatory requirements for reproducibility. Prepared films accommodated a drug loading of up to 9 (w/w) %. Unit doses released about 90% of ibuprofen and 75% of griseofulvin. Changing the thickness of a non-porous cast cover or the porosity of the matrix could enable one to vary the drug release profile from unit doses.

CHAPTER 7

CONCLUDING REMARKS

7.1 Summary

As the field of medicine and pharmaceutics is evolving into the domain of patient specific and sub-population drug delivery, the search for efficient, cost-effective and linearly scalable methods of manufacturing of unit dosages is paramount. This has activated researches in the area of Drop-on-Demand since it is a very promising approach that meets the necessary requirements. DOD greatly enables distributed manufacturing as dosages can be easily manufactured for different subsets of the populations with similar genetic map. Clinical trial quantities can also be easily manufactured without huge cost.

Additionally, control of content uniformity in dosage manufacturing is another high point that makes DOD special as drops with active pharmaceutical ingredients can be deposited and arranged on a carrier substrate without significant variations in volume and contents. This is very important when working with highly expensive pharmaceutical materials where unduly waste of material is undesirable. Also, drug dissolution and release characteristic can be tailored by manipulation of microdrops containing API. Another advantage of using DOD in dosage manufacturing is the ability to vary parameters very easily without huge setbacks; for example, multiple drugs and multi-architecture dosage forms can be designed for engineered release profiles. These functionalities have made DOD technique very desirable for

pharmaceutical applications. The existing DOD techniques used in other fields such as inkjet printing are limited due to new functional requirements in pharmaceutical materials. As the properties of pharmaceutical materials vary over a wide range, the application of current DOD systems become a big challenge as extensive trial and error process required for each new product is impractical for the pharmaceutical domain because the continuous introduction of innovative new drug products does not allow extended development periods, especially not for clinical trials purposes.

This dissertation dealt with a proposed electric field based DOD method of printing pharmaceutical products which addresses the critical limitations facing current DOD methods (Chapters 1-3). To advance beyond trial and error empirical design and operating modes, this dissertation determined operating regimes, studied the regimes and understood the mechanisms and essential physics governing field based drop formation and deposition. A dynamic model for the field driven evolution of a pendant drop and scaling analysis for prediction of drop deposition regimes was developed (Chapters 4-5).

A demonstration of the ability of the field based DOD printing method for producing customized unit doses was carried out by preparing assembled unit dosages by loading freeze dried porous HPMC film with microdrops containing active pharmaceutical ingredients. The dissolution tests on the assembled unit dosages showed that electrodeless DOD printing method satisfied reproducibility requirements critical for the control of content uniformity in dosages manufacturing (Chapter 6). The release characteristics suggests that the freeze dried porous film loaded with API could be used in the design of fast dissolvable oral unit dosages.

7.2 Future Studies

1. Characterization of Drops Deposited on Substrates and the Crystallization Kinetics of Deposited PEG-based Drug Formulations

As the form and microstructure of the drug inside the porous substrate is not known, understanding and control of the final microstructure of the solid phase that is formed when solidification occurs upon deposition is an area of deep further studies. This will lead to methods of control of final microstructure of the solid phase when solidification occurs after drop deposition. This study will involve probing the molecular phase and the drop crystallization kinetics within the substrate, control of solidification/drying rate and provisions for enhancing product stability through microstructure stabilization. Tools such as Modulated Differential Scanning Calorimetry, X-ray Diffractometry, Raman Spectroscopy, Nuclear Magnetic Resonance Spectroscopy NMR and Chemical Imaging systems will be very useful in these studies.

2. Deposition of Multi-layer Systems with Multiple Drugs for Engineered Release Profiles

Another area of study is the deposition and design of multi-layered dosage forms. The effect of layering on time release of drug and the stability of the dosage units will be active areas of investigation. Also the effect of multiple drugs on the design of dosage forms will be an interesting area of study.

3. Study the Interaction of Deposited Drops with Substrate: Spreading, Penetration and Imbibition of Drop on Porous Substrate

Incomplete and/or inadequate understanding of impact/spreading and imbibitions of drops of complex fluids on porous and solid substrate is a key limitation in the process of designing unit dosages through the deposition of many micro drops containing actives on a carrier substrate. Further studies in this area will bring insight on driving factors for

content uniformity. This will involve the examinations of compatibility between substrate and fluid properties.

APPENDIX A

MINIMIZATION OF VARIATION IN DROP POTENTIAL

In other to minimize variation in drop potential, a large energized electrode was used. In Figure A.1 the capacitance of the nozzle C_w is calculated from Equation A.1 which defines the capacitance of a cylindrical capacitor, where L_{Nozzle} is the length of the nozzle in contact with the energized electrode.

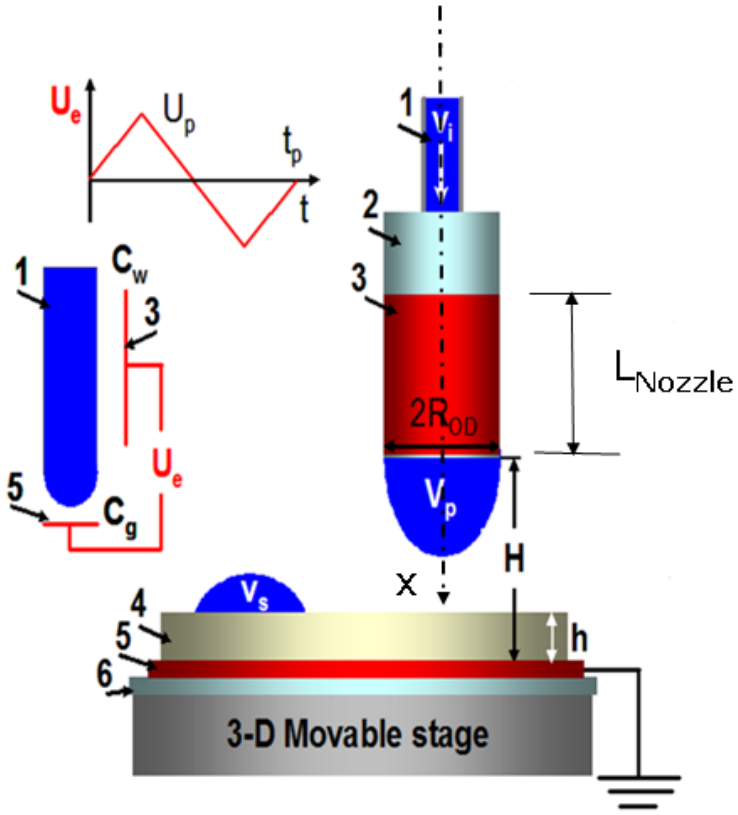

Figure A.1 Nozzle configuration and minimization of variation in drop potential.

$$C_W = \frac{2\pi\varepsilon_o\varepsilon_r R_{OD}\bar{L}_{Nozzle}}{Log_e\left(\frac{R_{OD}}{R_{ID}}\right)} \qquad (A.1)$$

The second capacitance $C_g(x)$ between the drop tip and ground electrode is calculated from Equation A.2 usually employed in nanoscale capacitance microscopy for the measurement of the dielectric constant of thin films placed on a ground electrode.

$$C_g(\bar{x})=2\pi\varepsilon_o\bar{R}_c R_{OD}\mathrm{Log}_e\left[1+\frac{\bar{R}_c(1-\mathrm{Sin}\theta)}{\bar{x}+\bar{h}/\varepsilon_r}\right] \tag{A.2}$$

Therefore, spatial variation in drop potential is given by Equation A.3 such that for $C_w >> C_g(x)$ variation in drop potential is insignificant.

$$U_f \sim U_e \Big/ \left(1+C_g(\bar{x})/C_w\right) \tag{A.3}$$

APPENDIX B

PARAMETERS FOR TRIANGULAR PULSE

The damped harmonic oscillator model as written in Equation B.1 contains a forcing function $f(\tau)$.

$$a\frac{d^2\bar{x}}{d\tau^2}+b\frac{d\bar{x}}{d\tau}+c\bar{x}=f_E(\bar{x})f(\tau)$$
$$\bar{x}\big|_{\tau=0}=0 \quad \text{and} \quad d\bar{x}/d\tau\big|_{\tau=0}=0 \tag{B.1}$$

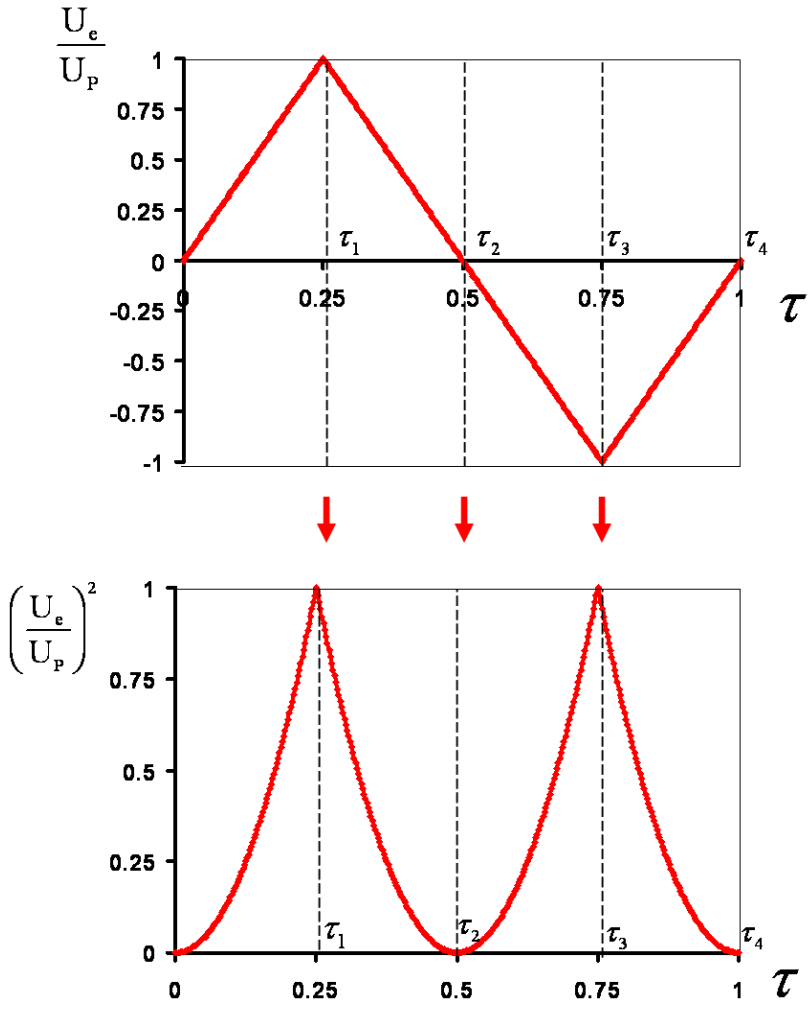

Figure B.1 Triangular pulse applied to the pendant drop (for $t_p=t_c$).

For the triangular pulse applied (shown in Figure B.1), the function $f(\tau)$ for the intervals of the pulse are given in Table B.1 where $\tau_1=0.25t_p/t_c$ $\tau_2=0.5t_p/t_c$ $\tau_3=0.75t_p/t_c$, $\tau_4=t_p/t_c$.

Table B.1 Pulse Forcing Functions for Different Intervals Within The Pulse

Range	**Pulse Interval**	**Pulse Function**
1st Quarter	$0 \le \tau \le \tau_1$	$f(\tau)=\left(\frac{\tau}{\tau_1}\right)^2$
2nd Quarter	$\tau_1 \le \tau \le \tau_2$	$f(\tau)=\left(\frac{\tau-\tau_2}{\tau_1-\tau_2}\right)^2$
3rd Quarter	$\tau_2 \le \tau \le \tau_3$	$f(\tau)=\left(\frac{\tau-\tau_2}{\tau_3-\tau_2}\right)^2$
4th Quarter	$\tau_3 \le \tau \le \tau_4$	$f(\tau)=\left(\frac{\tau-\tau_4}{\tau_3-\tau_4}\right)^2$
Pulse duration is finished	$\tau > \tau_4$	$f(\tau)=0$

APPENDIX C

ELECTRIC FORCE AND DEFROMATION OF PENDANT DROP

As the initial spherical segment with α~0.325 (fat drop i.e. $0 < \alpha < 1$) deforms into an hemispheroid with the same tip position as the initial drop (i.e. $R=L_o$), the initial hemispheroid parameters are L_o, R_o, e_o, R_c, and θ_o which are the major radius, minor, radius, eccentricity, radius of the spherical apex at the foci and the tip angle. Since there is no change in volume of the drop, these initial parameters can be estimated as: $R_o = \sqrt{\frac{3V_p}{2\pi L_o}}$, $e_o = \sqrt{1-\left(\frac{R_o}{L_o}\right)^2}$, $R_c = R_o\sqrt{1-e_o^2}$, and $\theta_o = \frac{180}{2\pi}\tan^{-1}(e)$.

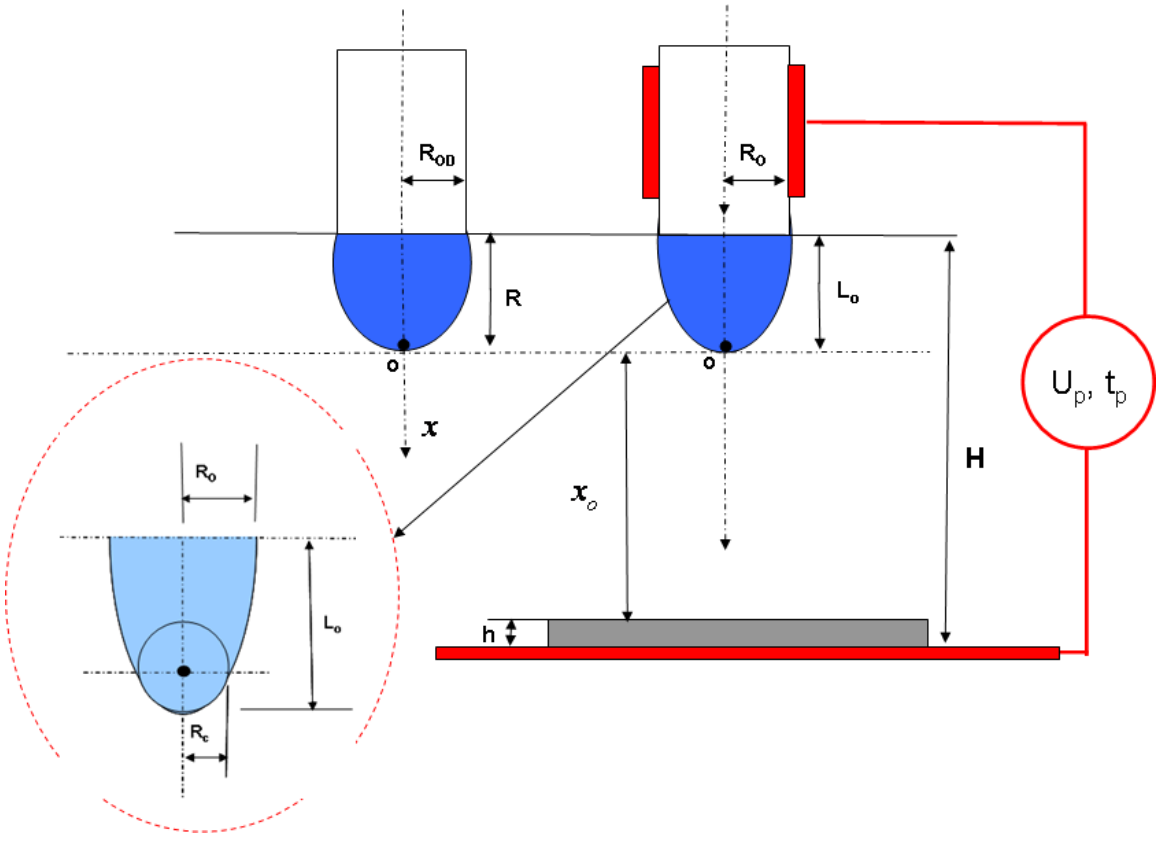

Figure C.1 Deformation of pendant drop by electric force.

The initial capacitance is calculated using these parameters in conjunction with the initial displacement x_o between the tip of the drop and the substrate.

The force acting on the drop is approximated from two components, (1) The Taylor force acting on a hemispheroidal conductor as in Chapter 5, Equation 5.3 and the electrostatic force on a spherical apex in Equation 5.4 which is obtained by taking the derivative of the capacitance as in Equation C.1.

$$f_{Sperical\_apex}(\overline{x}) = -\frac{1}{2}\frac{\partial C(\overline{x})}{\partial \overline{x}} U_f^2 \qquad (C.1)$$

APPENDIX D

FORMATION OF MICROPOROUS SUBSTRATE

Non porous substrates are formed through casting of required concentration of a HPMC polymer solution. However, porous substrates are formed through freeze drying of the polymer solution in a Labconco Benchtop freeze drier shown in Figure D.1. 3 dimensional porous gel networks are usually formed by crosslinks of polymer chains formed by covalent bonds, hydrophobic interaction, hydrogen bonds or physical enlargement (Kato and Gehrke 2004). Usually, as water freezes causing the polymer to condense around ice, these porous networks remain after sublimation of ice resulting in a microporous substrate.

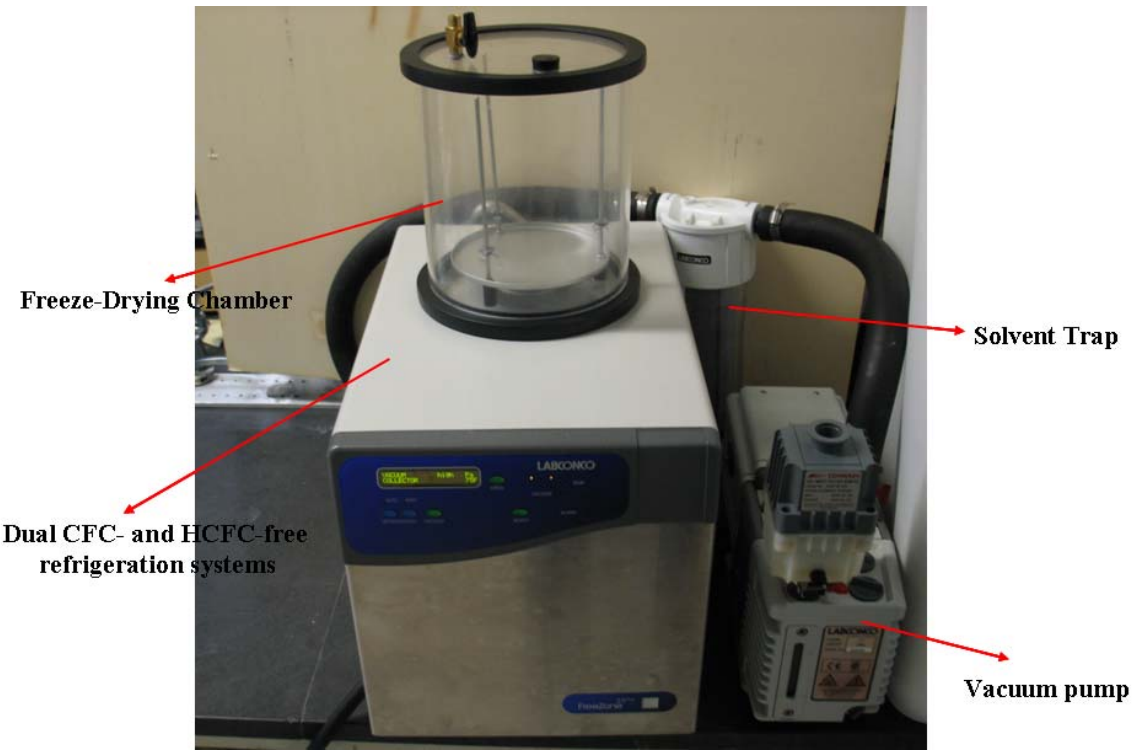

Figure D.1 Labconco Benchtop Freeze Drier.

Typically, shrinking in these gels is low because of the low diffusion coefficient of the polymer. Porosity is controlled by the concentration of polymer solution before freeze drying. However, interesting characteristic of such porous substrate includes their swelling and absorbent property which makes it useful for drug delivery. Table D.1 shows polymer concentration, film porosity and thickness.

Table D.1 Film Configurations

Method	**HPMC Weight Ratio** φ_p	**Water Weight Ratio** φ_w	**HPMC (w/w)%**	**Film Thickness** μm	**Film Porosity** φ
Freeze drying	1	19	5	500	0.95
Freeze drying	1	5	20	1000	0.83
Casting	1	5	5	80	Non Porous

$\phi = \frac{\varphi_W \rho_P}{\varphi_W \rho_P + \varphi_P \rho_W}$ where $\rho_P \sim 1000 kg/m^3$ and $\rho_W \sim 1000 kg/m^3$ are the true density of HPMC and water respectively.

APPENDIX E

MEASUREMENT OF FLUID DIELECTRIC PROPERTIES

Conductivity measurements were done on the low frequency module of a broadband dielectric spectrometer (BDS-80) shown in Figure E.1 and Figure E.2. BDS Cells for liquids with high and low permittivity were used. A cell containing a sample is placed under two electrodes in the low frequency module, a voltage of 1V was applied and the sample dielectric properties were measured over a wide frequency range, 1Hz-3MHz. Temperature was controlled at 25°C degree with the aid of liquid nitrogen and the feedback thermal control module on the broadband spectrometer. Temperature stabilization and accuracy was $\pm 0.01^{o}C$.

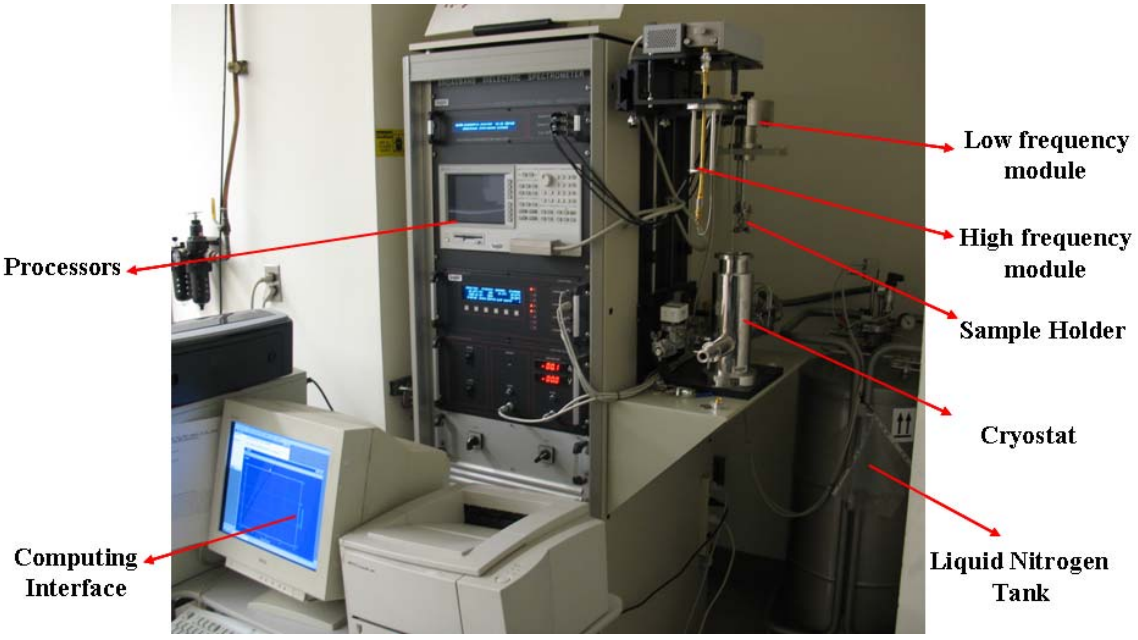

Figure E.1 Novocontrol Broadband Dielectric Spectrometer (BDS).

Calibrations were done with standard potassium chloride solution 0.035M (Sigma Aldrich) for high permittivity fluids and hexane (Sigma Aldrich) for low permittivity fluids. Measured properties were plotted as function of frequency over the whole frequency range (Figure E.3 and E.4). The real values were found at the plateau region of the curve where properties are frequency independent and free of polarization (inset, Figure E.3 and Figure E.4).

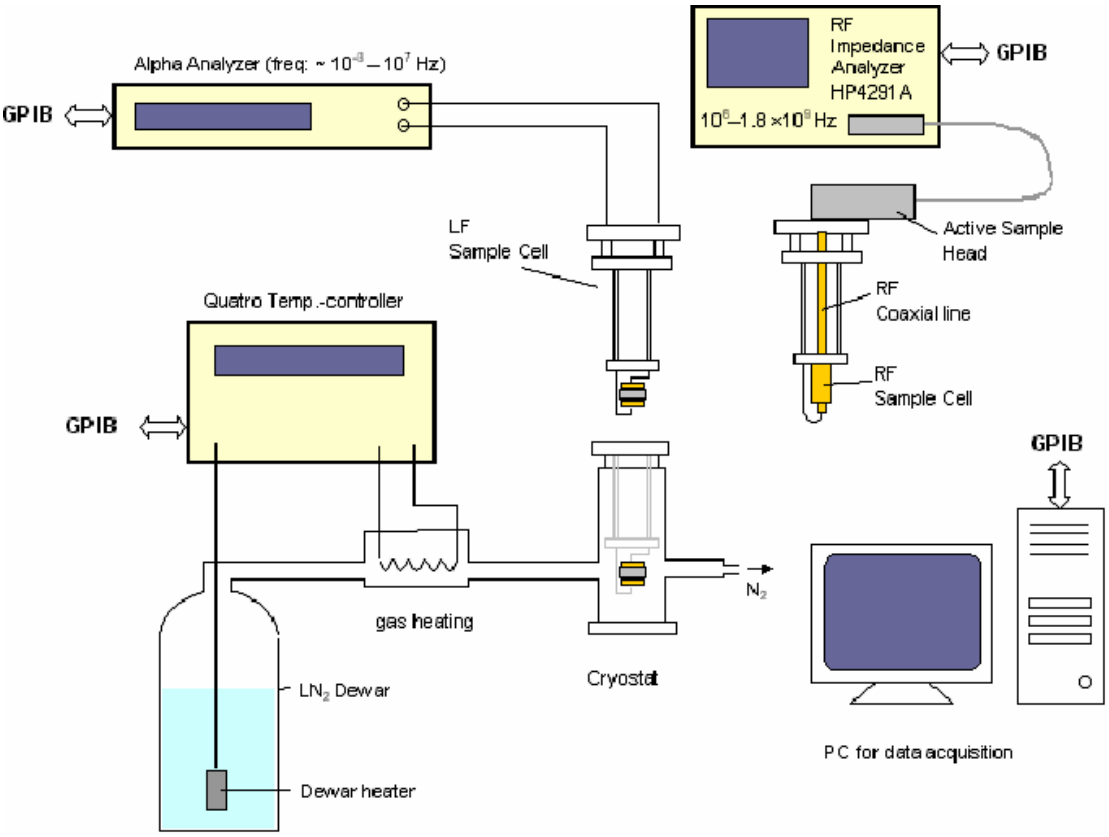

Figure E.2 Broadband Dielectric Spectrometer Schematics.

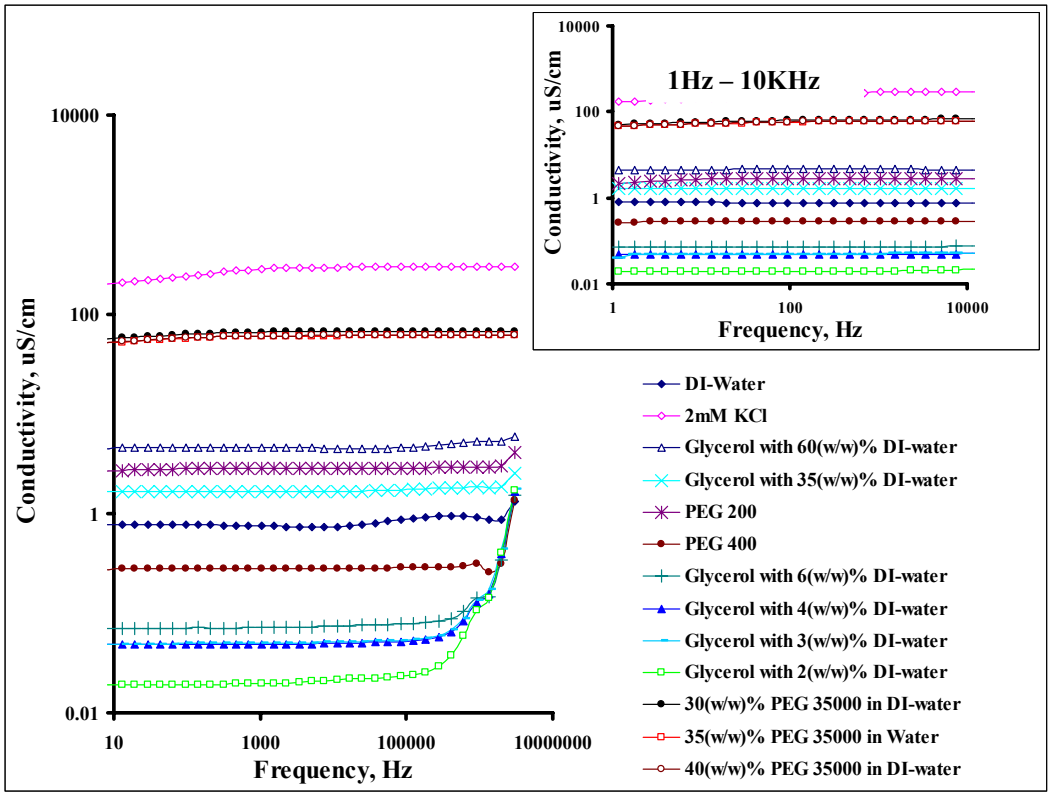

Figure E.3 Conductivity spectrum of different fluids.

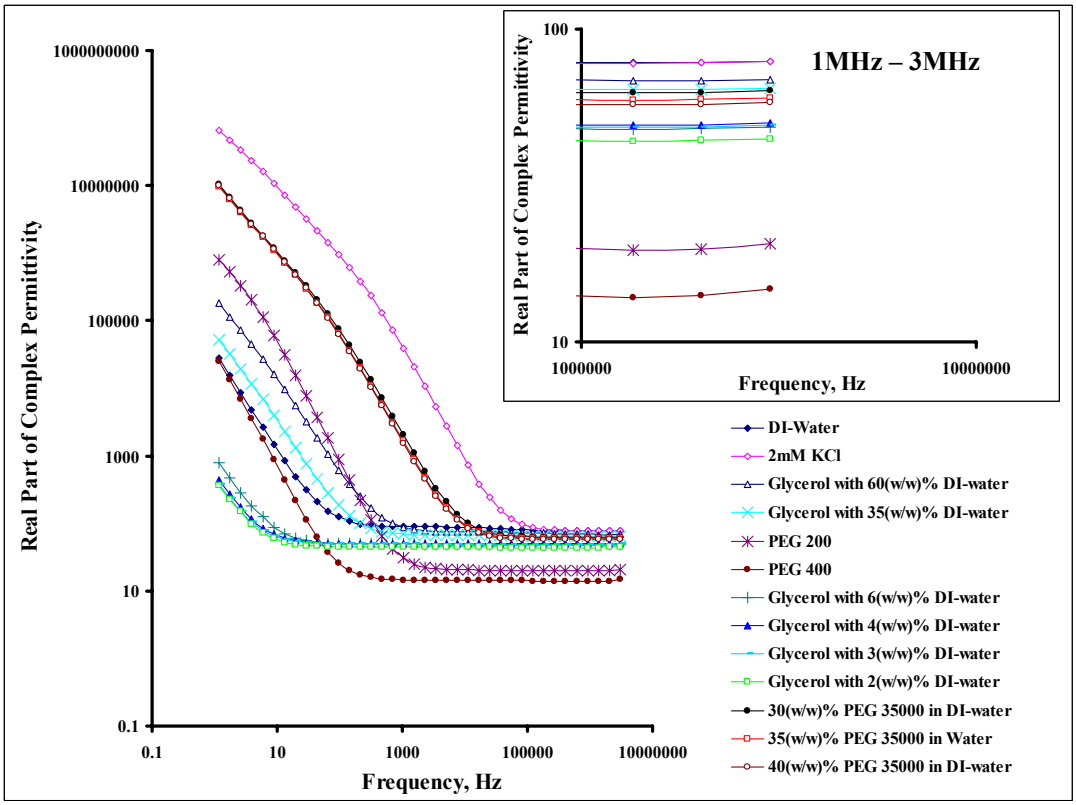

Figure E.4 Spectrum of real part of dielectric permittivity for different fluids.

The complex dielectric permittivity of a material is expressed as $\varepsilon = \varepsilon' + i\varepsilon''$ where ε' is the real part or the dielectric constant while ε'' is the imaginary part. The frequency dependence of conductivity of the material can be calculated from ε'' as in Equation E.1

$$\sigma = 2\pi\varepsilon_o\varepsilon''f \quad \textbf{(E.1)}$$

Where f is the frequency.

APPENDIX F

THERMO-OPTICAL MEASUREMENTS

The melting point of different materials was measured on a thermo-optical system consisting of a Mettler-Toledo FP84 Hot Stage connected to an FP 90 central processor, Visualization of materials behavior during melting can be carried out on a computer to which a Nikon SMZ 1500 microscope with a CCD camera (High resolution CoolSNAP HQ 2) is connected (Figure F.1).

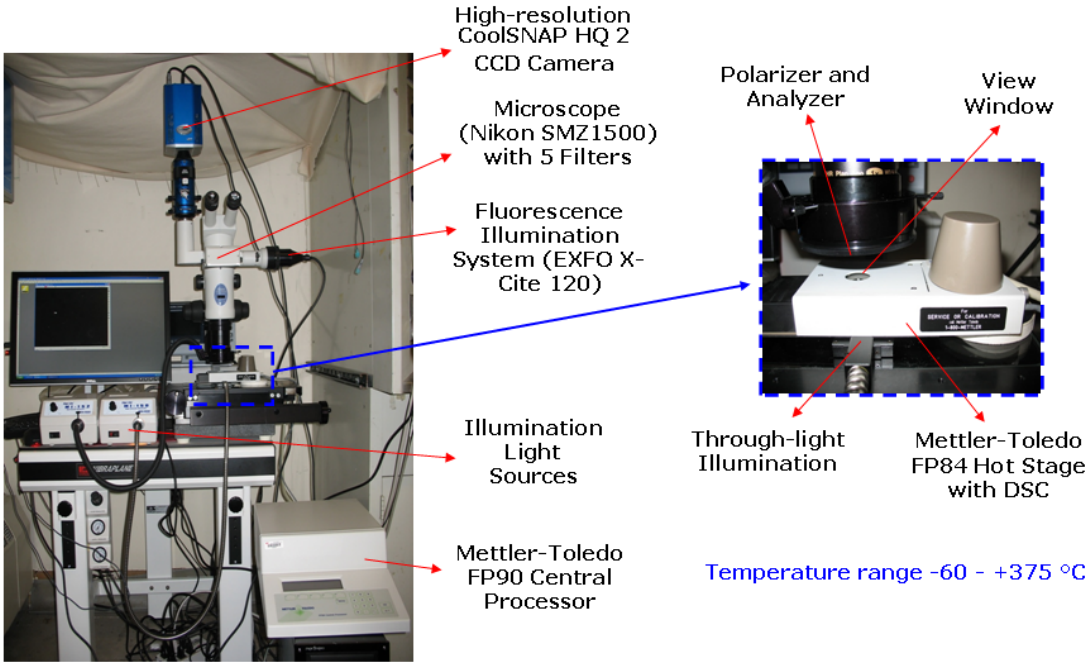

Figure F.1 Experimental Setup for thermo-optical analysis.

The endothermic peak/melting point was found for all materials used in experiments (Figure F.2). The melting points are in agreement with literature values.

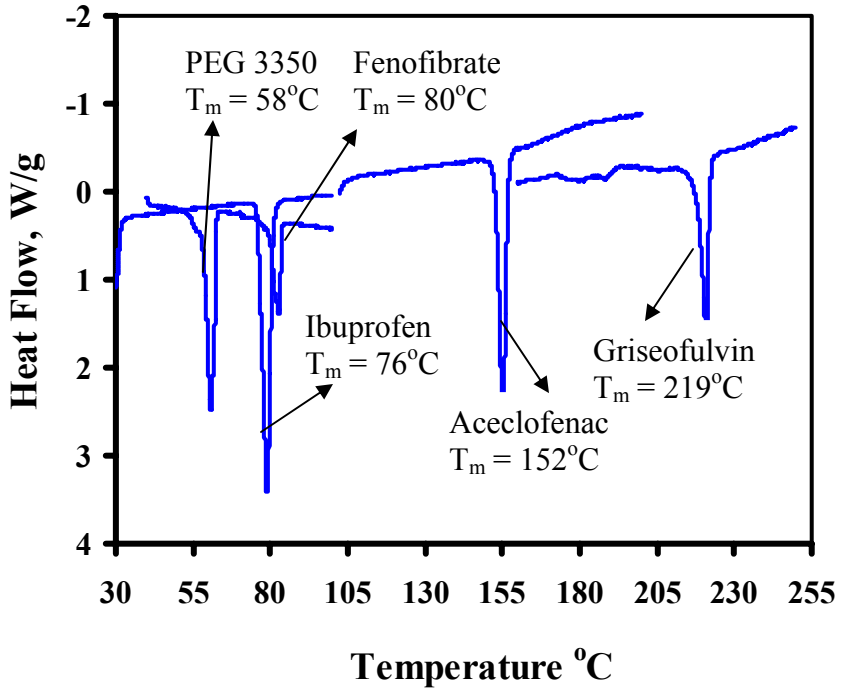

Figure F.2 DSC Thermograms at 5°C/min showing the melting temperature of different materials.

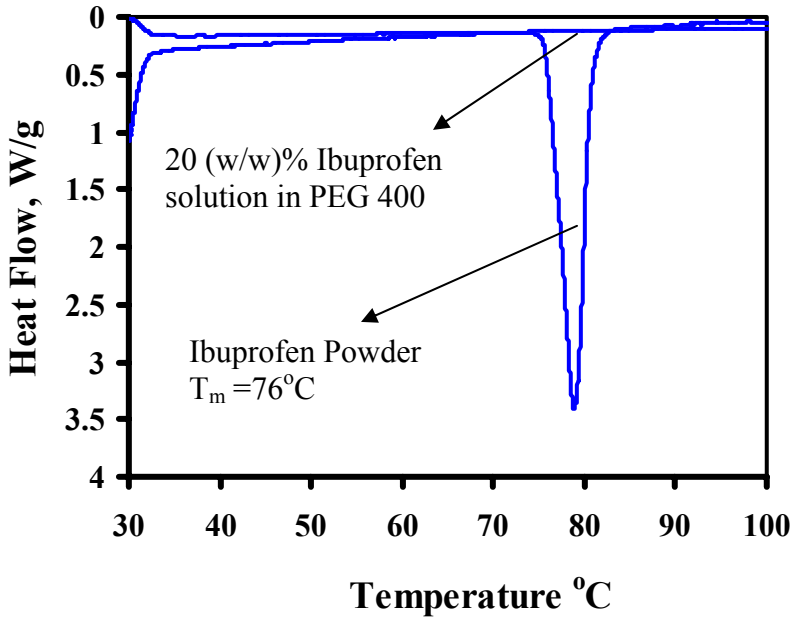

Figure F.3 DSC Thermograms of 7.2mg Ibuprofen powder and 36mg solution of 20 (w/w)% Ibuprofen solution in PEG 400 at 5°C/min.

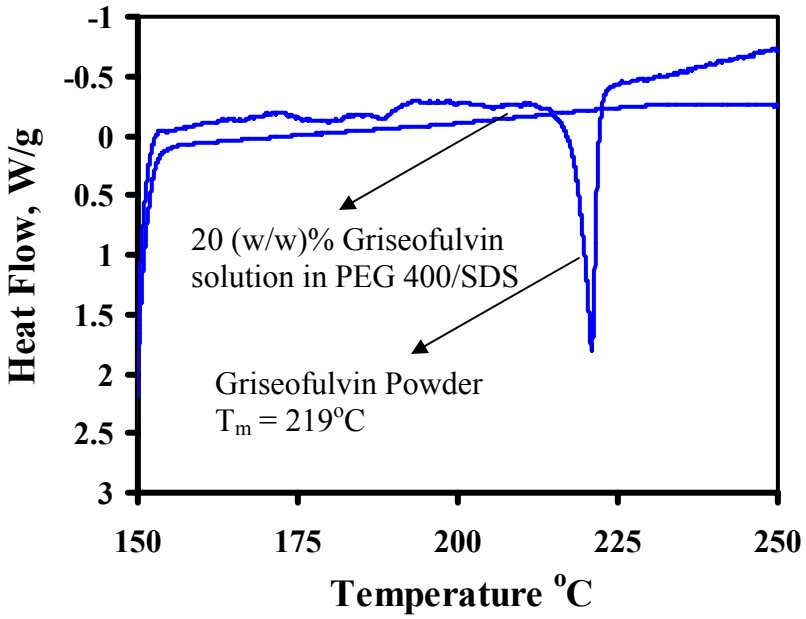

Figure F.4 DSC Thermograms of 7.5mg Ibuprofen powder and 37.5mg solution of 20 (w/w)% griseofulvin solution in PEG 400 at 5°C/min.

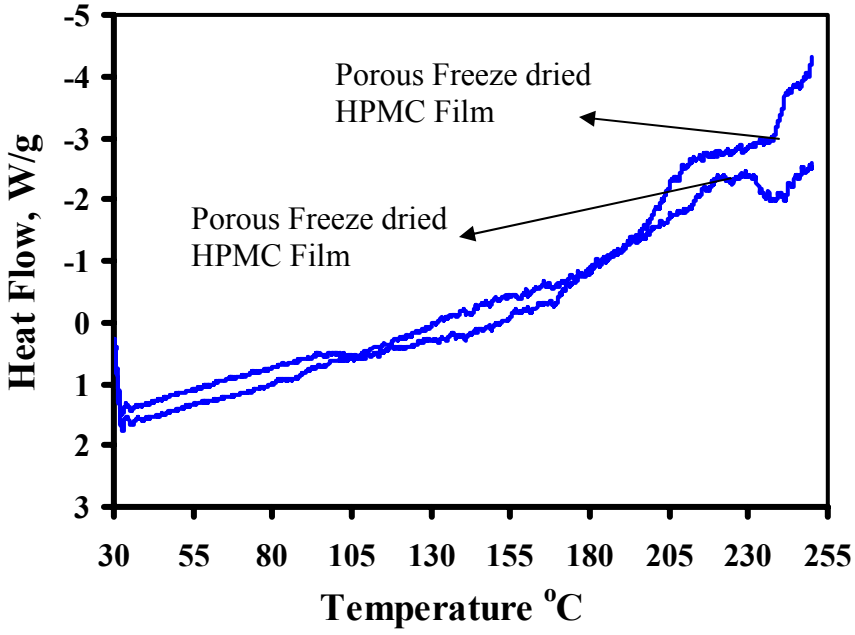

Figure F.5 DSC Thermograms of 1.5mg HPMC powder and 1.5mg porous freeze dried HPMC film at 5°C/min.

Differential scanning calorimetry (DSC) experiments on 7.2mg sample of Ibuprofen powder and 36mg of Ibuprofen solution in PEG 400 showed that the endothermic peak was found in the powder but could not be found in the solution (Figure F.3). The same observation was made on griseofulvin powder and its solution in PEG 400 and SDS (Figure F.4). It may be that both drugs dissolved in PEG 400 might have formed a continuous solid solution such that the instrument does not have the required sensitivity to detect the drugs (Leuner and Dressman 2000; Bikiaris, Papageorgiou et al. 2005). Also, drops of drug solutions printed on substrate could not be directed by DSC experiments. However, the DSC curve of HPMC powder and freeze dried porous film appears to be similar.

APPENDIX G

CHARGE RELAXATION TIME AND FLUID BEHAVIOR

Example of charge relaxation time relaxation time $t_e=\varepsilon_f\varepsilon_0/\sigma_f$ computed for fluids with low Ohnesorge number shows that $t_e << t_p$ and fluid behaves like a conductor.

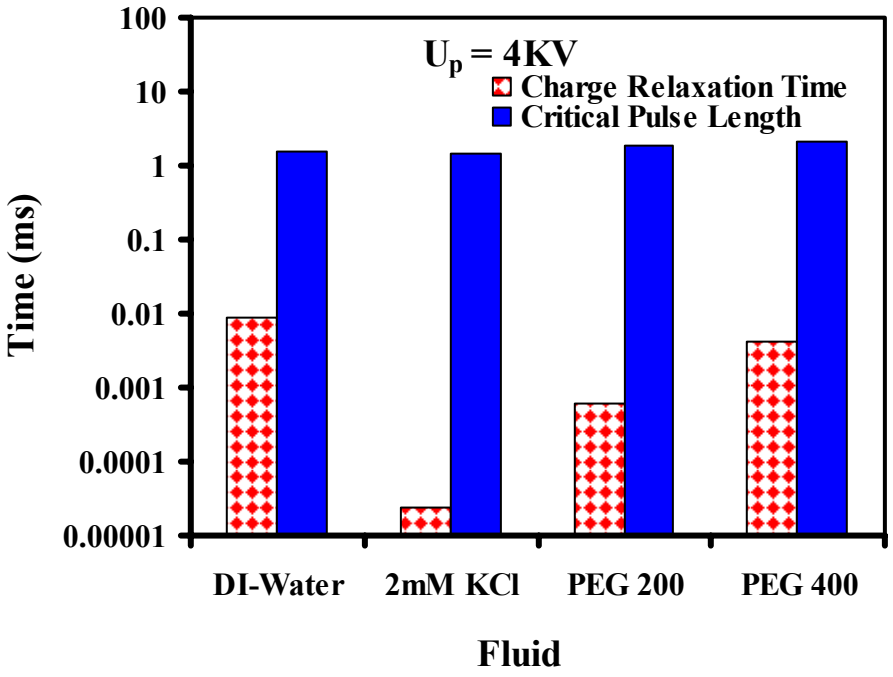

Figure G.1 Charge relaxation time compared to pulse length for fluids with Oh≤1.

APPENDIX H

CRITICAL PULSE AND RESONANCE TIME

Comparison of resonance time $T=2\pi\sqrt{\frac{m}{\Omega^2\gamma_f}}$ and critical pulse length shows that pulse length at the critical liquid bridge line is below resonance, where m is the mass of pendant drop, γ_f the fluid surface tension and Ω the resonance parameter in the damped harmonic oscillator equation.

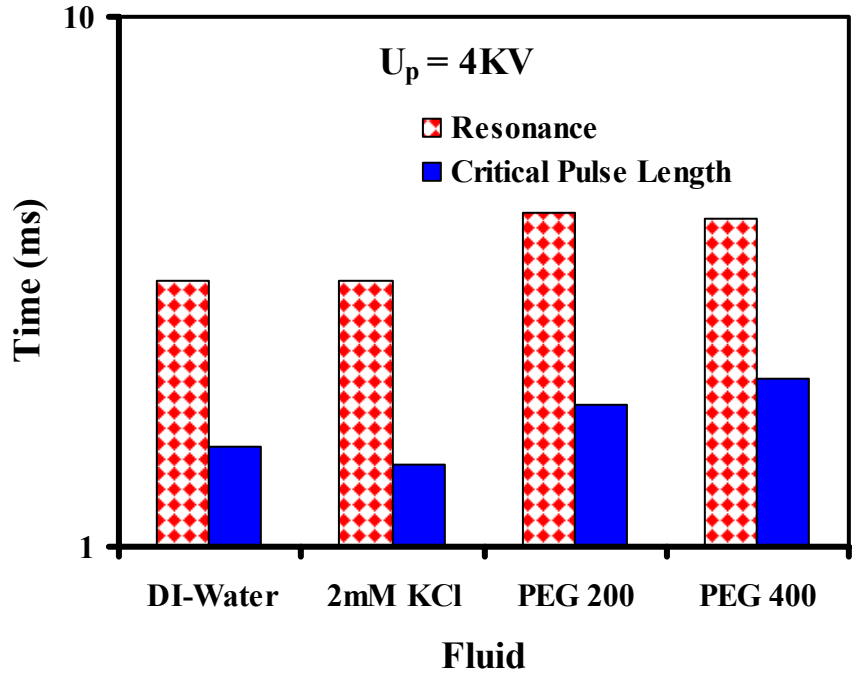

Figure H.1 Comparison of resonance time and pulse length for fluids with Oh≤1.

REFERENCES

Allen, L. V., N. G. Popovich, et al. (2004). Ansel's Pharmaceutical Dosage Forms and Drug Delivery Systems. Philadelphia, Lippincott Williams & Wilkins.

Amidon, G. L., H. Lennernäs, et al. (1995). "A Theoretical Basis for a Biopharmaceutic Drug Classification: The Correlation of *in Vitro* Drug Product Dissolution and *in Vivo* Bioavailability." Pharmaceutical Research **12**(3): 413-420.

BALAKRISHNAN, A., B. D. REGE, et al. (2004). "Surfactant-Mediated Dissolution: Contributions of Solubility Enhancement and Relatively Low Micelle Diffusivity." JOURNAL OF PHARMACEUTICAL SCIENCES **93**(8): 2064–2075.

Basaran, O. A. (2002). "Small-scale free surface flows with breakup: Drop formation and emerging applications." AIChE Journal **48**(9): 1842-1848.

Basaran, O. A. and D. W. DePaoli (1994). "Nonlinear oscillations of pendant drops." Physics of Fluids **6**(9): 2923-2943.

Batchelor, G. K. (1967). An Introduction to Fluid Dynamics. Cambridge, Cambridge University Press.

Belaidi, S., P. Girard, et al. (1997). "Electrostatic forces acting on the tip in atomic force microscopy: Modelization and comparison with analytic expressions." Journal of Applied Physics **81**(3): 1023-1030.

Bikiaris, D., G. Z. Papageorgiou, et al. (2005). "Physicochemical studies on solid dispersions of poorly water-soluble drugs: Evaluation of capabilities and limitations of thermal analysis techniques." Thermochimica Acta **439**(1-2): 58-67.

Casuso, I., L. Fumagalli, et al. (2007). "Nondestructive thickness measurement of biological layers at the nanoscale by simultaneous topography and capacitance imaging." Applied Physics Letters **91**(6): 063111-063113.

Chen, C. H., D. A. Saville, et al. (2006). "Scaling laws for pulsed electrohydrodynamic drop formation." Applied Physics Letters **89**(12): 124103-124103.

Choi, H. K., J.-U. Park, et al. (2008). "Scaling laws for jet pulsations associated with high-resolution electrohydrodynamic printing." Applied Physics Letters **92**(12): 123109-123103.

Chow, K., H. H. Y. Tong, et al. (2008). "Engineering of pharmaceutical materials: An industrial perspective." JOURNAL OF PHARMACEUTICAL SCIENCES **97**(8): 2855-2877.

Cloupeau, M. and B. Prunet-Foch (1994). "Electrohydrodynamic spraying functioning modes: a critical review." Journal of Aerosol Science **25**(6): 1021-1036.

Costa, P. and J. M. Sousa Lobo (2001). "Modeling and comparison of dissolution profiles." European Journal of Pharmaceutical Sciences **13**(2): 123-133.

Dixit, R. P. and S. P. Puthli (2009). "Oral strip technology: Overview and future potential." Journal of Controlled Release **139**(2): 94-107.

Eggers, J. (1997). "Nonlinear dynamics and breakup of free-surface flows." Reviews of Modern Physics **69**(3): 865.

Elmqvist, R. (1951). Measuring instrument of the recording type. U. S. P. Office. United States.

Espino, J. L., J. Meseguer, et al. (2002). "An experimental study of the breakage of liquid bridges at stability limit of minimum volume." Physics of Fluids **14**(10): 3710-3713.

Fernández de la Mora, J. (2006). "The Fluid Dynamics of Taylor Cones." Annual Review of Fluid Mechanics **39**(1): 217-243.

Fujioka, Y., Y. Metsugi, et al. (2008). "Evaluation of in vivo dissolution behavior and GI transit of griseofulvin, a BCS class II drug." International Journal of Pharmaceutics **352**(1-2): 36-43.

Fumagalli, L., G. Ferrari, et al. (2007). "Dielectric-constant measurement of thin insulating films at low frequency by nanoscale capacitance microscopy." Applied Physics Letters **91**(24): 243110-243113.

Haddadin, R., F. Qian, et al. (2008). "Estimation of Drug Solubility in Polymers via Differential Scanning Calorimetry and Utilization of the Fox Equation." Pharmaceutical Development and Technology **14**(1): 19-27.

Hadimioglu, B., S. Elrod, et al. (2001). Acoustic ink printing: an application of ultrasonics for photographic quality printing at high speed. Ultrasonics Symposium, 2001 IEEE.

Hariharan, M. and B. A. Bogue (2009). "Orally dissolving film strips (ODFS): The Final Evolution of Orally Dissolving Dosage Forms." Drug Delivery Technology **9**(2): 24-28.

Harris, M. T. and O. A. Basaran (1993). "Capillary Electrohydrostatics of Conducting Drops Hanging from a Nozzle in an Electric Field." Journal of Colloid and Interface Science **161**(2): 389-413.

Hood, L., J. R. Heath, et al. (2004). "Systems Biology and New Technologies Enable Predictive and Preventative Medicine." Science **306**(5696): 640-643.

Jean, M. S., S. Hudlet, et al. (1999). "Van der Waals and capacitive forces in atomic force microscopies." Journal of Applied Physics **86**(9): 5245-5248.

Jørgensen, J. T. (2007). "From blockbuster medicine to personalized medicine." Personalized Medicine **5**(1): 55-63.

Kato, N. and S. H. Gehrke (2004). "Microporous, fast response cellulose ether hydrogel prepared by freeze-drying." Colloids and Surfaces B: Biointerfaces **38**(3-4): 191-196.

Katsanis, S. H., G. Javitt, et al. (2008). "A Case Study of Personalized Medicine." Science **320**(5872): 53-54.

Kim, J., H. Oh, et al. (2008). "Electrohydrodynamic drop-on-demand patterning in pulsed cone-jet mode at various frequencies." Journal of Aerosol Science **39**(9): 819-825.

Kipphan, H. (2001). Handbook of Print Media: Technologies and Production Methods. Berlin, Springer.

Kyser, E. L. and S. B. Sears (1976). Method and apparatus for recording with writing fluids and drop projection means therefore. U. S. P. Office. United States, Silonics Inc.

Le, H. P. (1998). "Progress and Trends in Ink-jet Printing Technology." The Journal of Imaging Science and Technology **42**(1): 49-62.

Lee, B. S., H.-J. Cho, et al. (2006). "Drop formation via breakup of a liquid bridge in an AC electric field." Journal of Colloid and Interface Science **302**(1): 294-307.

Leuner, C. and J. Dressman (2000). "Improving drug solubility for oral delivery using solid dispersions." European Journal of Pharmaceutics and Biopharmaceutics **50**(1): 47-60.

Li, C. L., L. G. Martini, et al. (2005). "The use of hypromellose in oral drug delivery." Journal of Pharmacy and Pharmacology **57**(5): 533-546.

Li, J. and P. Zhang (2009). "Formation and droplet size of EHD drippings induced by superimposing an electric pulse to background voltage." Journal of Electrostatics **67**(4): 562-567.

Lin, S. P. and R. D. Reitz (1998). "DROP AND SPRAY FORMATION FROM A LIQUID JET." Annual Review of Fluid Mechanics **30**(1): 85-105.

Magdassi, S. (2009). The chemistry of inkjet inks. Singapore, World Scientific Publishing Company.

Mashkevich, B. O. (2007). Drug delivery research advances. New York, Nova Science Inc.

Meléndez, P. A., K. M. Kane, et al. (2008). "Thermal inkjet application in the preparation of oral dosage forms: Dispensing of prednisolone solutions and polymorphic characterization by solid-state spectroscopic techniques." JOURNAL OF PHARMACEUTICAL SCIENCES **97**(7): 2619-2636.

Meseguer, J., J. L. Espino, et al. (2003). "On the breaking of long, axisymmetric liquid bridges between unequal supporting disks at minimum volume stability limit." European Journal of Mechanics - B/Fluids **22**(4): 355-368.

Meseguer, J., L. A. Slobozhanin, et al. (1995). "A review on the stability of liquid bridges." Advances in Space Research **16**(7): 5-14.

Mishra, S., K. L. Barton, et al. (2010). "High-speed and drop-on-demand printing with a pulsed electrohydrodynamic jet." Journal of Micromechanics and Microengineering **20**(9): 095026.

Moneghini, M., B. Bellich, et al. (2008). "Microwave generated solid dispersions containing Ibuprofen." International Journal of Pharmaceutics **361**(1-2): 125-130.

Moon, J. H., B. H. Kang, et al. (2006). "The lowest oscillation mode of a pendant drop." Physics of Fluids **18**(2): 021702-021704.

Newa, M., K. H. Bhandari, et al. (2007). "Preparation, characterization and in vivo evaluation of ibuprofen binary solid dispersions with poloxamer 188." International Journal of Pharmaceutics **343**(1-2): 228-237.

Radulescu, D., H. J. Trost, et al. (2005). "3D Printing of Biological Materials for Drug Delivery and Tissue Engineering Applications." Digital Fabrication September 18-21.

Rayleigh, L. (1878). "On The Instability Of Jets." Proceedings of the London Mathematical Society **s1-10**(1): 4-13.

Roth, E. A., T. Xu, et al. (2004). "Inkjet printing for high-throughput cell patterning." Biomaterials **25**(17): 3707-3715.

Sandler, N., A. Määttänen, et al. (2011). "Inkjet printing of drug substances and use of porous substrates-towards individualized dosing." JOURNAL OF PHARMACEUTICAL SCIENCES: doi: 10.1002/jps.22526.

Saville, D. A. (1997). "ELECTROHYDRODYNAMICS:The Taylor-Melcher Leaky Dielectric Model." Annual Review of Fluid Mechanics **29**(1): 27-64.

Schena, M. (2005). Protein Microarrays. Sudbury, Jones and Bartlett.

Siepmann, J. and N. A. Peppas (2001). "Modeling of drug release from delivery systems based on hydroxypropyl methylcellulose (HPMC)." Advanced Drug Delivery Reviews **48**(2-3): 139-157.

Slobozhanin, L. A. and J. I. D. Alexander (1998). "Combined effect of disk inequality and axial gravity on axisymmetric liquid bridge stability." Physics of Fluids **10**(10): 2473-2488.

Slobozhanin, L. A., J. I. D. Alexander, et al. (2002). "The stability margin for stable weightless liquid bridges." Physics of Fluids **14**(1): 209-224.

Stachewicz, U., C. U. Yurteri, et al. (2009). "Stability regime of pulse frequency for single event electrospraying." Applied Physics Letters **95**(22): 224105-224103.

Strani, M. and F. Sabetta (1984). "Free vibrations of a drop in partial contact with a solid support." Journal of Fluid Mechanics **141**: 233-247.

Strani, M. and F. Sabetta (1988). "Viscous oscillations of a supported drop in an immiscible fluid." Journal of Fluid Mechanics **189**: 397-421.

Taylor, G. (1964). "Disintegration of Water Drops in an Electric Field." Proceedings of the Royal Society of London. Series A, Mathematical and Physical Sciences **280**(1382): 383-397.

Taylor, G. (1966). "The Force Exerted by an Electric Field on a Long Cylindrical Conductor." Proceedings of the Royal Society of London. Series A, Mathematical and Physical Sciences **291**(1425): 145-158.

Taylor, G. (1969). "Electrically Driven Jets." Proceedings of the Royal Society of London. Series A, Mathematical and Physical Sciences **313**(1515): 453-475.

Tsukada, T., M. Sato, et al. (1987). "A Theoretical and experimental study on the oscillation of a hanging drop." Journal of Chemical Engineering of Japan **20**(88).

USP (2004). "Pharmacopeial Previews." **30**: 351-363.

Wilkes, E. D. and O. A. Basaran (1997). "Forced oscillations of pendant (sessile) drops." Physics of Fluids **9**(6): 1512-1528.

Wulff, M. and M. Aldén (1995). “Phase equilibria in drug-polymer-surfactant systems.” Thermochimica Acta **256**(1): 151-165.

Wulff, M., M. Aldén, et al. (1996). “An investigation into the critical surfactant concentration for solid solubility of hydrophobic drug in different polyethylene glycols.” International Journal of Pharmaceutics **142**(2): 189-198.

Xu, T., J. Jin, et al. (2005). "Inkjet printing of viable mammalian cells.” Biomaterials **26**(1): 93-99.

Yeo, Y., O. A. Basaran, et al. (2003). “A new process for making reservoir-type microcapsules using ink-jet technology and interfacial phase separation.” Journal of Controlled Release **93**(2): 161-173.

Yogi, O., T. Kawakami, et al. (2001). “On-Demand Droplet Spotter for Preparing Pico- to Femtoliter Droplets on Surfaces.” Analytical Chemistry **73**(8): 1896-1902.

Yu, D.-g., W.-x. Yan, et al. (2008). “Rheological characteristics of drug-loaded microemulsions and their printability in three dimensional printing systems.” Journal of Central South University of Technology **15**(0): 88-92.

Yu, L. X., G. L. Amidon, et al. (2002). “Biopharmaceutics Classification System: The Scientific Basis for Biowaiver Extensions.” Pharmaceutical Research **19**(7): 921-925.

Zoltan, S. L. (1972). Pulse droplet ejection system. U. S. P. Office. United States, Clevite Corporation.